Development of Adsorber Beds for Air Conditioning in Vehicle Applications

by

Seyyed Mahdi Nemati Mehr

B.Sc., Sharif University of Technology, 2011

Thesis Submitted in Partial Fulfillment of the
Requirements for the Degree of
Master of Applied Science

in the
School of Mechatronic Systems Engineering
Faculty of Applied Sciences

SIMON FRASER UNIVERSITY

Summer 2016

Approval

Name:	**Seyyed Mahdi Nemati Mehr**
Degree:	**Master of Applied Science**
Title:	***Development of Adsorber Beds for Air Conditioning in Vehicle Applications***

Examining Committee: **Chair:** Flavio Firmani
Lecturer

Majid Bahrami
Senior Supervisor
Professor _____

Jiacheng (Jason) Wang
Supervisor
Assistant Professor _____

Michael Eikerling
Internal Examiner
Professor
Department of Chemistry _____

Date Defended/Approved: June 30, 2016

Abstract

This project set out to design and develop a better adsorber bed for an adsorption cooling system (ACS). The most important characteristic of an ACS is the specific cooling power (SCP), which is defined as the ratio of the cooling power at the evaporator to the product of the cycle time and mass of dry adsorbent. The performance of the ACS is evaluated using an in-situ mass measurement to determine the amount refrigerant that has been adsorbed. A numerical model for the adsorption process within an adsorber bed was developed in ANSYS Fluent with an added user defined function (UDF) module and a comparison was made between the results of the numerical model and the experimental tests. Although the numerical model always over predicts the value for SCP, the results show good agreement. The validated numerical model can be used to predict the performance of the ACS at different working conditions and with different adsorber bed geometries.

Keywords: Adsorption; Specific Cooling Power; In-Situ; Experimental Setup; Numerical Modeling

Dedicated to my beloved father, mother, and my dear family

Acknowledgements

First and foremost, I would like to express my sincere gratitude to my supervisor Dr. Majid Bahrami for his years of guidance, encouragement and patience towards me during my M.A.Sc. studies. I really appreciate the inspirations arising from his deep insights and broad knowledge and provoking comments on various aspects of my research. Without his help, I definitely could not have learnt so much in the past two years.

Secondly, I would like to thank my friend and the Ph.D. student in our lab, Dr. Amir Sharafian for his patience and accompany during my research. I also thank our other group members Dr. Wendell Huttema, Dr. Claire McCague, Marius Haiducu, Khorshid Fayazmanesh, Poovana Cheppudira and Mayank Kalra. They helped me on different aspects of this research and this research could not have been this successful without their sincere helps. I would not forget those memorable moments with them and I really cherish the friendship we have developed.

Table of Contents

List of Tables

List of Figures

List of Acronyms

AC	Air Conditioning
ACS	Adsorption Cooling System
CFC	Chlorofluorocarbon
CFD	Computational Fluid Dynamics
COP	Coefficient Of Performance
GWP	Global Warming Potential
HCFC	Hydrochlorofluorocarbon
HFC	Hydrofluorocarbons
HVAC	Heating, Ventilation, and Air Conditioning
ICE	Internal Combustion Engine
IUPAC	International Union of Pure Applied Chemistry
LAEC	Laboratory for Alternative Energy Conversion
NTU	Number of Transfer Units
RSC	Reversed Stirling Cycle
TGA	Thermogravimetric Analysis
VCR	Vapor Compression Refrigeration

List of Subscripts

ads	Adsorber
fg	Fluid-gas phase change
ref	Refrigerant

Glossary

Adsorber Bed to Adsorbent Mass Ratio (AAMR)	Ratio of the metal mass of an adsorber bed to the dry mass of adsorbent material
Coefficient of Performance	Ratio of evaporative cooling energy to the waste heat energy supplied to the adsorber bed
Specific Cooling Power	Ratio of evaporative cooling energy to dry mass of adsorbent multiplied by the cycle time
Uptake	Ratio of the adsorbed material mass to the dry adsorbent mass

Executive Summary

Motivation

The conventional refrigeration cycle, which is used for air conditioning (AC) systems, is a cycle based on the vapor compression refrigeration (VCR) cycle. There are four main components in this cycle: a compressor, an evaporator, a condenser, and an expansion valve. To run this cycle, external work is required to run the compressor. In stationary applications, this work is usually supplied by electricity, however, in mobile applications like vehicles and reefers, the power to run the compressor is often provided through a direct mechanical connection to the engine of the vehicle. It has been shown that for a typical passenger vehicle, this connection can add up to 6 kW to the power consumption to the engine. This power is equivalent to the power needed to drive a 1200 kg sedan at the constant speed of 56 km/h. One of the main drawbacks associated with internal combustion engines (ICE), is their low efficiency. In a typical ICE, about 70% of the total released energy is wasted as heat through the radiator and the exhaust gas. This raises the possibility of utilizing this waste heat to run the AC system. A number of different technologies have been introduced in this regard, such as thermoelectric cooling, the reverse Stirling cycle, absorption refrigeration, and adsorption refrigeration. This thesis focuses on adsorption cooling systems (ACS) as a promising approach for vehicle applications. The materials used in an adsorption cooling system (both adsorber and adsorbent) are mostly non-toxic, non-corrosive, and environmentally friendly. The only moving parts in ACS are valves and, therefore, these systems are quiet, and require minimal maintenance. However, there are some drawbacks associated with ACS, which make them heavy and bulky. As a result, of these disadvantages, ACS have not been commercialized in mobile applications, even though they can utilize the waste heat and are environmentally friendly. In this thesis, heat and mass transfer within adsorber bed are studied, and a new design for the adsorber bed is introduced to enhance the overall adsorption cycle performance.

Objectives

The main objective of this project is to investigate the mass and heat transfer processes within the adsorber bed and improve the performance of a two-adsorber bed ACS. This project is divided into two main parts: experimental setup and numerical modeling. Each of these parts will be discussed in details in the following chapters. To achieve the ultimate goal, which is performance enhancement, the following objectives were set:

- Review of the available theoretical and experimental research on ACS.
- Review of the available adsorption working pairs and a comprehensive comparison between them.
- Develop a numerical model that can be used in different working conditions and geometries to predict the performance of new designs.
- Build a test facility to understand the adsorption and desorption processes inside an adsorber bed and investigate the effects of changing different parameters.

Methodology

Two heat exchanger designs were studied experimentally at the *Laboratory for Alternative Energy Conversion* (LAEC). The study focused on uptake rate measurements, which can be used to calculate the specific cooling power (SCP) of the system. Uptake measurements were performed using an in-situ technique in which the mass of the adsorber bed is measured with a scale in real time. The changes in the mass of the adsorber bed over time show how much refrigerant is adsorbed or desorbed.

A computational fluid dynamics (CFD) model was developed based on the linear driving force (LDF) and data extracted from thermogravimetric analysis (TGA). This numerical model can be used for any working pairs if the governing equations of the adsorption process are known. In addition, CFD model can be used for different geometries if correct boundary conditions are applied. The numerical model was validated with the results of the experiments and after validation; the model was used to predict the performance of other designs and different boundary conditions. Parametric studies of

different parameters were performed, and the importance of each property was evaluated using this model.

Thesis outline

This thesis consists of four chapters. The first chapter is an introduction to the adsorption process and its utilization in refrigeration applications. A comprehensive literature review on adsorption cooling systems is presented in chapter two. Chapter three describes the design of a test facility that was used to measure the performance of two adsorber bed designs under different working conditions. The developed numerical model is presented in chapter four. Assumptions and simplifications that were used in this model are described in detail, and results from the numerical model are shown. This chapter contains comparisons between the numerical and experimental results and discusses possible explanations for the discrepancies between the results of these two methods.

Chapter 1. Introduction

In this chapter, an introduction to adsorption cooling systems is presented. First, the commonly used vapor compression refrigeration cycle is introduced and then some alternatives are discussed. The adsorption cooling cycle is presented in detail, a summary of working pairs is shown, and different adsorption cooling systems are introduced.

1.1. Vapor compression refrigeration cycle

Refrigeration and air conditioning systems are widely used in different applications, such as residential and industrial comfort cooling, food and medicine transportation, cold storage, etc. It is estimated that about 80 million air conditioning devices were sold in 2009 with a greater number being sold every year, which emphasizes on the importance of this market [1]. Most of this market is dominated by vapor compression refrigeration (VCR) systems, which are driven by high-grade electrical or mechanical energy. About 15% of worldwide electrical energy consumption is used to run refrigeration and air conditioning systems [2].

There are four main components in a VCR cycle: a compressor, an evaporator, a condenser, and an expansion valve. Refrigerant enters the compressor as a low pressure gas and exits the compressor as a hot, high pressure gas. In the condenser, refrigerant releases heat to ambient, cools down, and condenses. Liquid refrigerant passes through the expansion valve and its temperature and pressure drops. A cold mixture of liquid and gas enters the evaporator and cools down the secondary fluid. The cold vapor enters the compressor again to complete the cycle. A schematic of this cycle is shown in Figure 1-1.

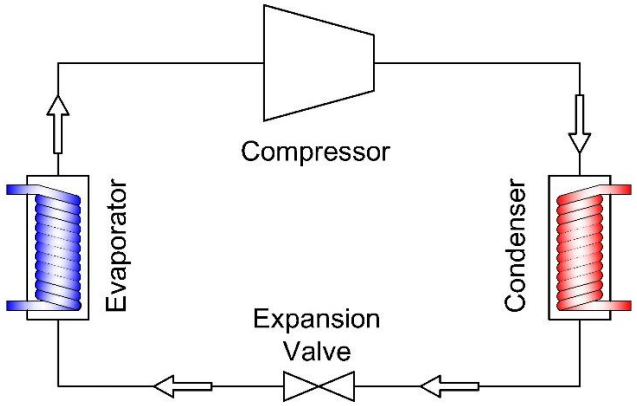

Figure 1-1 Schematic of vapor compression refrigeration cycle

There are two main concerns regarding using VCR systems: their energy consumption, and their effect on the environmental. These two concerns are discussed in more detail in the following sections.

1.1.1. Energy crisis

The conventional VCR cycle is generally run using electricity in stationary applications and a mechanical engine in mobile applications. According to data from US Department of Energy, HVAC systems are responsible for using 18.62%, 16.20%, and 2.34% of the total energy consumption in the residential, commercial and industrial sectors respectively [3]. The energy consumption in the mobile application is also important. In a typical passenger car, the compressor of the vehicle can add up to 6 kW of power consumption to the engine. This power is equivalent to the power required to drive a 1200 kg sedan at the constant speed of 56 km/h [4]. Annually about 40 billion liters of fuel is consumed in the US just to run the AC systems of light duty vehicles [4]. Therefore, a commercially reasonable replacement for VCR systems in both mobile and stationary applications can be received by the market. Different technologies have been introduced, such as thermoelectric cooling, reverse Stirling cycle, absorption refrigeration cycle, and adsorption refrigeration cycle.

1.1.2. Environmental effects

The environmental effects of VCR systems can be divided into three aspects: ozone depletion, global warming, and air pollution. Most of the refrigerant being used in VCR systems are CFC (chlorofluorocarbon) and HCFC (hydrochlorofluorocarbon) based materials. The ozone layer protects the Earth from cancer-causing ultraviolet solar radiation. It has been shown CFC and HCFC molecules break apart when they are exposed to ultraviolet radiation in the stratosphere and release chlorine atoms. Chlorine atoms react with ozone and destroy it. The final product of this reaction is an oxygen molecule, which does not have protective effects of ozone[5]. Based on Montreal Protocol (initiated in 1987) and its amendments, the use of CFCs and HCFCs should be eliminated gradually until 2030. In addition, according to EU regulations, all AC devices using HFCF22 should be replaced with devices do not work with ozone depleting refrigerants [6]. The second environmental problem associated with VCR air conditioning systems is the greenhouse effects of the refrigerants used and their very high global warming potential (GWP). CFCs are one of the six main gasses showing greenhouse effects and based on Kyoto Protocol, the use of them has to be limited. The 100 year GWP of R134a, which is one of the most commonly used refrigerants in VCR systems, is 1430 compared to methane which is 25 [7]. Based on the fluorinated greenhouse gases (F-gas) regulations, the use of the refrigerants with a global warming potential of greater than 150 is prohibited in new vehicle AC systems in the European Union since 2011, and has to be eliminated from all vehicles globally after 2017 [8]. These refrigerants enter the air through direct release due to leaks, equipment maintenance, and retirement. It is also important to mention that transportation is responsible for the most refrigerant leakage in the world [9]. The greenhouse effect causes global warming, which results in greater cooling demand and, therefore, creates a positive feedback loop.

The third environmental effect, which is possibly the most important, is that these systems use mechanical or electrical energy to run the compressor. Most of the electricity worldwide comes from burning fossil fuels at power plants. The main product of combustion process is CO_2, which is a greenhouse gas and contributes to global warming. In addition to CO_2, there are several byproducts of the combustion process, like CO, NOx and Sulphur oxides, which are air pollutants.

1.2. Waste-heat driven cooling cycles

A solution proposed to overcome problems associated with conventional refrigeration cycle is using waste-heat driven cooling cycles. “Waste heat is defined as heat that is produced in a process by way of fuel combustion or chemical reaction and then dumped into the environment even though it could be still reused for some useful and economic processes” [10]. One of the best applications for waste-heat driven systems is in vehicles driven by an internal combustion engines (ICE), as a significant part of combustion energy is wasted as heat. Following is a brief introduction to few waste-heat driven cycles have been proposed so far.

1.2.1. Thermoelectric cooling

In this technique, a thermoelectric cooling system and a thermoelectric generator are needed. The thermoelectric generator is made of two different semiconductor materials that can produce electricity when they are subjected to temperature difference through a process called Seebeck effect [11]. To create a temperature difference between the two sides of the thermoelectric generator, one side of it is exposed to the hot exhaust gas of the engine, while the other side exposed to the ambient air. The efficiency of current thermoelectric generators is less than 9%. When considering the amount of available waste heat in a vehicle, about 450 W of electricity can be produced, which is not enough for a vehicle AC system [12]. The electrical power generated by thermoelectric generator should be transferred to the thermoelectric cooling system. The COP of a typical Peltier cooler is less than 0.6, which makes the overall efficiency of the thermoelectric system less than 5.4% [13]. Therefore, thermoelectric cooling cannot be a solution for mobile air conditioning systems unless the overall efficiency can be improved [14].

1.2.2. Reverse Stirling cycle

The reverse Stirling cycle (RSC) consists of two isothermal and two constant volume processes. This system is internally reversible, and its COP is similar to a Carnot cycle working at the same cold and hot source temperature [11]. However, applying this cycle to a waste heat driven refrigeration has faced many technical difficulties in mobile

applications. The other drawback of these systems is their low power density (around 1 W/kg), which makes them heavy and bulky [14].

1.2.3. Absorption cooling cycle

The absorption cooling cycle is a heat driven refrigeration cycle, which is based on absorption of a refrigerant by a transform medium. Different refrigerant and transform medium have been proposed for different applications, however, the most commonly used pairs are ammonia - water, and water - lithium bromide. Absorption cycle is very similar to vapor compression cycle, except that the compressor is replaced with an absorption mechanism. The absorber mechanism has a low pressure and high-pressure region. The desorber and condenser work in the high-pressure region and the absorber and evaporator work in the low-pressure region. In a water – lithium bromide single effect absorption chiller, water and lithium bromide work as refrigerant and absorber, respectively. Dilute solution of lithium bromide and water is heated up in generator and produced water vapor is condensed on condenser. The water then goes to the evaporator, cools it down, and evaporates. Water vapor then is mixed with concentrated lithium bromide and moves toward the generator, and this cycle repeats. Typical COP values for an absorption refrigeration cycle are 0.65-0.70 [11]. Although this heat driven cycle has been commercialized and widely used in stationary applications, two main problems have made using this cycle in mobile applications extremely challenging. First, NH_3 shows corrosive and toxic characteristics, and second, water separation can be affected significantly by the vehicle's vibrations [15,16].

1.2.4. Adsorption cooling cycle

The adsorption cooling cycle is based on the exothermic physical (or chemical) adsorption process where the molecules of adsorbate material are bound to surface of the adsorbent material by Van-der-Waal forces (or chemical bonds) [17,18]. Adsorbents are porous materials, like silica gel, zeolite, and activated carbon that can adsorb an adsorbate, such as water, methanol, ethanol or ammonia. Different working pairs used in adsorption cooling system will be discussed in the following chapter. The adsorption refrigeration cycle uses two heat sources and two heat sinks, and operates at three

temperature levels. Desorption process happens at high temperature, adsorption and condensation occur at intermediate temperature, and evaporator operates at low temperature. A schematic is shown in Figure 1-2.

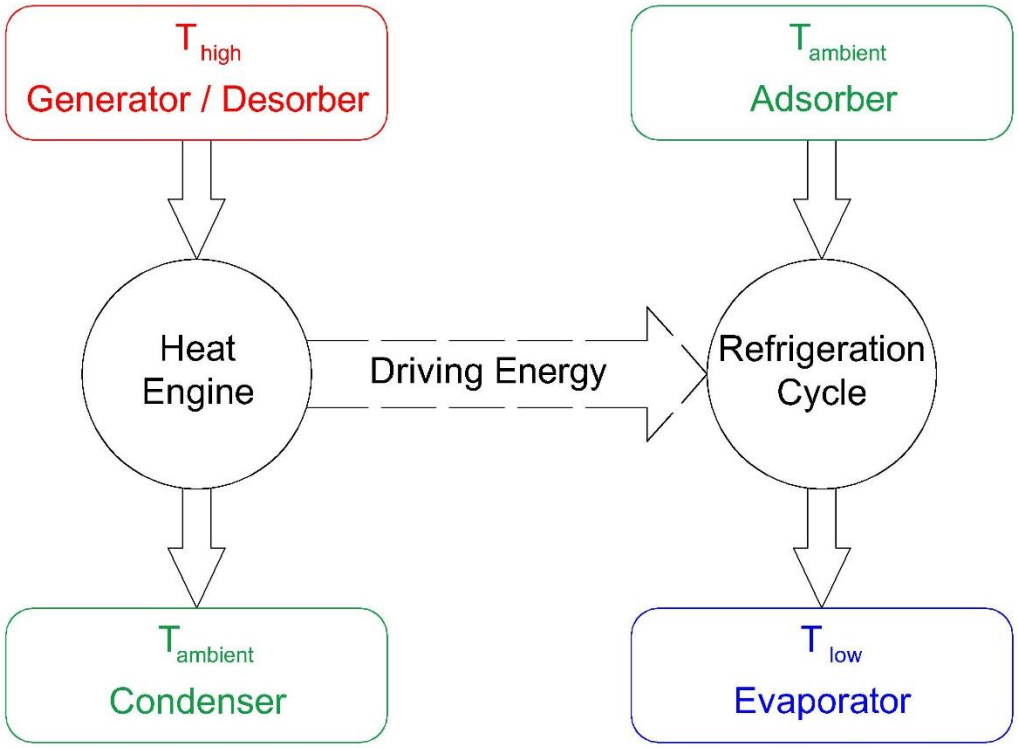

Figure 1-2 Schematic of adsorption cooling cycle

It must be mentioned that like any other technology, there are some advantages and disadvantages associated with adsorption cooling systems. The main advantages of these systems are [19]:

- They utilize low-grade thermal energy from sources like waste heat, solar, or geothermal energy.
- The only moving parts in adsorption system are the valves, which makes their maintenance costs minimal.
- Due to lack of moving parts, these systems are quiet and do not create vibrations.
- Most materials used in adsorption systems are environmental friendly and do not contain toxic or hazardous compounds.

However, the following drawbacks have prevented this technology from being competitive with VCR systems:

- Most working pairs used in ACSs operate at very low pressure (near vacuum condition), which makes these systems heavy and bulky.
- Working at low pressure can also requires high quality vacuum sealing and increases the risk of air leakage and shut down of refrigeration system
- Adsorption systems show relatively low COP values compared to other commercialized refrigeration cycles
- There are few suppliers in the market and there is no pricing regulation for this emerging technology

1.2.5. Adsorption vs. absorption

Adsorption and absorption are both refrigeration cycles that can be run by waste heat. Although absorption technology is now more developed compared to adsorption, there are more advantages associated with adsorption, which make it more promising as the next generation of refrigeration cycles.

Operational considerations

Adsorption cycle uses solid adsorbent and vaporous refrigerant, while in absorption there is a solution of a refrigerant and transform medium is in liquid shape. Therefore, absorption systems are sensitive to shocks, vibration, and position of installation, which limits the use of absorption cycle to stationary applications [17]. The other problem that most absorption chiller can face is crystallization which drops the performance significantly [20]. The other operational consideration that needs to be pointed is maintenance. There is no moving part (except valves) in adsorption cycle, while there is a pump in absorption cycle. Therefore, there is a chance that absorption cycle may need frequent maintenance and even repairs.

Performance

Although different setups and designs can have different performance and efficiency, it can be said that performance of absorption cycle is higher than adsorption

cycle on average (especially in cases with lower thermal energy quality) [21]. However, as these two cycles are waste-heat driven cycles, the efficiency is not the first parameter for the comparison and many other aspects need to be considered for the best choice of a certain application.

Complexity

Both adsorption and absorption systems are more complicated compared to vapor compression cycles, however, absorption cycle is much more complicated than adsorption cycle. The reason for that is having chemical reactions in absorption cycle, which makes it chemically complex, while the complexity of adsorption cycle is mostly due to mechanical difficulties.

1.3. Adsorption process

The process of adsorption of vapors on a solid surface was found by Scheele and Fontana separately in eighteenth century. They found that when charcoal is heated in a test tube, it desorbs gasses. These gasses were adsorbed again when the charcoal was cooled down [22]. The nature of sorption process was controversial for a long time over nineteenth century. Faraday in 1834 discussed the possibility of gasses being held on the surface of adsorbent by an electrical force and suggested that gasses could react more easily in the adsorbed state. In 1836, Berzelius observed that porous materials work better as the adsorbent. Therefore, he suggested that sorption is a phenomenon in which surface tension or another force causes the gas to be condensed on to the pores of the porous material. However, it was shown that pore condensation alone cannot explain the sorption process accurately [22]. The sorption process can be divided into two types: physical sorption (physisorption) and chemical sorption (chemisorption). In physisorption, the Vander Waal's forces are the most dominant force, and since the attraction between the vapor and adsorbent is weak, this type of adsorption can be easily reversed when heated. In chemisorption the attraction forces have the same strength as chemical bonds and therefore this type of adsorption cannot be reversed easily. Air conditioning systems work in repetitive cycles, therefore, interaction between adsorbent and adsorbate needs to be reversible in air conditioning and refrigeration applications [23]. On the other hand,

chemisorption can be used in applications where reversibility of adsorption is undesirable like material removal. A short review on properties of physisorption working pairs used in refrigeration systems is provided in Table 1-1 [23].

Table 1-1 Properties of working pairs observed in different physisorption refrigeration systems, reprinted with permission from Elsevier [23]

Working pair	Maximum uptake capacity (kg/kg)	Average heat of adsorption (kJ/kg)	Temperature range (°C)
Water-zeolite 4A	0.22	4400	30-350
Water-zeolite 5A	0.22	4180	30-350
Water-zeolite MgA	0.29	3400	60-250
Water-zeolite 13X	0.30	4400	30-350
Water-zeolite 13X	0.27	-	20-300
Water-zeolite 13X	0.27	3400	30-350
Water-zeolite 10A	0.20	4000	50-250
Water-clinoptilolite	0.12	3000	20-240
Water–mordenite	0.11	4000	30-350
Water–chabazite	0.17	3000	30-250
Water–charcoal	0.40	2320	30-250
Water–ac. alumina	0.19	2480	30-150
Water–silica gel	0.37	2560	30-150
Water–silica gel	0.20	2500	20-130
Methanol–zeolite 13X	0.20	2400	-
Methanol–zeolite 4A	0.16	2300	-
Methanol–zeolite 5A	0.17	2300	-
Methanol–ac. carbon	0.32	1400	20-140

1.4. Adsorption isotherms

Adsorption isotherms are useful curves that show the adsorption behavior for different working pairs. These graphs show the amount of adsorbed material as a function of pressure at a constant temperature. Adsorption isotherms can be fitted to empirical Freundlich model, the Langmuir model, Brunauer-Emmet-Teller (BET) model, linear

solvation energy relationships (LSERs) model, Prausnitz model, ideal adsorbed phase (IAP) model, and Langmuir–Freundlich generalized models [24]. Based on the general form of isotherms, and according to international union of pure and applied chemistry (IUPAC) adsorption materials are divided into six types and each type shows different behavior during adsorption and desorption [25]. Detail explanation of these curves is beyond the scope of this research.

1.5. Adsorption measurement methods

To establish adsorption features like isotherms, kinetics, and heat of adsorption for any working pair it is necessary to perform measurements. These features are essential in numerical modeling and can be used in the prediction of system performance. Two main measurement techniques for adsorption are volumetric, and gravimetric. In the volumetric method the adsorption isotherm is calculated using the state equation of adsorbate vapor (the relation between pressure, temperature and volume) [26]. In the gravimetric measuring method, a very small amount of adsorbent is completely dried out using vacuum and heat, and then it is exposed to adsorbate vapor at a certain pressure and temperature. As adsorption occurs, the weight of sample increases and isotherm data can be derived [27].

1.6. The adsorption cooling cycle

The cooling effect in an adsorption chiller is generated during the adsorption process while the adsorber bed is connected to the evaporator. The adsorption cycle can be explained using the Clapeyron diagram (Ln *P* vs. -1/*T*), which is illustrated in Figure 1-3. There are two main portions in an ideal adsorption cooling cycle: the heating-desorption-condensation portion and the cooling-adsorption-evaporation portion [28]. During the first period, the adsorber bed is exposed to the heat source (state A). The source heat increases the temperature of the bed to a certain temperature T_b (state B), which raises the vapor pressure of the desorbed refrigerant to the condensing pressure (P_c). Desorption is started at a constant pressure, and the desorbed refrigerant vapor is condensed in the condenser and flows to the evaporator. As the heat is being supplied to the adsorber bed,

the maximum temperature of the cycle is achieved at the end of this period (state D). During the second portion, which is cooling-adsorption-evaporation, the adsorber bed is cooled down and its temperature drops down to the lower temperature (T_f). This decrease in temperature produces a drop in pressure to the evaporation pressure (P_e). Then adsorption and evaporation take place while the adsorber bed is cooling down at the constant pressure of the evaporator until it reaches T_a, which is the starting point.

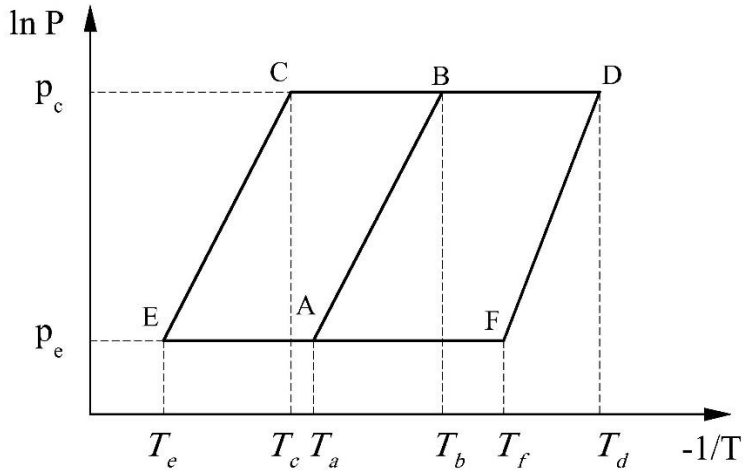

Figure 1-3 Clapeyron diagram for adsorption refrigeration cycle

From the Clapeyron diagram, it can be seen that the total heat supplied to the cycle (Q_{AD}) equals the sum of the energy used to increase the temperature of the bed and refrigerant from T_a to T_b (Q_{AB}) plus the energy used to heat the bed up to T_d and desorb the adsorber material (Q_{BD}):

$$Q_{AD} = Q_{AB} + Q_{BD} \tag{1-1}$$

$$Q_{AB} = \left\{ M_{ads} \left(c_{p,ads} + \omega_a c_{p,ref} \right) + M_{bed} c_{p,bed} \right\} \left(T_b - T_a \right) \tag{1-2}$$

$$Q_{BD} = \left\{ M_{ads} \left(c_{p,ads} + \frac{\left(\omega_a + \omega_d \right) c_{p,ref}}{2} \right) + M_{bed} c_{p,bed} \right\} \left(T_d - T_b \right) + H_{ads} M_{ads} \left(\omega_a - \omega_d \right) \tag{1-3}$$

The cooling produced in the evaporator is

$$Q_{re} = M_{ads}\left(\omega_a - \omega_d\right)H_{fg,ref} \quad \text{1-4}$$

Part of this produced cooling effect is used to cool down the bed from the condensing temperature (T_c) to evaporation temperature (T_e). This energy is

$$Q_{ce} = \left\{M_{ads}\left(\omega_a - \omega_d\right)c_{p,ref} + M_{bed}c_{p,bed}\right\}\left(T_c - T_e\right) \quad \text{1-5}$$

The COP of a refrigerant system is defined as the ratio of supplied energy to the amount of cooling at the evaporator, which is defined as

$$COP_{cyc} = \frac{Q_{re} - Q_{ce}}{Q_{AD}} \quad \text{1-6}$$

The cycle described above produces intermittent cooling. To have continuous cooling in the evaporator more than one adsorber bed is necessary. By having at least two beds, one bed can be undergoing adsorption (generating cooling) while the other bed is undergoing desorption (endothermic process).

1.7. Working pairs

The term “working pair” refers to two materials: the first one is adsorber or adsorbent material, which is the material that can adsorb another material when it is cooled down and releases it when it is heated up. The most commonly used adsorbent materials are silica gel, zeolite, and activated carbon. The second material can be adsorbed by the adsorbent and it is called the adsorbate. Adsorbate is in the liquid phase when it is adsorbed and after desorption, it changes phase into vapor. The best choice of working pair depends on many parameters such as temperature range, heat of adsorption, working pressure, etc., but the following parameters need to be addressed to select a proper working pair [29]:

- Ability to adsorb large amount of adsorbate at the temperature of the cold source.
- Ability to desorb adsorbate at the temperature of regeneration.

- Having a high heat of adsorption to release and absorb as much energy as possible.
- Showing non-corrosive behaviour to the materials in adsorber bed.
- Being widely available at reasonable price.
- Not being toxic or hazardous, especially for sensitive applications.

1.7.1. Adsorbent materials

In this section, only physical adsorption is studied. Physical adsorption is adhesion of adsorbate to the surface of the adsorbent material through Van de Walls force between the molecules. The most commonly used adsorbent materials are silica gel, zeolite, and activated carbon. A very short introduction to these materials is provided in the following.

Silica gel

Silica gel based adsorber materials have been the subject of many studies in recent years [30,31]. Silica gel is synthetic amorphous silica and it is a continuous net of colloidal silica, connected to grains of hydrated SiO_4. The array of SiO_4 in silica gel is shown in Figure 1-4 [32]. Silica Gel is highly porous material and it is a good adsorbent material with a low regeneration temperature when it is paired with water (as low as 75°C) [33]. One of the key parameters in performance assessment of silica gel is its pore distribution. Type A silica gel is a fine pore silica gel that has a large internal surface area. The average pore diameter for this type is 2.0-3.0 nm, and the surface area is 650-800 m^2/g [34]. Average pore size for type B silica gel is about 0.7 nm and its specific surface area ranges from 100 to 1000 m^2/g [34]. Silica gel is usually paired up with water in an adsorption system. The specific heat of adsorption for this pair is about 2800 kJ/kg, which is predominantly due to the heat of condensation of water [35].

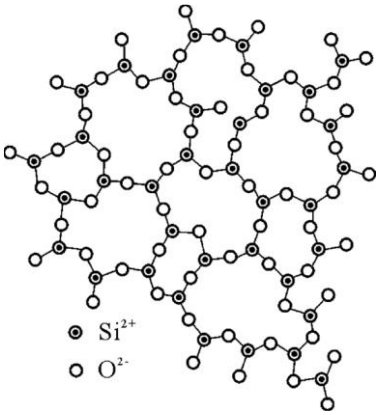

Figure 1-4 Array of SiO_4 in silica gel, reprinted with permission from Elsevier [32]

Zeolite

Zeolite is an alumina-silicate based highly porous material that is used as adsorber material. The structure of zeolite is a three-dimensional pore structure with a general chemical formula in the form of $M_{y/n}[(AlO_2)_y(SiO_2)_m]zH_2O$ where y and m are all integers, m/y is equal or larger than unity, n is the chemical valence of the positive ion of M, and z is the number of the water molecule in a crystal cell unit [32]. The arrangement of these crystals determines the type and properties of the zeolites. There are two main zeolite types that are being used in adsorption cooling: type A and type X, as illustrated in Figure 1-5 (A) and (B) respectively [32].

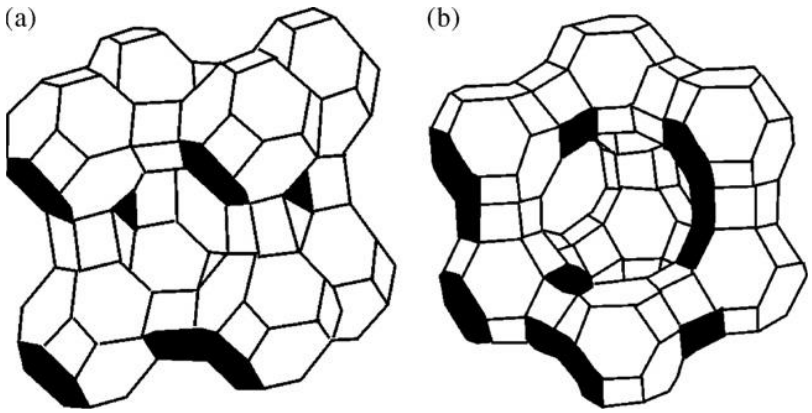

Figure 1-5 Crystal unit of zeolite (a) Type A, (b) Type X, reprinted with permission from Elsevier [32]

One of the most commonly used zeolites in adsorption cooling is 13X zeolite. The heat of adsorption for zeolite is relatively high compared to other adsorbent materials (3300-4200 kJ/kg), and high desorption temperature is required for these materials (around 200°C). Zeolite adsorbents are mostly used in designs where the heat source temperature is between 200-300°C [18].

Activated carbon

Activated carbons are popular materials in adsorption cooling systems due to their highly porous surface area. The specific surface area of activated carbon is between 500 and 1500 m^2/g [36]. Activated carbon can be found in different sizes, and in a powder, granular, and extruded form [36,37]. The structure of activated carbon is composed of irregular channels with a larger pore size at the surface and narrow pores within the grain as shown in Figure 1-6 [36–38]. The heat of adsorption of activated carbons is lower than other adsorbents. This is the result of the non-polarity of the surface of activated carbon [36]. Activated carbon can be in the form of grains and fibers. It has been shown that activated carbon fiber has more specific surface area, more uniform pore sizes, and better heat transfer performance compared to granular activated carbon [32].

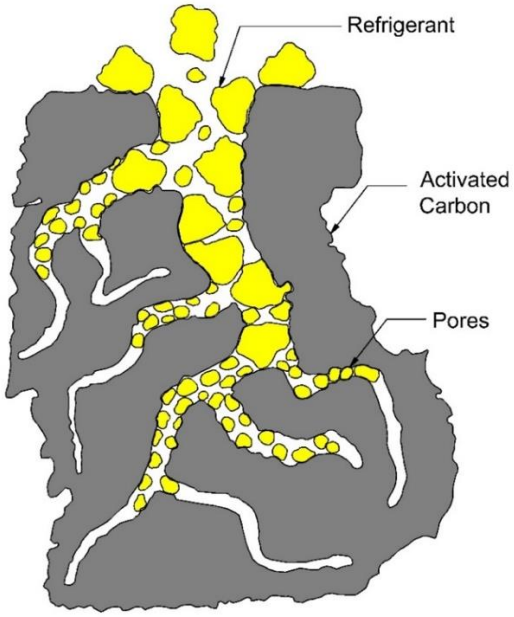

Figure 1-6 structure of activated carbon

1.7.2. Adsorbate materials

Selection of proper adsorbate/adsorbent pair depends on the application, but in general, the following characteristics are desirable for the adsorbate:

- Small size molecules so it can easily penetrate through the adsorbent pores.
- High latent heat of vaporization and high heat of adsorption.
- Thermal stability at cyclic operation conditions.
- Non-toxic, non-corrosive and non-flammable.
- Saturation pressure close to one atmosphere at the working temperature range.

Unfortunately, no refrigerant has all these properties, however, based on the application and working conditions, a suitable refrigerant can be selected. The best refrigerant is the one that meets the maximum number of the above considerations. The commonly used refrigerants in adsorption refrigeration are water, ammonia, methanol, and ethanol. Physical properties these refrigerants are shown in Table 1-2. There are some other refrigerants like hydrogen, oxygen, R134a, R22, R732, and R407 that have not been used commercially yet due to technological or financial considerations.

Table 1-2 Physical properties of common refrigerants for adsorption systems, reprinted with permission from Elsevier [32]

Refrigerant	Chemical formula	Normal boiling point (°C)	Molecular weight	Latent heat of vaporization H_{fg} (kJ/kg)	Density ρ (kg/m^3)	ρ×L (MJ/m^3)
Ammonia	NH_3	-34	17	1368	681	932
Water	H_2O	100	18	2258	958	2163
Methanol	CH_3OH	65	32	1102	791	872
Ethanol	C_2H_5OH	79	46	842	789	665

1.8. Important parameters in adsorber bed performance

One of the main components of the adsorption cooling system is the adsorber bed, which creates the refrigerant flow in refrigeration cycle. There are several parameters that affect performance of adsorber bed. Here, a short review of these parameters is provided.

Adsorbent porosity

The porosity of a porous material is defined as the ratio of void space to the total volume of the medium. It has been shown that the heat and mass transfer are influenced significantly by the porosity [39]. As the porosity increases, the specific surface area of the adsorbent increases, and since adsorption is a surface phenomenon, amount of adsorption will increase as well. However, increasing the porosity decreases the overall thermal conductivity and heat transfer rate of the adsorbent. Therefore, there is an optimum for the porosity of an adsorbent to have the maximum amount of refrigerant adsorbed. In a parametric study, Demir et al. have shown that having low porosity will increase the pressure gradient at the beginning of the adsorption process, but it soon reaches steady state conditions [39]. This is due to high rate of adsorption at the beginning of each process, which increases the refrigerant flow and pressure drop.

Pore size

Pore size is related to porosity, and porosity generally increases when pore size is increased. Higher porosity shows higher specific surface area and leads to higher adsorption performance. On the other hand, smaller pore sizes require more adsorption

isosteric energy and subsequently higher regeneration temperature. One of the main criteria for selecting the appropriate working pair is the compatibility between the pore size of the adsorbent and the molecule size of the adsorbate. If the pore size is too small for an adsorbate, the kinetics of adsorption will be reduced significantly [29].

Grain size

Grain size can affect both heat and mass transfer in an adsorber bed [40]. By decreasing the particle size, thermal contact resistance between the particles and the heat exchanger surface can be reduced. In addition, with smaller particle size, more continuity and uniformity of heat transfer is observed within the adsorber bed, as the voids between grains are reduced in number and size [41]. There are two mechanisms for mass transfer of refrigerant within adsorber bed: mass transfer within the adsorbent grains (intra-particle), and mass transfer between grains (inter-particle). The intra-particle mass transfer performance of small grains is better than that of large particles. This is because of the higher total surface area of the bulk grains for smaller particle sizes. The larger particle size has more voids between particles, and therefore, the inter-particle mass transfer performance (or permeability) is higher for large particle sizes. This is more critical when the evaporative pressure for the refrigerant is low (water, methanol, and ethanol) [42].

Adsorbent / metal mass ratio

Having more adsorbent increases the maximum adsorbed refrigerant. However, with more adsorbent packed in the adsorber bed the thermal resistance of the system increases, since the thermal conductivity of most adsorbents is very low. The solution to this problem is to put more fins in the heat exchanger with lower fin spacing. Although this solution increases the SCP of the system, it decreases the COP of the cycle, due to the heat adsorbed by the metal during desorption process [43]. Therefore, it is crucial to have an optimal fin spacing to compromise between COP and SCP.

Chapter 2. Literature Review

2.1. Introduction

This chapter starts with a historical overview of development of refrigeration and air conditioning systems. Next, different designs for adsorption cycles are introduced, and studies on the design of adsorber beds are overviewed. Finally, a literature review on numerical studies of adsorber beds is provided.

2.2. The history of different air conditioning systems

Living in comfortable conditions has always been one of the main concerns of human race and development of air conditioning systems has played a significant role in fulfilling that goal. Air conditioning in ancient times was limited to the use of man powered elementary central heating systems, and evaporative cooling methods like wind catchers [44,45]. The development of industrialized air conditioning systems started in 1902 when the first year-round air conditioning system was installed in a printing factory [46]. The use of air conditioning units in industrial applications quickly increased with General Electric designing the first room air conditioner in 1920. During last 70 years, the use of air conditioning units has increased in different applications from mobile to stationary, small scale to large scale, and with different operating conditions. However, as energy consumption and environmental effects of these systems has become an issue, research into alternative air conditioning systems has grown [46].

2.3. Different configurations of adsorption cooling systems

The adsorption and desorption processes are the main processes in an adsorption refrigeration cycle; however, different configurations of the cycle elements can result in slightly different cycles in terms of performance, temperature range, and usage. A few different adsorption-based refrigeration cycles are introduced in the following section.

2.3.1. Single bed adsorption refrigeration cycle

A simple one-bed adsorption cycle consists of four main components: an adsorber bed, an evaporator, a condenser, and an expansion valve [47]. The adsorber bed is packed (or coated) with adsorbent and will adsorb or desorb the refrigerant during the adsorption or desorption process. Flow diagrams of this cycle are shown in Figure 2-1. The operation of a single bed ACS can be divided into two part: adsorption, and desorption. During adsorption, bed is connected to the evaporator and disconnected from the condenser while being charged (Figure 2-1 (A)). During desorption, valve configuration is reversed and bed is connected to the condenser instead of the evaporator (Figure 2-1 (B)). Heat transfer fluid supplies the heat for desorption and extracts heat during the adsorption process. The problem with a single bed cycle is that the cooling effect at the evaporator is intermittent. That is why a simple two-bed cycle is introduced to provide continuous cooling.

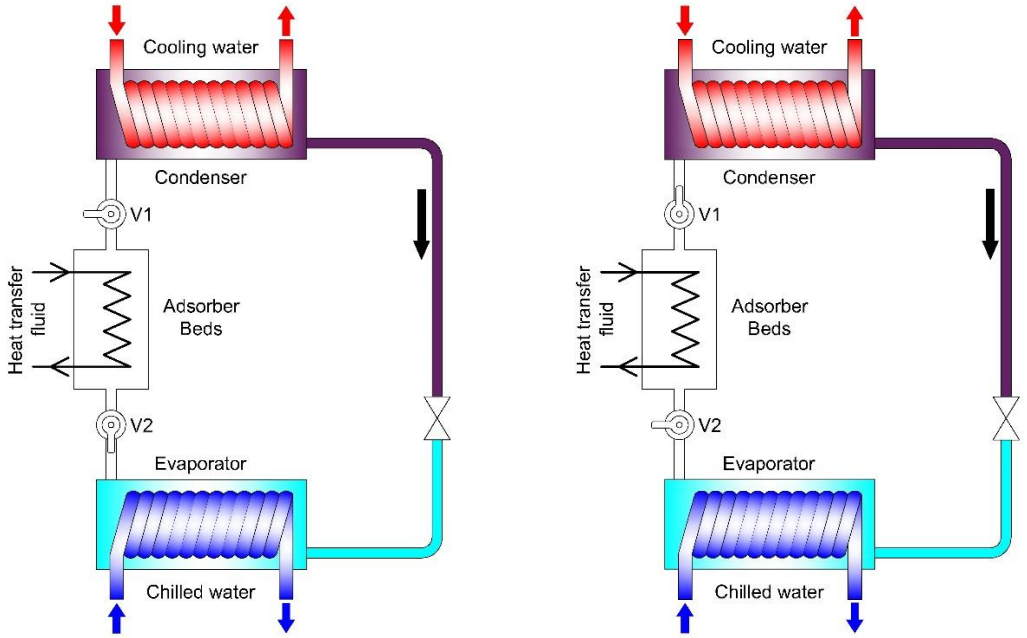

(A) (B)

Figure 2-1 Flow diagram of a single bed adsorption refrigeration cycle

2.3.2. Simple two-bed adsorption refrigeration cycle

A simple two-bed adsorption cycle consists of five main components: two adsorber beds, an evaporator, a condenser, and an expansion valve [48]. Similar to a single bed cycle, adsorber beds are packed (or coated) with adsorbent and will adsorb or desorb the refrigerant during the adsorption or desorption process. Interconnecting valves control the flow of refrigerant in the cycle as shown in Figure 2-2. The valves positions during each of the four processes of an adsorption cooling cycle are described in Table 2-1 [49,50].

Table 2-1 Two-bed cyclic operation and valve status

Process	Bed A	Bed B	V1	V2	V3	V4
Isosteric	Heating	Cooling	X	X	X	X
Isobaric	Heating	Cooling	O	X	O	X
Isosteric	Cooling	Heating	X	X	X	X
Isobaric	Cooling	Heating	X	O	X	O

X: closed O: Open

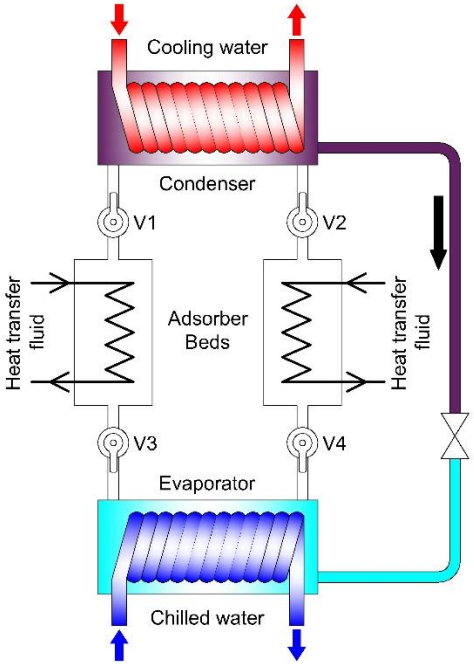

Figure 2-2 Flow diagram of simple two-bed adsorption refrigeration cycle

Heat and/or mass recovery can be added to the two-bed adsorption cycle to increase performance [51–54]. In mass recovery, the two beds are connected to each other to speed up the pressure increase in the cold bed and pressure decrease in the hot bed [55]. In heat recovery, cooling fluid first flows through the hot bed and then through the cold bed. This will reduce the required heat for regeneration and improve cycle performance [51,56]. Operating modes of a two-adsorber bed system without heat and mass recovery are shown in Figure 2-3.

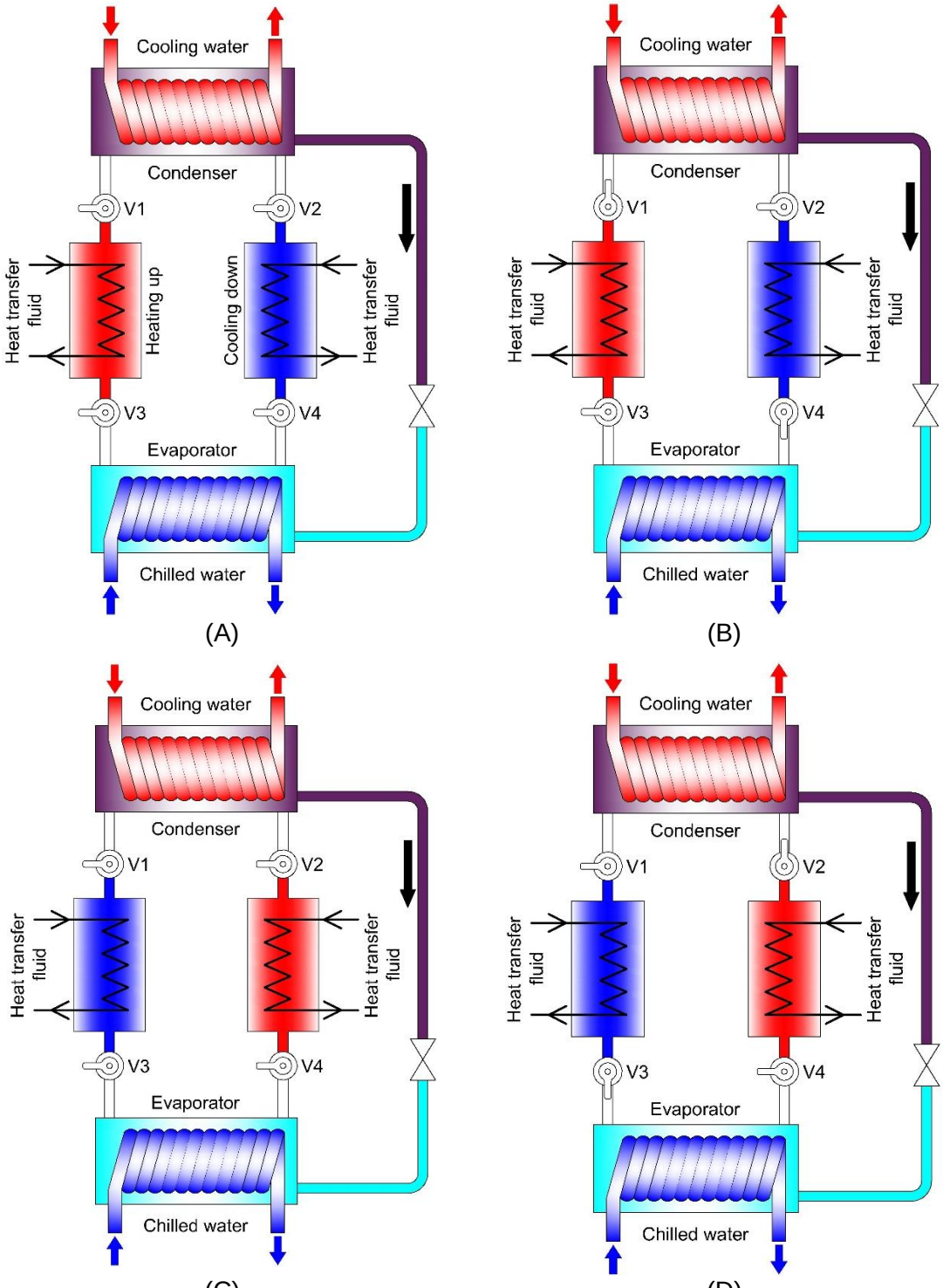

Figure 2-3 Two bed adsorption cycle operating modes; A: Isosteric cooling/heating, B: Isobaric cooling/heating, C: Isosteric cooling/heating, D: Isobaric cooling/heating

2.3.3. Integrated adsorption refrigeration cycle

An integrated adsorption cycle consists of two separate units. Each unit has its own bed, evaporator. and condenser [57]. The main advantage of this design is the elimination of the switching modes. No control system or valves are required for the flow of refrigerant in this design, which makes it more reliable [58]. However, some control valves are required to control the flow of secondary fluid to each unit. As shown in Figure 2-4, bed A is heated up with the heating fluid. At the same time, condenser A cools down the desorbed refrigerant and condense it. Simultaneously, bed B is being cooled down by cooling fluid and adsorbs the vapor refrigerant generated by evaporator B. After half a cycle the valve configuration will change to switch the hot and cold beds. The performance of an integrated adsorption cycle can be improved by using heat and/or mass recovery.

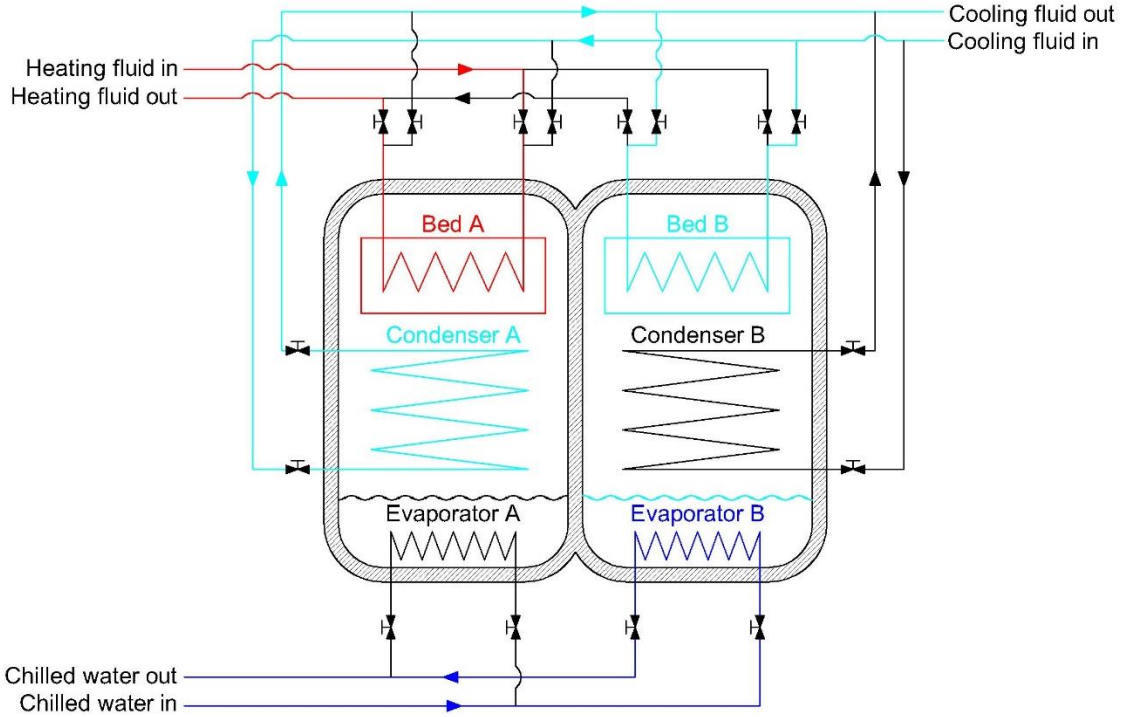

Figure 2-4 Schematic of integrated adsorption chiller

2.3.4. Compact two-bed adsorption refrigeration cycle

This cycle is very similar to a simple two-bed adsorption refrigeration cycle in operation; however, this design is much more compact compared to that. In compact ACS the evaporator, condenser, and beds share walls, which makes them lighter and less bulky. In addition, piping is not needed in this configuration and thus pressure drop between different components is minimized [38,59]. The schematic of a compact two-bed adsorption cycle is shown in Figure 2-5. This design has been commercialized with the brand name of SorTech in different cooling capacities. The final product of SorTech adsorption chiller is shown in Figure 2-6.

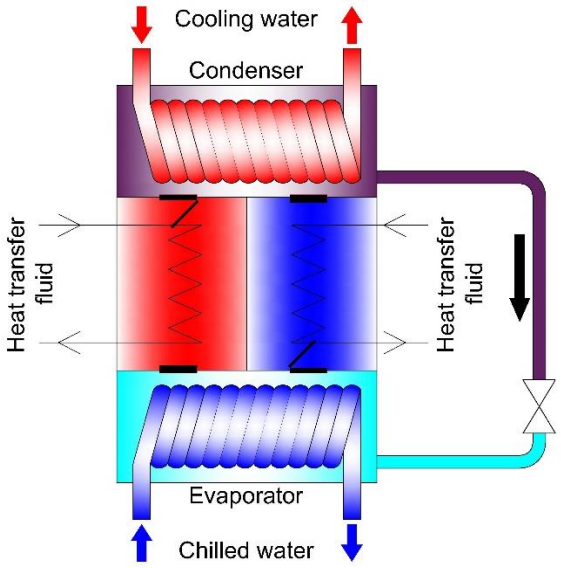

Figure 2-5 Schematics of a compact two-bed adsorption system

Figure 2-6 Commercialized compact adsorption chiller by SorTech [59]

2.3.5. Three-bed adsorption cycle

This cycle consists of three adsorber beds, a condenser, and an evaporator. The goal of this design is to have a more continuous cooling effect in the evaporator. This cycle

has 12 operating steps, and each adsorber bed goes through four operating modes: preheating, desorbing, precooling, and adsorbing [60]. The schematic of a three-bed adsorption cycle is shown in Figure 2-7. Interconnecting valves are closed during the preheating and precooling modes to change the pressure within the bed. During adsorption mode for each bed, the valves are set in a configuration which connects it to the evaporator and during desorption, the bed is connected to the condenser. The mode of each bed over a full cycle time in three-bed adsorption cycle is described in Table 2-2 [49,60]. Mass recovery can be added to three-bed adsorption cycle to increase the performance [61].

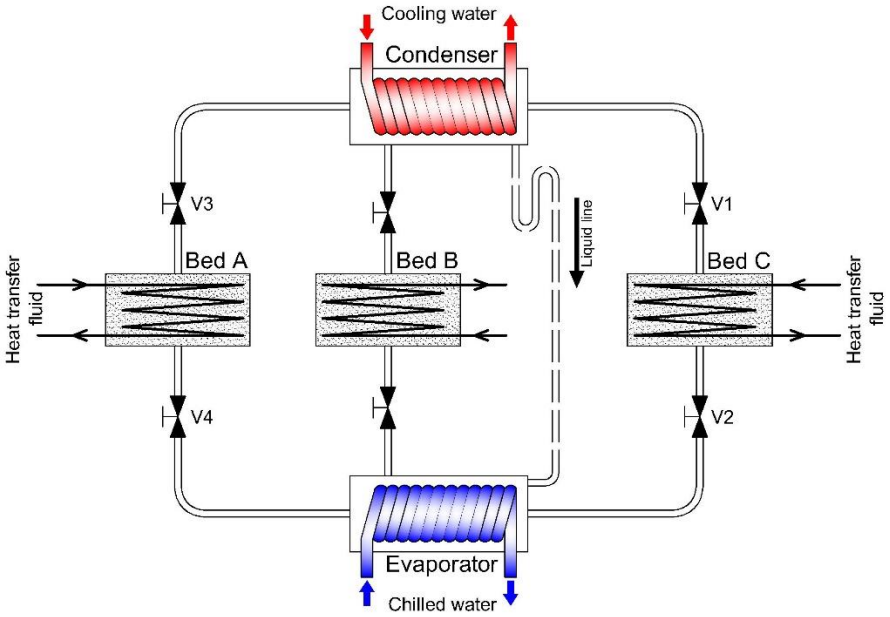

Figure 2-7 Schematic diagram for three-bed adsorption cycle

Table 2-2 Operating modes of three-bed adsorption cycle

Step	Bed A	Bed B	Bed C
Step 1	Desorption	Adsorption	Desorption
Step 2	Desorption	Adsorption	Precooling
Step 3	Desorption	Adsorption	Adsorption
Step 4	Desorption	Preheating	Adsorption
Step 5	Desorption	Desorption	Adsorption
Step 6	Precooling	Desorption	Adsorption
Step 7	Adsorption	Desorption	Adsorption
Step 8	Adsorption	Desorption	Preheating
Step 9	Adsorption	Desorption	Desorption
Step 10	Adsorption	Precooling	Desorption
Step 11	Adsorption	Adsorption	Desorption
Step 12	Preheating	Adsorption	Desorption

2.3.6. Three bed with dual evaporator adsorption refrigeration cycle

The idea of this design is to have two evaporators to enhance the performance of the cycle. The main components of this design are three adsorber beds, a condenser, a low pressure evaporator, and a high pressure evaporator [62]. Each bed experiences six different modes during a cycle: desorption, precooling, lower pressure adsorption, higher pressure adsorption, and preheating. These processes are alternatively performed in the three adsorbent beds. While an adsorber bed is connected to the condenser, it is heated up and desorbs refrigerant. After that, the bed is disconnected from the evaporator and condenser and the precooling process begins to decrease the temperature and pressure of the bed. During low pressure desorption, the bed is connected to low pressure evaporator and adsorbs refrigerant. The low-pressure evaporator with water as refrigerant works at approximately 1.0 kPa (7°C). After a certain amount of low-pressure adsorption, the bed is disconnected from low-pressure evaporator and connected to the high-pressure evaporator. The pressure in high-pressure evaporator is approximately 1.8 kPa, which increases the amount of adsorbed refrigerant. After this mode, the preheating process starts and temperature and pressure of the bed increases while all interconnecting valves are closed. The operating modes of each bed in a three-bed adsorption cycle are described in Table 2-3 [49,62]. The schematic diagram of this cycle is shown in Figure 2-8.

Table 2-3 Operating modes of three-bed dual evaporator adsorption refrigeration cycle

Step	Bed A	Bed B	Bed C
Step 1	Desorption	HP adsorption	LP adsorption
Step 2	Precooling	Preheating	LP adsorption
Step 3	LP adsorption	Desorption	HP adsorption
Step 4	LP adsorption	Precooling	Preheating
Step 5	HP adsorption	LP adsorption	Desorption
Step 6	Preheating	LP adsorption	Precooling

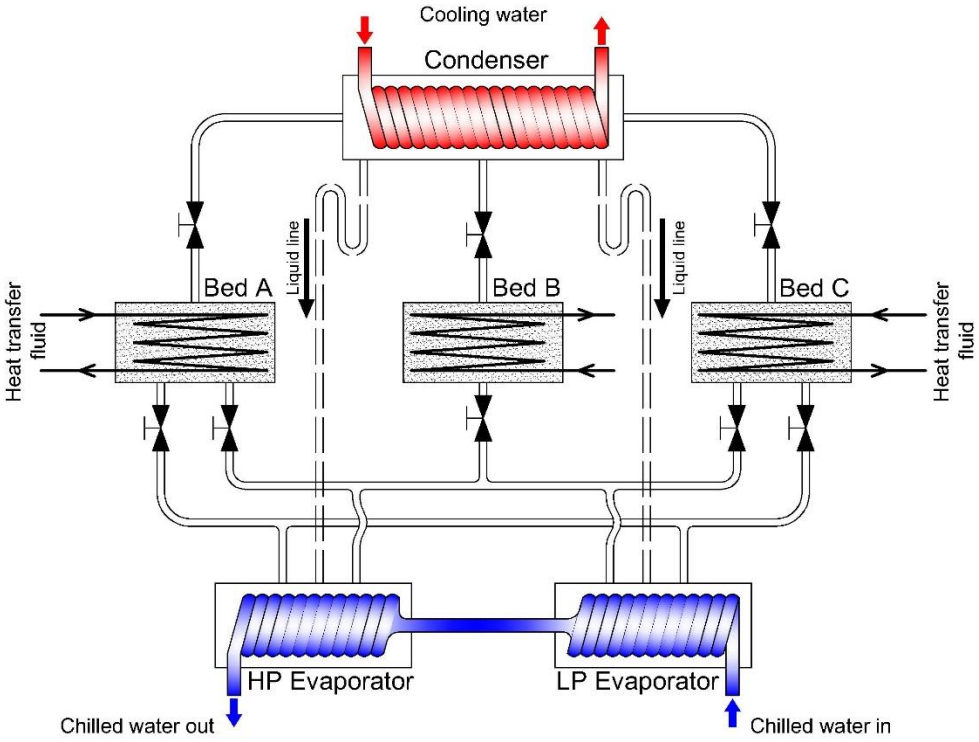

Figure 2-8 Schematic diagram of three-bed dual evaporator adsorption refrigeration cycle

2.3.7. Multi-stage adsorption refrigeration cycle

The multi-stage adsorption refrigeration cycle is used when low regeneration temperature (45-60°C) is available. The heat sink and evaporative temperatures are similar to a simple two-bed adsorption cycle, about 30°C and 7°C, respectively [63,64]. At low desorption temperatures, previously mentioned designs do not show acceptable performance [65]. In this cycle, the pressure increases from the evaporation pressure to

the condensation pressure through three different beds at the same adsorption/desorption temperatures. Figure 2-9 shows the schematic of this design. Valve positions and operating modes for a three-stage adsorption refrigeration cycle are presented in Table 2-4 [49,64].

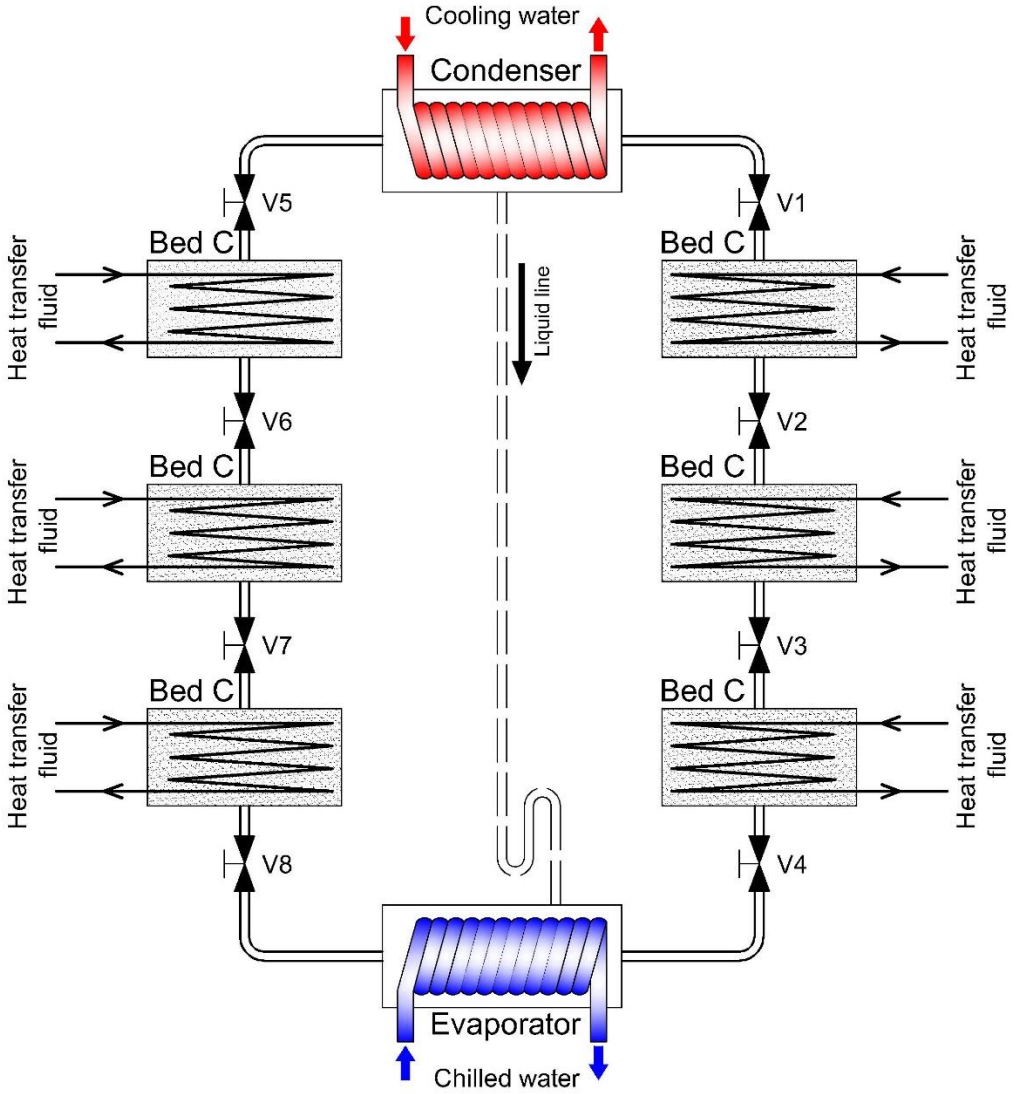

Figure 2-9 Schematic diagram of three-stage adsorption refrigeration cycle

Table 2-4 Modes and valving in a three-stage adsorption refrigeration cycle

Component	Mode A	Mode B	Mode C	Mode D
Bed 1	Precooling	Adsorption	Preheating	Desorption
Bed 2	Preheating	Desorption	Precooling	Adsorption
Bed 3	Preheating	Desorption	Precooling	Adsorption
Bed 4	Precooling	Desorption	Preheating	Desorption
Bed 5	Precooling	Adsorption	Preheating	Desorption
Bed 6	Preheating	Adsorption	Precooling	Adsorption
V1	X	O	X	X
V2	X	X	X	O
V3	X	O	X	X
V4	X	X	X	O
V5	X	X	X	O
V6	X	O	X	X
V7	X	X	X	O
V8	X	O	X	X

Each different design has its advantages and disadvantages, however, based on the desired application, certain designs can be more feasible to use. Constraints like temperature range, weight, and volume can be important for the configuration that is being chosen.

2.4. Adsorber bed design

The focus of this project is on heat and mass transfer within an adsorber bed, as these two issues have a large effect on the performance of an ACS. Heat transfer is effected by two phenomena: thermal contact resistance, and heat conduction. Thermal contact resistance can play a major role in granular adsorber beds. In this configuration, thermal contact between particles and the heat exchanger, and between particles is limited to Hertzian contact which strongly depends on the pressure applied between the two surfaces. Ideas like consolidated adsorbent and material coating are introduced to address this issue. Heat conduction is affected by thermal conductivity of heat transfer medium. Adsorbent material usually show very low thermal conductivity values, which makes these systems bulky and heavy. To overcome this issue, adding conductive material to the adsorbent is suggested [66,67]. The other problem in adsorber bed is mass

transfer. The main mass transfer mode in adsorber bed is through mass diffusion, and the low working pressure of the adsorption cycle can aggravate this issue.

Different types of heat exchangers have been studied to mitigate heat and mass transfer problems. Sharafian and Bahrami have performed a comprehensive review of different heat exchanger types used as adsorber beds and compared them with respect to COP and SCP [68]. Based on this article, nine different types of heat exchangers have been used in adsorber beds: spiral plate, shell and tube, hairpin, annulus tube, plate fin, finned tube, plate tube, simple tube, and plate heat exchanger. A summary of the existing adsorber beds used for adsorption cooling cycles is shown in Table 2-5. Ref. [68] claims that a finned tube heat exchanger has the best performance when SCP and COP are studied simultaneously. Sharafian et al. have provided a critical literature review on different cycle control strategies [69]. They reduced the total mass of their ACS by 10.5 kg by using expansion valve and control valves. Sharafian and Bahrami have provided detail data about different finned tube heat exchangers used in adsorption cooling systems. The summary of this performance analysis is shown into Table 2-5.

Table 2-5 Summary of existing studies on adsorption cooling systems, reprinted with permission from Elsevier [68]

Working pair	Adsorber bed HEX type	Cycle time [min] (ads/des)	COP	SCP	Cooling capacity	Adsorbent mass (kg)	Reference
Zeolite/water, Act. Carbon/methanol	3 hairpin HEX	164 (1)	0.65	23	1.44 kW	63.5	[125]
Consolidated Act. Carbon/ammonia	Aluminum finned tube HEX	20 (1)	0.061	33	52.8 W	0.8	[126–128]
Silica gel/methanol	Stainless steel finned tube HEX	65 (1)	-	30	23 W	0.6	[129]
Zeolite 13X/water	Stainless still cylindrical finned tube HEX	131.5 (1)	0.38	22.8	242.6 W	6.2	[130–132]
Zeolite 13X/water	Finned tube HEX	180 (2)	0.25	28.5	6 kW	140	[133,134]
Silica gel+CaCl2 / water	Stainless steel finned tube HEX	167 (0.75)	0.43	23.5	60 W	1.1	[135]
AQSOA-FAM-Z02/water	Aluminum finned tube HEX	8.6 (1)	0.27	131.5	1 kW	1.9	[136]
Silica gel/water	Finned tube HEX	34 (1)	0.43	48	9.6 kW	50	[137–139]
Coated hydrophobic Y zeolite / methanol	Stainless steel finned tube HEX	18 (1)	0.11	25	-	-	[140]
Silica gel / water	Finned tube HEX	37 (1)	0.29	35	700 W	5	[141]
Act. Carbon+CaCl2 / ammonia	Finned tube HEX	40 (1)	0.19	70.8	680 W	2.4	[142–144]
Silica gel+CaCl2 / water	Aluminum finned tube HEX	10 (1)	0.15	137	480 W	1.75	[145]
Silica gel+CaCl2 / water	Finned tube HEX	100 (1)	0.23	43	103 W	1.2	[146]
LiNO3-silica KSK / water	Stainless steel annulus tube HEX	6.4 (2.5)	0.176	318	155 W	0.350	[119,147]

Table 2-5 (cont'd) Summary of existing studies on adsorption cooling systems, reprinted with permission from Elsevier [68]

Working pair	Adsorber bed HEX type	Cycle time [min] (ads/des)	COP	SCP	Cooling capacity	Adsorbent mass	Reference
Silica gel / water	Aluminum finned tube HEX	6 (1)	0.29	158	1.9 kW	3	[148]
Consolidated graphite + zeolite 13X/water	Stainless steel finned tube HEX	72 (1)	0.28	38	213 W	2.8	[149]
Consolidated zeolite/water	Annulus tube HEX	60 (1)	0.41	97	3.14 kW	8.1	[112]
Act. Carbon / methanol	Stainless steel spiral plate HEX	100 (1)	0.2	-	-	6	[150][151]
Act. Carbon / ammonia	Plate tube HEX	40 (1)	0.37	152	15.8 kW	26	[54,152,153]
Act. Carbon / methanol	Shell and tube HEX	50 (1)	0.08	7.6	1.7 kW	56	[154][155]
Act. Carbon / ammonia	Shell and tube HEX	-	0.06	-	-	8	[156]
Consolidated zeolite/ammonia	Tube	3.3 (1) 5 (1) 10 (1)	0.19 0.18 0.22	550 350 200	42 W 27 W 16 W	0.077 0.077 0.077	[113,157–159]
Consolidated zeolite/ammonia	Plate HEX	1 (1)	0.22	800	1.6 kW	1	[160–162]
Silica gel / water	Plate HEX	4.6 (1)	0.33	118	-	36	[163]
Silica gel / water	Plate fin HEX	20 (1)	0.51	57	21.4 kW	47	[164][165]
Silica gel / water	Plate fin HEX	17.66 (1)	0.21	26.5	2.8 kW	26.4	[57,166,167]
Silica gel / water	Plate fin HEX	17 (1)	0.36	132	8.5 kW	16	[168]
Silica gel / water	Flat tube HEX with corrugated fins	12 (1)	0.45	87.8	4.3 kW	24.5	[169]
Silica gel / water	HEX	45 (1)	0.5	26	3.7 kW	35	[170]

2.5. In-situ mass measurement

Thermogravimetric analysis (TGA) is a well-known technique for measuring the adsorbate uptake of an adsorbent material. In a TGA, mass changes of few milligrams of an adsorbent are measured during adsorption or desorption under a controlled temperature and pressure. The water vapor sorption isotherms of FAM-Z02 measured by a TGA can be found in Refs. [70–73]. The nominal adsorption and desorption temperatures of a waste heat-driven FAM-Z02 ACS reported in the open literature were 30°C and 90°C. TGA measurements showed that the equilibrium water uptakes of FAM-Z02 at 30°C and 90°C were 0.33 and 0.023 kg/kg with the water vapor source temperature maintained constant at 20°C [72]. Therefore, the equilibrium water uptake difference of FAM-Z02 under these operating conditions was 0.307 kg/kg. In a real application, however, adsorption and desorption occur under large pressure jumps and non-isothermal conditions, making the operating conditions far from the ideal found in a TGA.

Adsorbate uptake capability of an adsorbent material packed in an adsorber bed may be further reduced by the adsorber bed design, interparticle mass transfer resistance, and pressure drop within the adsorber bed, as well as effects from other components of the ACS, e.g. condenser and evaporator. A metallic wire mesh or perforated sheet is necessary for holding loose adsorbent grains inside the adsorber bed, which contributes to the pressure drop and mass transfer resistance. More importantly, an ACS is a dynamic system and, as a result of adsorption and desorption within short cycle times (less than 30 min), the adsorbate uptake of an adsorbent material does not reach the equilibrium value measured by a TGA. Due to these geometrical and operational constrains, the adsorbate uptake capability of an adsorbent material reduces in the short periods of adsorption and desorption processes. To quantify these effects and measure the adsorbate uptake rate of adsorbent materials in conditions close to reality than in a TGA, a variety of experiments have been designed, as summarized in Table 2-6.

Table 2-6 In-situ adsorbate uptake rate measurements of different adsorbent materials in a large-scale test bed, reprinted with permission from Elsevier [74].

Ref.	Adsorbent-adsorbate pair	Adsorbent mass	Purpose
Dawoud and Aristov [75]	Mesoporous silica gel-water Alumina-water Silica gel + $CaCl_2$ (SWS-1L)-water Alumina + $CaCl_2$ (SWS-1A)-water	3 g	Measuring the kinetics of water sorption of loose adsorbent grains under real ACS operating conditions
Aristov et al. [76,77]	Silica gel + $CaCl_2$ (SWS-1L)-water	0.022 - 0.025 g	Effects of grain size (0.7-2.8 mm) and temperature (33-69°C) on the kinetics of water sorption of SWS-1L under real ACS operating conditions
Dawoud [70]	FAM-Z02-water	0.150 g	Effects of grain size (0.7-2.6 mm) on water sorption rate of FAM-Z02 under real ACS operating conditions
Dawoud et al. [78]	Consolidated zeolite-water	3 g	Measuring the kinetics of water sorption of consolidated zeolite layer with 0.7 mm thickness on an aluminum substrate under real ACS operating conditions
Glaznev and Aristov [40,79,80]	Silica gel + $CaCl_2$ (SWS-1L)-water RD silica gel-water	0.420 - 0.425 g	Effects of residual air on water sorption rate of adsorbents under real ACS operating conditions
Glaznev et al. [81]	FAM-Z02-water		
Storch et al. [82]	Zeolite 13X-water	180 g	Effects of 3500 adsorption / desorption cycles on the equilibrium water uptake of zeolite 13X
Schnabel et al. [83]	Coated zeolite A-water	0.170 g	Measuring water uptake rate of zeolite coated directly on a metallic substrate
	Coated zeolite X-water	1.030 g	

Riffel et al. [84]	Silica gel-water Zeolite water	1.051 kg 1.093 kg	Measuring water uptake rate of two different adsorbent materials packed in a finned tube heat exchanger under real ACS operating conditions
Solmuş et al. [85]	Natural zeolite-water	1.667 g	Measuring equilibrium water uptake of zeolite packed in an adsorber bed
Ovoshchnikov et al. [86]	Silica gel + $CaCl_2$ (SWS-1L)-water	-	Measuring water uptake rate of SWS-1L to find different water diffusion mechanism inside SWS-1L
Askalany et al. [87]	Activated carbon-R134a	-	Measuring equilibrium R134a uptake of granular activated carbon
Aristov et al. [88] Aristov [89] Chakraborty et al. [90]	RD silica gel-water	-	Effects of adsorbent grain size and number of adsorbent layers on its water uptake rate under large temperature jumps
Dawoud [91]	FAM-Z02-water	204 g 1.5-2.53 kg	Calculating the kinetics of water uptake of FAM-Z02 indirectly by using the performance analysis of an adsorption heat pump
Gordeeva et al. [92]	LiBr + silica gel-ethanol	0.300 g 56-76 g	Measuring in-situ ethanol uptake rate of loose LiBr+silica gel grains packed in finned tube heat exchangers with different length/height ratios
Santamaria et al. [93]	FAM-Z02-water	72-90 g	Effect of heat exchanger geometry, adsorbent grain size and heat transfer fluid flow rate on in-situ water uptake rate measurement of FAM-Z02

Frazzica et al. [94]	SAPO 34 + bentonite clay + carbon fiber-water	0.26-0.85 g	Measuring the water uptake rate of the composite adsorbent coated on a metallic plate with different thicknesses
Sapienza et al. [95]	SAPO 34-water	4.49-33.13 g	Effects of adsorbent grain size and number of adsorbent layers on in-situ water uptake rate measurement of SAPO 34 under real ACS operating conditions
Gordeeva and Aristov [96]	Activated carbon ACM-35.4-methanol	0.5 g	Effects of 0.8-4.0 mm adsorbents and number of adsorbent layers on water uptake rate of activated carbon ACM-35.4
Freni et al. [97]	Coated SAPO 34-water	84 g	Measuring in-situ water uptake rate of SAPO 34 with 0.1 mm thickness coated on an aluminum heat exchanger under real ACS operating conditions

The main goal of these studies tabulated in Table 2-6 was to find the effects of large-scale masses (> 1 mg) of different adsorbent materials with different grain sizes and number of adsorbent layers on their in-situ adsorbate uptake rate. Riffel et al. [84], Dawoud [91], Gordeeva et al. [92] and Santamaria et al. [93] also studied the effects of different adsorber bed designs on the adsorbate uptake rate of adsorbent materials. Riffel et al. [84] measured the water uptake rate of silica gel and zeolite packed in a finned tube heat exchanger for adsorption times of less than 3 min. They have mentioned that the scale had to be calibrated for each set of experiments because of the flexible tubes and different heat exchangers. However, they had not noted the effects of the density change of the heat transfer fluid during adsorption and desorption on the adsorber bed mass measurements. Dawoud [91] measured the water uptake rate of FAM-Z02 indirectly from the performance analysis of an adsorption heat pump. Using this method can be misleading because of the thermal masses of condenser and evaporator. For example, the thermal mass of an evaporator delays the heat transfer from the chilled water to the adsorbate and calculating the adsorbate uptake of an adsorbent material from the chilled

water cooling power results in underestimating the water uptake. To minimize such errors, therefore, in-situ adsorbate uptake rate measurements are preferred. Santamaria et al. [93] calculated the performance of an ACS by measuring the water uptake of FAM-Z02 with 72-90 g mass. Their measurements showed 6-8 times higher values than what they found in their large-scale tests because of mass transfer resistances between particles and the metal mesh wrapped around the adsorber bed, and the designs of the condenser and evaporator of the ACS [93].

2.6. Numerical modeling of an adsorption refrigeration cycle

Numerical studies in the field of adsorption cooling systems can be divided into two main groups: thermodynamic cycle modeling, and computational fluid dynamics (CFD) modeling. In the first group, numerical tools are employed to solve the governing ordinary differential equations (ODEs) or partial differential equations (PDEs) of the ACS. In this approach, each component of the ACS behaves as a lumped body, and the details of adsorption/desorption processes are not taken into account. Lumped-body models can be categorized into quasi-steady state models, dynamic models with perfect condenser and evaporator models, and fully dynamic models. Further information about thermodynamic modeling of adsorption refrigeration cycle is provided in [98]. In the latter group, the spatial dimensions of ACS components are included in the modeling and PDEs are solved using CFD techniques. In the field of ACS, CFD modeling is mostly used to simulate the adsorption/desorption processes inside the adsorber beds. CFD models, once validated, can be used in parametric studies to investigate the effects of different properties (thermal conductivities, permeability, specific heat, etc.) and working conditions (temperature ranges, working pressure, cycle time, etc.). Numerical modeling can also help to predict the performance of new designs. Several CFD models of adsorber beds are available in the literature, however, a comprehensive model that takes into account all the phenomena, like thermal contact resistance and temperature dependent properties at the same time, is missing. A comprehensive literature review of available CFD models and their geometry is provided in Table 2-7.

Table 2-7 CFD studies on adsorption cooling systems

Ref.	Year	Working pair	Geometry and model	Assumptions
[99]	1995	Zeolite 13X / Water Zeolite 13X / Ammonia	1D axial heat and mass transfer in cylindrical coordinate	1. Identical and uniformly distributed particles 2. Local thermal equilibrium between solid and gaseous phases 3. Ideal gas behavior for the gaseous phase 4. Negligible mass dispersion of gaseous phase 5. Constant specific heats, heat of adsorption and viscosity for materials

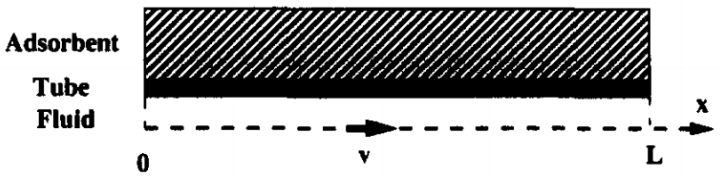

Reprinted with permission from Elsevier [99]

[100]	1996	Zeolite NaX / water Activated carbon AX21 / Ammonia	1D axial heat and mass transfer in cylindrical coordinate	1. Uniformly sized particles and isotropic properties 2. Local equilibrium between solid and gaseous phase, for heat and mass transfer 3. Ideal gas behavior for gaseous phase 4. Darcy law for velocity calculations 5. Constant thermophysical properties for materials 6. Negligible thermal energy induced by gas compression 7. No heat loss in the circulating fluid loop

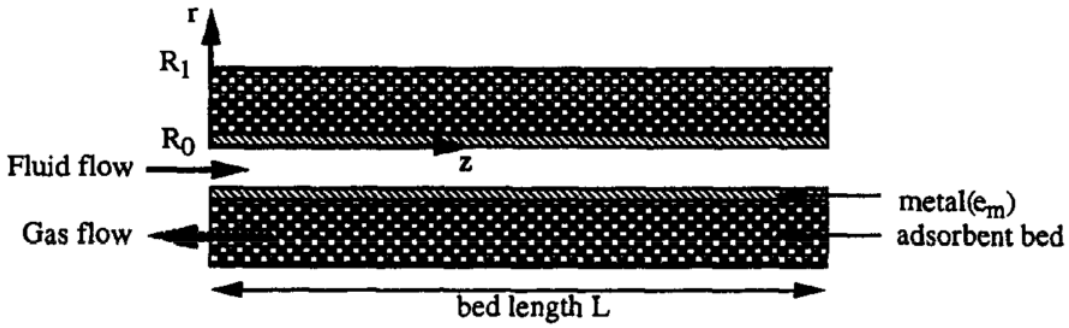

Reprinted with permission from Elsevier [100]

[101]	2000	Zeolite 13X / Water	1D heat transfer in metal tube, 2D heat transfer in fins, 3D heat and mass transfer in adsorbent	1. Liquid phase for adsorbed phase and ideal gas behavior for vaporous adsorbate 2. Constant specific heat and density for the adsorbate 3. Uniformly sized particles and isotropic properties 4. Ideal evaporator and condenser with infinite heat transfer coefficient

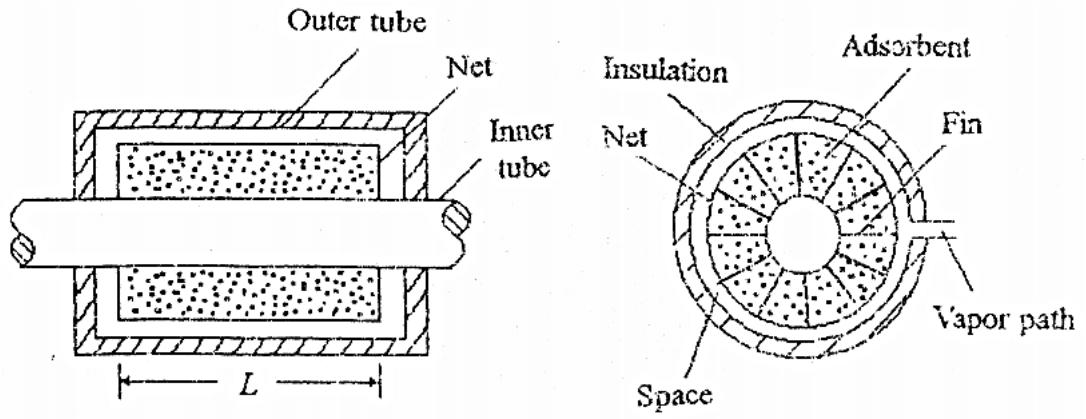

Reprinted with permission from Elsevier [101]

[102]	2002	Consolidated zeolite 4A / water	1D heat transfer in HTF*, 2D heat and mass transfer in adsorbent	1. Uniformly sized particles and isotropic properties 2. Thermal equilibrium between solid and vapor phase 3. Ideal gas model for vaporous adsorbate 4. Constant thermophysical properties for metal and vaporous adsorbate 5. Temperature dependent properties for the thermal vector fluid and adsorbent 6. No heat loss

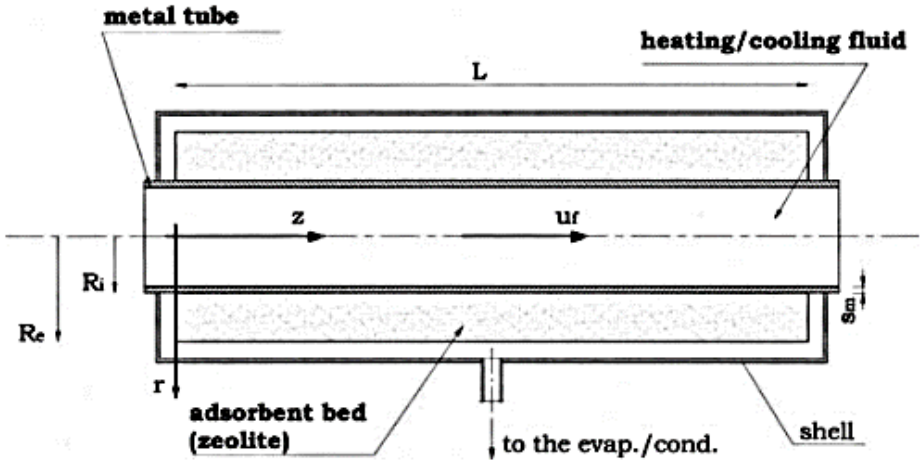

Reprinted with permission from Elsevier [102]

[103]	2002	Coated zeolite / water	1D radial heat and mass transfer in cylindrical coordinate	1. Non-uniform temperature and pressure within adsorber bed 2. Equivalent thermal conductivity, equivalent specific heat and sorption enthalpy as functions of pressure and temperature

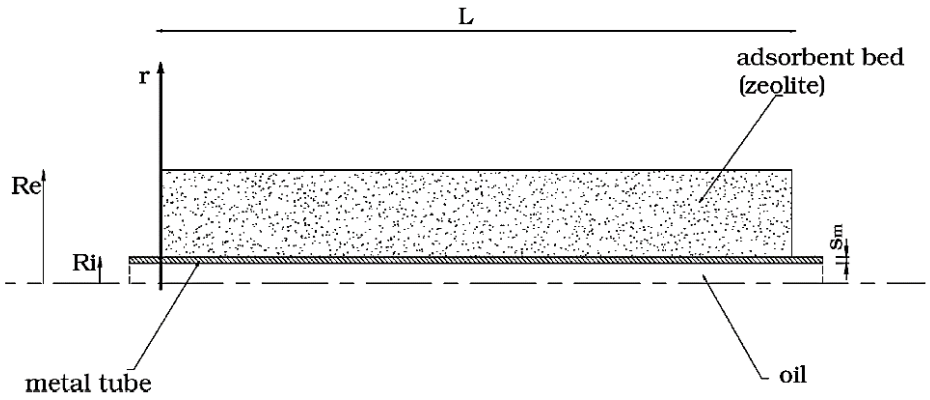

Reprinted with permission from Elsevier [103]

[104]	2004	Zeolite NaX / water	2D axial and radial heat and mass transfer in cylindrical coordinate	1. Liquid phase for adsorbed phase and ideal gas behavior for vaporous adsorbate 2. Uniformly sized particles and isotropic properties 3. Constant thermo-physical properties for heat transfer fluid, metal, and adsorbate (except density) 4. Zero heat loss 5. Neglected thermal contact resistant 6. Constant pressure and temperature in the condenser

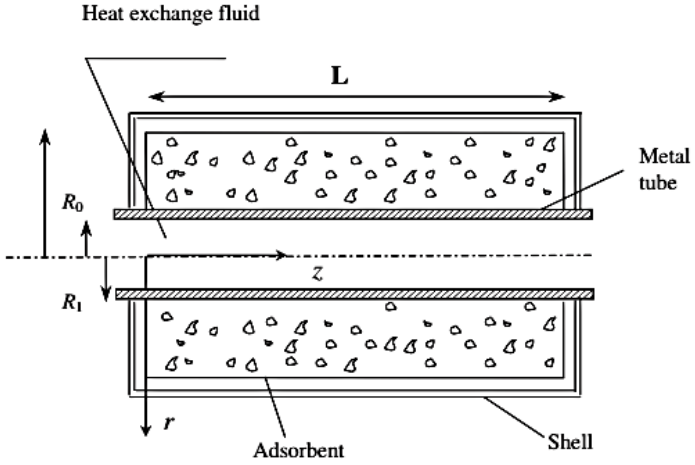

Reprinted with permission from Elsevier [104]

[105]	2004	Zeolite 13X / Water	2D cylindrical heat and mass transfer	1. Liquid phase for adsorbed phase and ideal gas behavior for vaporous adsorbate 2. Uniformly sized particles and isotropic properties 3. Constant thermophysical properties for heat transfer fluid, metal, and adsorbate (except density) 4. No heat loss 5. No TCR between adsorbent and heat transfer surfaces

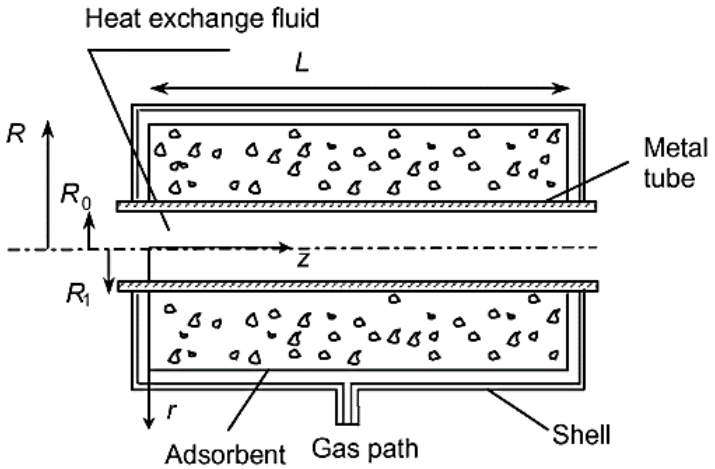

Reprinted with permission from Elsevier [105]

[106]	2008	Zeolite NaX / Water	2D cylindrical heat and mass transfer	1. Liquid phase for adsorbed phase and ideal gas behavior for vaporous adsorbate 2. Uniformly sized particles and isotropic properties 3. Constant thermophysical properties for heat transfer fluid, metal, and adsorbate (except density) 4. No heat loss 5. No TCR** between adsorbent and heat transfer surfaces 6. Constant pressure and temperature in the condenser

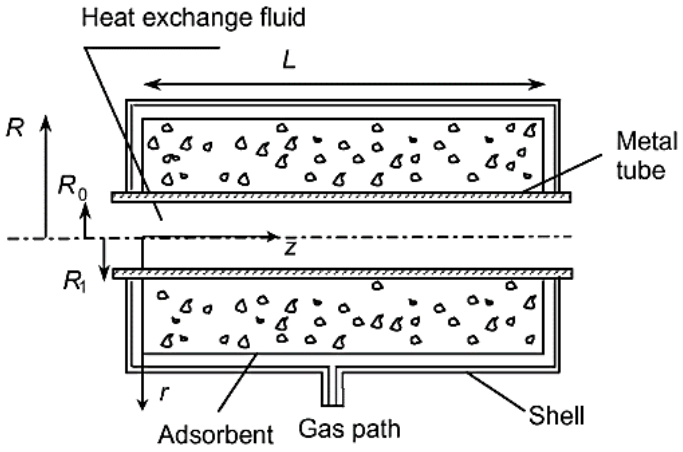

Reprinted with permission from Elsevier [106]

[84]	2010	Silica gel / water Zeolite / water	2D (radial and tangential) heat and mass transfer in cylindrical coordinate	1. Negligible convection and pressure drop in adsorbent 2. No heat loss 3. Uniformly sized particles and isotropic properties 4. Ideal gas behavior for adsorbate 5. Temperature dependent properties

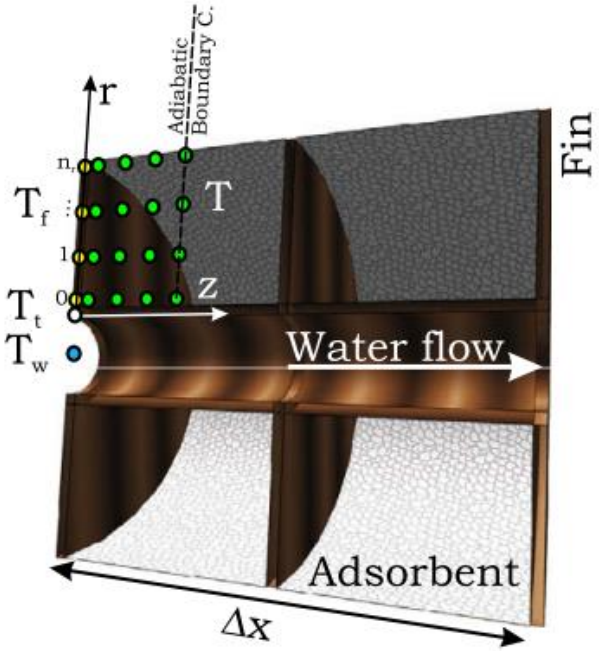

Reprinted with permission from Elsevier [84]

[107]	2011	Silica gel / water	2D (radial and tangential) heat and mass transfer in cylindrical coordinate	1. Uniformly sized particles and isotropic properties 2. Thermal equilibrium between solid and fluid phase 3. Negligible contact resistance 4. Temperature independent thermal conductivities, specific heat capacities, and viscosity

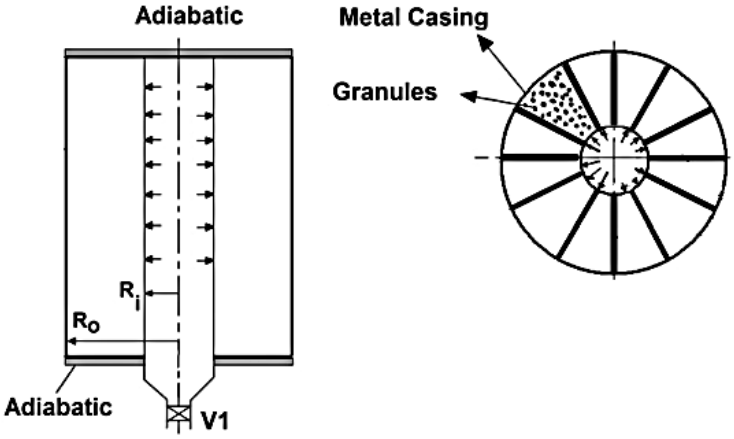

Reprinted with permission from Elsevier [107]

[108]	2012	Silica gel / water	1D heat transfer	1. Uniformly sized particles and isotropic properties 2. Ideal gas behavior for adsorbate 3. Negligible radiative heat transfer, viscous dissipation, and work done by pressure changes 4. Temperature independent thermal conductivities, specific heat capacities, and viscosity 5. Negligible thermal resistance in the wall of tube

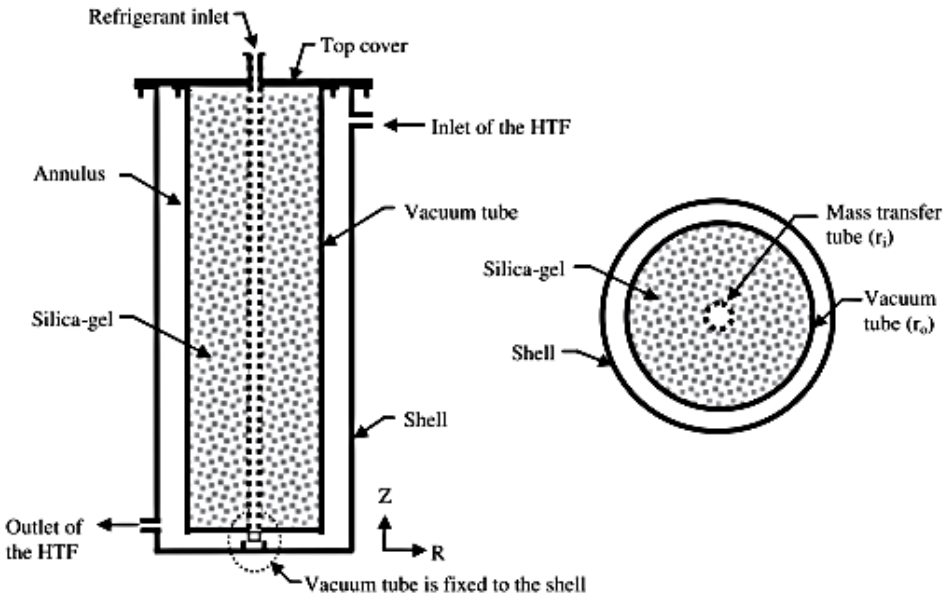

Reprinted with permission from Elsevier [108]

[109]	2012	Silica gel / Water	2D (radial and axial) heat and mass transfer in cylindrical coordinate	1. Liquid phase for adsorbed phase and ideal gas behavior for vaporous adsorbate 2. Uniformly sized and identical particles 3. Local thermal equilibrium between adsorbent and vaporous phase 4. Constant thermo-physical properties for materials, except density of the vaporous adsorbate 5. No thermal contact resistance 6. Spatially constant thermodynamic pressure inside chamber 7. Negligible heat losses through chamber walls

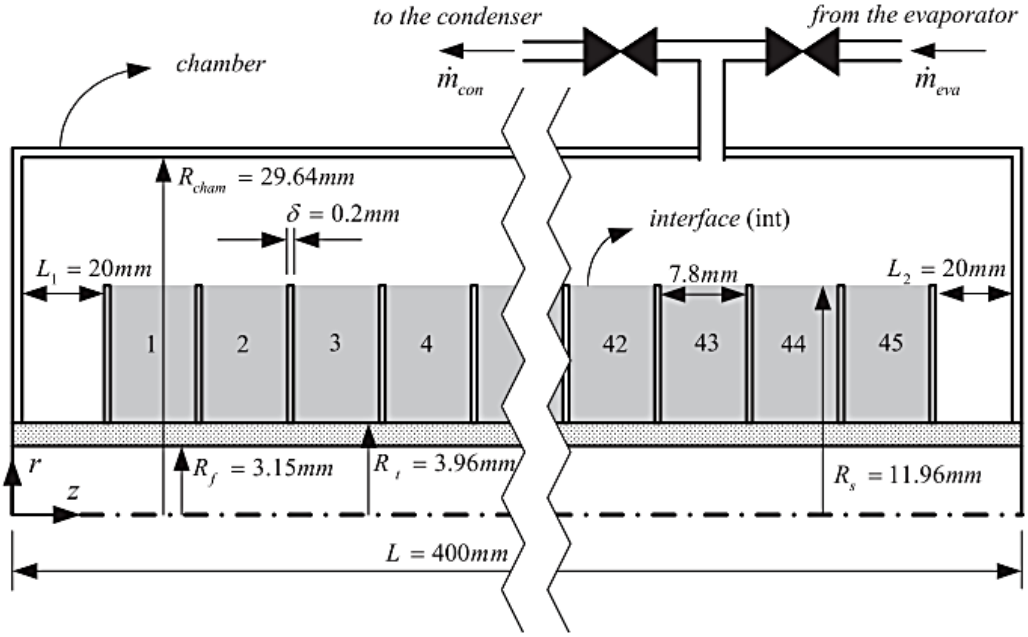

Reprinted with permission from Elsevier [109]

[110]	2012	SWS-1L / Water	3D non equilibrium heat and mass transfer	1. Spherical particles with uniform size and identical properties 2. No heat loss through wall chambers 3. Liquid phase and ideal gas behavior for adsorbed phase and refrigerant vapor respectively 4. Constant thermophysical properties for materials, except density of the vapor 5. Ideal condenser and evaporator with constant temperature during isobaric phases

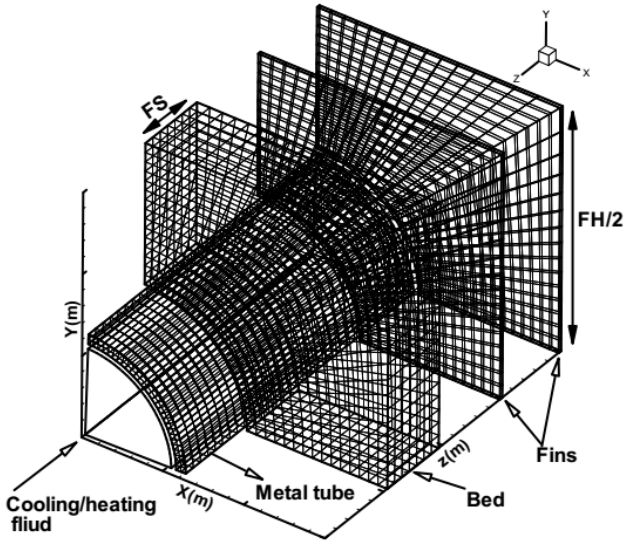

Reprinted with permission from Elsevier [110]

[111]	2013	Ethanol activated carbon	1D radial heat transfer in cylindrical coordinate	1. Negligible thermal resistance at the walls 2. Negligible heat transfer rate from outer wall of the bed 3. Constant thermophysical properties of the materials 4. Uniform pressure inside the bed

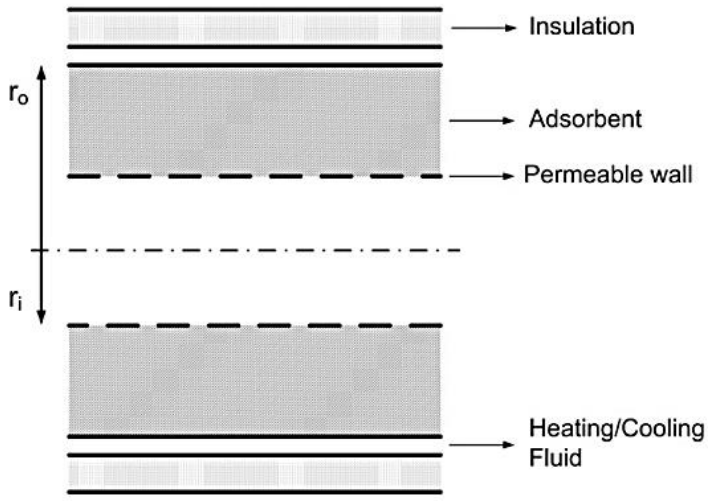

Reprinted with permission from Elsevier [111]

Chapter 3. Experimental Test

This chapter is reprinted version of one of my publications in Elsevier publishing company. The text and figures in this chapter are reprinted from Applied Thermal Engineering, Volume 98, Amir Sharafian, Seyyed Mahdi Nemati Mehr, Wendell Huttema, Majid Bahrami, Effects of different adsorber bed designs on in-situ water uptake rate measurements of AQSOA FAM-Z02 for vehicle air conditioning applications, Pages 568-574, 2016, with permission from Elsevier.

3.1. Introduction

Although adsorption cooling systems are promising technology for future of air conditioning, current ACS are limited in their usefulness for commercial vehicle applications, specifically light-duty vehicles, because of their bulkiness and heavy weight. The main challenges facing this technology are low coefficient of performance (COP = cooling energy / input energy) and low specific cooling power (SCP = cooling energy / (adsorbent mass × cycle time)), which originate from the low thermal conductivity of adsorbent particles (~0.1 to 0.4 W/m·K) [112–114] and the low mass diffusivity of adsorbent-adsorbate pairs (~10^{-8} to 10^{-14} m^2/s) [113,115].

To overcome these limitations, different composite adsorbent materials with high thermal conductivity and high adsorbate uptake have been developed [34,116]. AQSOA FAM-Z02 is one of these synthetic materials developed for air conditioning applications by Mitsubishi Chemical Ltd. [117]. FAM-Z02 showed high durability of 60,000 cycles with no reduction in its uptake capacity and it has a low desorption temperature of 75-95°C [117] making it a good candidate for ACS applications. In a thermogravimetric analyzer (TGA), mass changes of few milligrams of an adsorbent are measured during adsorption or desorption under a controlled temperature and pressure. The water vapor sorption isotherms of FAM-Z02 measured by a TGA can be found in Refs. [70–73]. The nominal adsorption and desorption temperatures of a waste heat-driven FAM-Z02 ACS were reported as 30°C and 90°C, respectively. TGA measurements showed that the equilibrium water uptake of FAM-Z02 at 30°C was 0.33 kg/kg and at 90°C was 0.023 kg/kg with the

water source temperature maintained constant at 20°C [72]. Therefore, the equilibrium water uptake difference of FAM-Z02 under these operating conditions was 0.307 kg/kg. In a real applications, however, adsorption and desorption occur under large pressure jumps and non-isothermal conditions, making the operating conditions far from the ideal found in a TGA.

3.1. Experimental test bed

To measure the mass exchange of an adsorbent packed in an adsorber bed under adsorption or desorption, an experimental test setup was designed and built as shown in Figure 3-1. The adsorber bed was placed on a scale (Setra, Supper II) with ±1 g accuracy and connected to cooling and heating fluid temperature control systems, TCS_{CF} and TCS_{HF}, for intermittent adsorption and desorption. A water source at a constant temperature, shown in Figure 3-1, was connected to the adsorber bed using a vacuum rated flexible hose. This water source served as an evaporator and a condenser during adsorption and desorption, respectively.

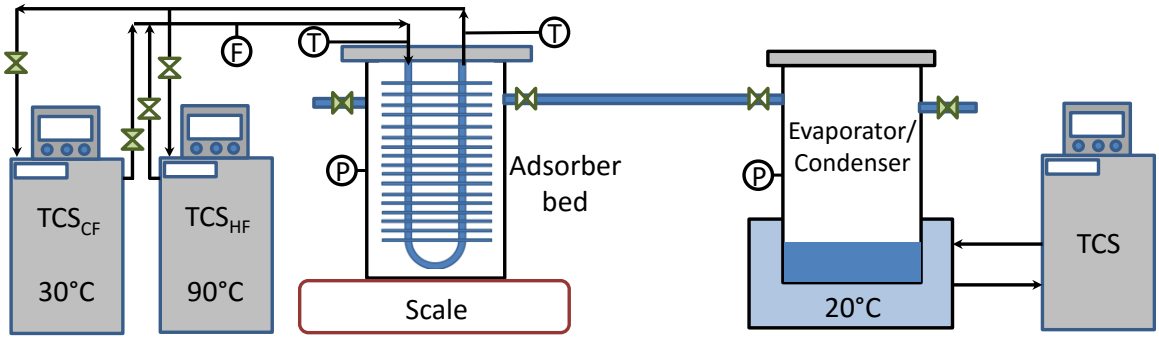

Figure 3-1 Schematic of the experimental test setup.

To test the effects of different adsorber bed designs, two heat exchangers with different geometries (No. 1 in Figure 3-2 (a) and Figure 3-2 (b)) were connected to the evaporator/condenser container (No. 3 in Figure 3-2a and Figure 3-2b). The first heat exchanger (called Design I) was built based on the results of Sharafian et al. [47] and was placed inside a vacuum chamber, as shown in Figure 3-2a. The second adsorber bed (called Design II), which was an engine oil cooler manufactured by Hayden Automotive (model #1268), was placed in a custom-built vacuum chamber, as shown in Figure 3-2b.

The fin spacing and heat transfer surface area of heat exchangers in Designs I and II were 8.47 mm and 0.235 m^2, and 2.54 mm and 2.8 m^2, respectively. To measure the temperature and pressure of the adsorber beds and evaporator/condenser container, thermocouples type T (Omega, model #5SRTC-TT-T-36-36) with accuracy of 0.75% of reading, and two pressure transducers (Omega, model #PX309-005AI) with 0-34.5 kPa absolute pressure range and ±0.4 kPa accuracy were installed. A positive displacement flow meter (FLOMEC, Model # OM015S001-222) with accuracy of 0.5% of reading was installed on the adsorber bed to measure the heating and cooling fluid flow rates. Table 3-1shows further details on the adsorber bed geometries and operating conditions. It can be seen in Table 3-1 that the amount of adsorbent material inside the adsorber bed of Design II is more than that of Design I. To supply enough water vapor during adsorption process, two evaporators of the same type were connected to the adsorber bed of Design II, as shown in Figure 3-2b.

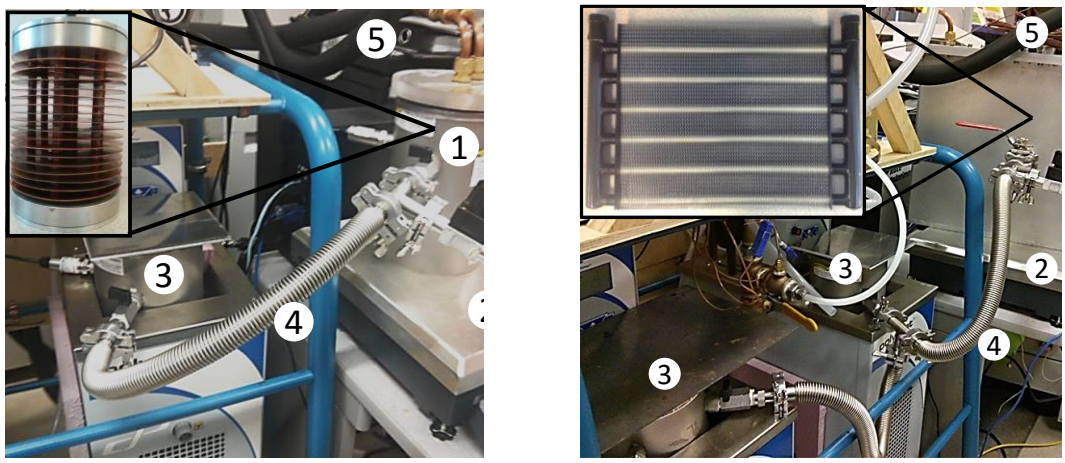

(a) (b)

Figure 3-2. Details of the experimental setup for (a) Design I and (b) Design II. 1: adsorber bed, 2: scale, 3: evaporator/condenser, 4: flexible hose, and 5: heating/cooling fluid ports

Table 3-1 Specifications of adsorber beds and operating conditions.

Parameter	Design I	Design II
Working pairs	AQSOA FAM-Z02/water	
Adsorbent particles diameter (m)	0.002	
Mass of adsorbent (kg)	0.62	1.50
Metal mass of adsorber bed (kg)	2.80	2.87
Adsorber bed heat transfer surface area, A_{bed}, (m^2)	0.235	2.80
Fin spacing (mm)	8.47 (3 fpi)	2.54 (10 fpi)
Fin dimensions	12.7 cm (5") diameter	43.18×30.48 cm (17"×12")
Heating fluid mass flow rate to adsorber bed (kg/s)	0.058 (4.1 L/min of silicone oil)	
Cooling fluid mass flow rate to adsorber bed (kg/s)	0.062 (4.1 L/min of silicone oil)	
Heat capacity of silicone oil (kJ/kgK)	1.8	
Heating fluid inlet temperature (°C)	90	
Cooling fluid inlet temperature (°C)	30	
Evaporation/condensation temperature (°C)	20	

The adsorber bed, packed with the FAM-Z02, was heated using a 90°C heating fluid and simultaneously evacuated for 8 hours to be completely dried out. The adsorber bed was then placed on the scale and connected to the evaporator, TCS_{HF}, and TCS_{CF}. For an adsorption process, TCS_{CF} circulated a 30°C cooling fluid to the adsorber bed and once the valve between the adsorber bed and the evaporator was opened the FAM-Z02 adsorbed the water vapor from the evaporator. This adsorption caused the adsorber bed mass to increase over time. For a desorption process, the adsorber bed was heated up with a 90°C heating fluid and the adsorber bed mass reduced due to desorption of water.

3.2. Data analysis

The performance of the adsorber beds is evaluated by calculating the COP and SCP of the ACS. 3-1 gives the ideal evaporation cooling energy, calculated based on the in-situ water uptake rate measurements of FAM-Z02:

$$Q_{evap,ideal}\left(J\right) = \Delta\omega_{adsorption} m_{adsorbent} h_{fg} \qquad 3\text{-}1$$

where $\Delta\omega_{\text{adsorption}}$ is equal to $\Delta m_{\text{adsrobate uptake}}/m_{\text{adsorbent}}$, i.e. the amount of water adsorbed during an adsorption process over the mass of dry adsorbent, and h_{fg} is the enthalpy of evaporation of water at the evaporator temperature. In this study, the ideal evaporation cooling energy refers to an evaporator with the effectiveness of one and thermal mass of zero in which there is no temperature drop between the refrigerant and the chilled water circulated inside the evaporator. This assumption is in agreement with the data measured using a TGA such as the data reported in [70]. The total heat transfer to the adsorbent material during a desorption process is:

$$Q_{total\ heating}\left(J\right)=\int_{desorption}\dot{m}_{fg}c_{p,hf}\left(T_{hf,i}-T_{hf,o}\right)dt \qquad 3\text{-}2$$

where $\dot{m}_{hf}$ is the heating fluid mass flow rate and $T_{hf,i}$ - $T_{hf,o}$ is the temperature difference between the inlet and outlet of the adsorber bed. Using 3-1 and 3-2, the ideal COP and SCP of the ACS can be calculated:

$$COP_{ideal}=\frac{Q_{evap,ideal}}{Q_{total\ heating}} \qquad 3\text{-}3$$

$$SCP_{ideal}\left(W/\text{kg}\right)=\frac{Q_{evap,ideal}}{m_{adsorbent}\tau_{cycle}} \qquad 3\text{-}4$$

where τ_{cycle} in 3-4 is the cycle time.

3.3. Results and discussion

3.3.1. Effects of adsorber bed design on the equilibrium water uptake of FAM-Z02

To compare the equilibrium data collected using our experimental setup and the TGA data reported in literature [72], two adsorption and desorption isotherm tests were run under the operating conditions summarized in Table 3-1. To run the equilibrium adsorption test, the dried FAM-Z02 packed in the adsorber beds of Designs I and II was exposed to the water vapor provided by the evaporator at a constant temperature of 20°C. As shown in Figure 3-3a, the FAM-Z02 adsorbs the water vapor and the adsorber bed

mass increases until it reaches a constant value of 30% kg/kg. It can be seen in Figure 3-3a that the mass of the adsorber bed in Design II increases faster than that in Design I. This is because of the higher heat transfer surface area and faster removal of the heat of adsorption from the adsorber bed. At the adsorption time of 240 min, the equilibrium water uptakes of both adsorber beds reach the same value. Figure 3-3a also indicates that the equilibrium water uptakes measured using Designs I and II are 3% (= 33% - 30%) less than that measured by the TGA.

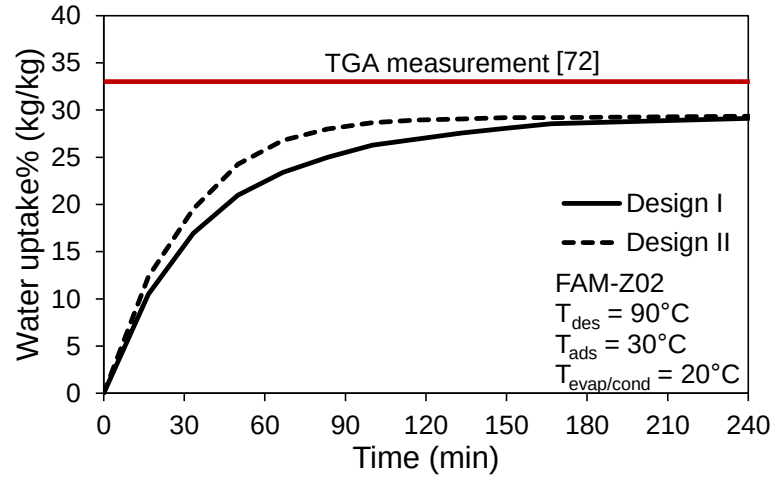

(a)

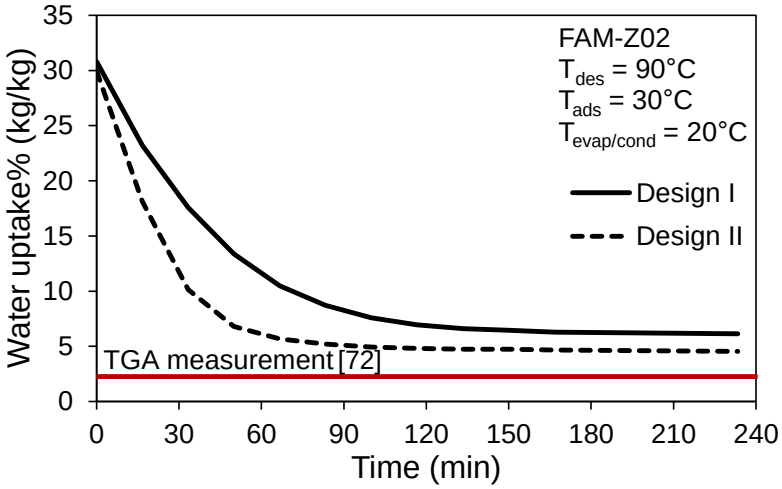

(b)

Figure 3-3. (a) Adsorption and (b) desorption isotherms measured by using Designs I and II, and compared against the TGA data measurements reported [72]**.**

Figure 3-3b shows the desorption curves for Designs I and II under the operating conditions tabulated in Table 3-1. Figure 3-3b demonstrates that the adsorber bed of Design II results in faster water desorption from the FAM-Z02 due to the higher heat transfer rate. In addition, at the end of the desorption process the equilibrium water uptake of FAM-Z02 in Design II is 0.016 kg/kg less than that in Design I. The equilibrium water uptakes at the end of the desorption tests of Designs I and II are 0.038% and 0.022% kg/kg more than that of the TGA measurement. Finally, by comparing the running times of adsorption and desorption processes in Design II, one can conclude that the desorption time of water (120 min) is almost two times shorter than the adsorption time of water (240 min) by FAM-Z02 under the defined operating conditions.

3.3.2. Effects of adsorber designs on the performance of an ACS

Figure 3-4 shows the variations in the heating and cooling fluid inlet and outlet temperatures, and the mass changes of the adsorber bed in Design II during adsorption and desorption at cycle time of 60 min. It can be seen in Figure 3-4 that by cooling the adsorber bed in Design II, adsorption process starts and mass of adsorber bed increases. At the end of adsorption process, the mass of adsorber bed reaches its maximum value. By heating the adsorber bed, the adsorbate is desorbed from the FAM-Z02 and flows to the condenser, and as a result, the mass of adsorber bed starts reducing, as shown in Figure 3-4b.

The heat transfer fluid used for heating and cooling of the adsorber beds was silicone oil (Julabo, Thermal P60), which had a density change from 909 kg/m^3 at 30°C to 854 kg/m^3 at 90°C. Further, the stiffness of the hosing connected to the adsorber beds changed during heating and cooling processes and affected the mass measurements. To eliminate these undesirable changes in the adsorber bed mass measurements, the adsorber beds were disconnected from the evaporator/condenser container, and heating and cooling processes were performed to measure the adsorber bed mass change caused only by the variations of heat transfer fluid density and the stiffness of the hosing. Figure 3-4b indicates that these variations can have significant effects on the adsorber bed mass measurement and, consequently, the water uptake rate calculations and should thus be de-convoluted from the measured data.

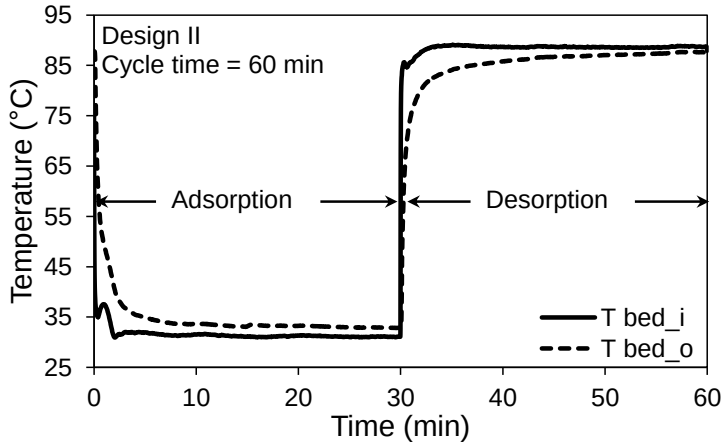

(a)

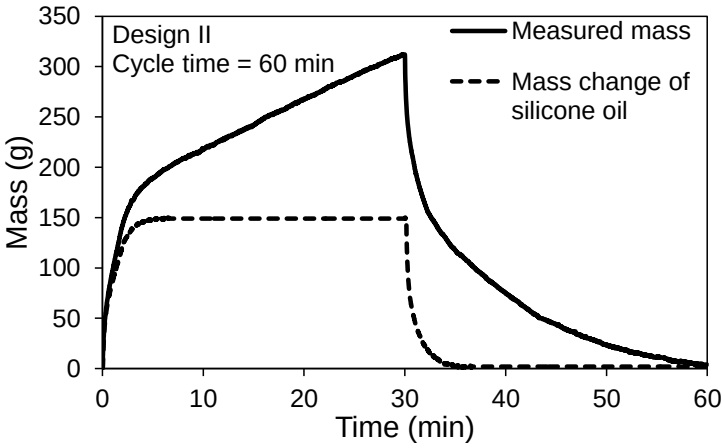

(b)

Figure 3-4. (a) Heating and cooling fluid inlet and outlet temperatures and (b) mass changes of adsorber bed in Design II and silicone oil during adsorption and desorption under cycle time of 60 min.

Figure 3-5 shows the variation of evaporator/condenser pressure, $P_{evap/cond}$, for Designs I and II under a cycle time of 60 min. The red line in Figure 3-5 shows the saturation pressure of water at 20°C. It can be seen in Figure 3-5 that during the adsorption process, the adsorber beds in Designs I and II create suction, and $P_{evap/cond}$ reduces. This reduction in the evaporator pressure causes water to start evaporating inside the evaporator. Figure 3-5 also indicates that $P_{evap/cond}$ is lower when the evaporator is connected to the adsorber bed in Design II than when it is connected to the adsorber bed

in Design I, because of higher suction created by the adsorber bed in Design II. Higher suction by the adsorber bed in Design II causes more water evaporation and, as a result, the FAM-Z02 adsorbs more water vapor within a constant adsorption time. By heating the adsorber beds in the desorption process, water is desorbed from the FAM-Z02 and pressures of the adsorber beds increase. Due to the pressure gradient between the adsorber bed and the condenser container, water vapor is pushed from the adsorber beds to the condenser.

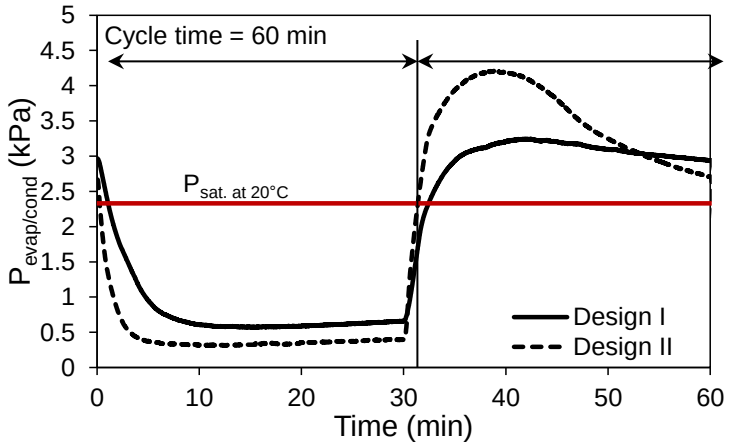

Figure 3-5. Variations in $P_{evap/cond}$ due to the different adsorber beds in Designs I and II during the adsorption and desorption processes. The red line demarcates the saturation pressure of water at 20°C.

The FAM-Z02 water uptake differences, $\Delta\omega$, between two continuous adsorption and desorption processes were measured in-situ under different cycle times, as shown in Figure 3-6a. It can be seen in Figure 3-6a that the adsorber bed in Design II provides higher $\Delta\omega$ than that in Design I for a constant cycle time. For example, under the cycle time of 60 min, the adsorber beds in Designs I and II provide $\Delta\omega$ of 0.035% and 0.108% kg/kg, respectively (a three times higher uptake for Design II). The main reasons for this significant difference between the $\Delta\omega$ of Designs I and II are the high heat transfer surface area and small fin spacing of the adsorber bed in Design II. These features help the FAM-Z02 adsorb more water vapor during adsorption by more quickly removing the heat of adsorption. Using the measured $\Delta\omega$, the SCP_{ideal} and COP_{ideal} of Designs I and II can be calculated.

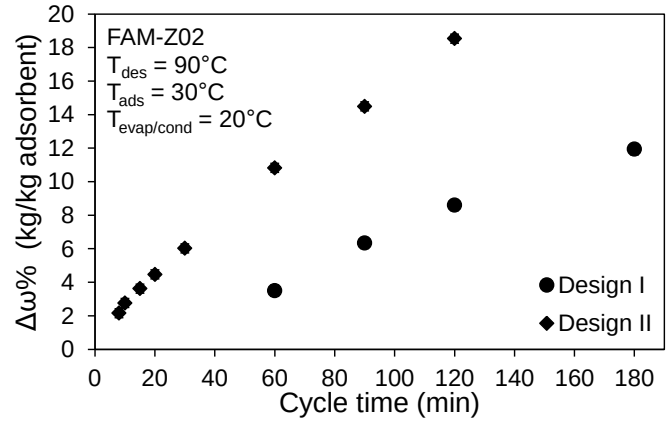

(a)

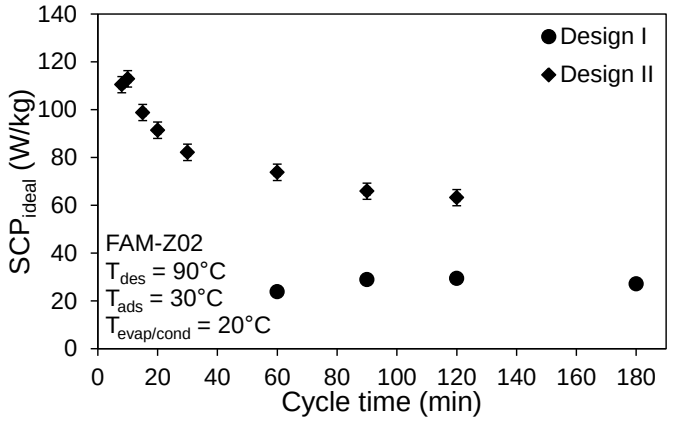

(b)

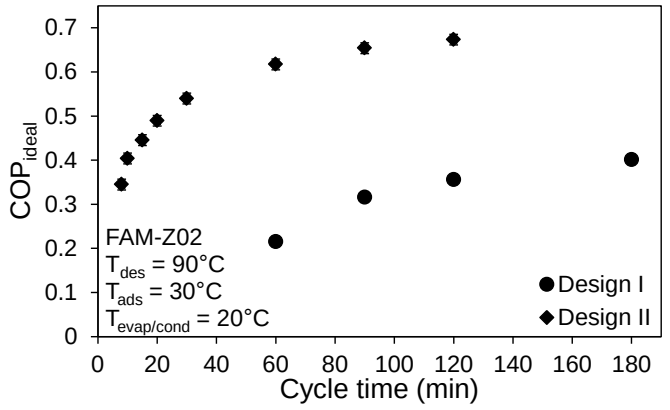

(c)

Figure 3-6. (a) FAM-Z02 water uptake difference between adsorption and desorption processes, (b) SCP_{ideal} and (c) COP_{ideal} in Designs I and II vs. different cycle times

Figure 3-6b shows that the SCP_{ideal} of Design I varies between 23.8-29.3 W/kg for cycle times of 60-180 min. In contrast, the SCP_{ideal} of Design II decreases from 112.9 to 63.2 W/kg by increasing the cycle time from 10 to 120 min. Figure 3-6c displays that the COP_{ideal} of Design I increases from 0.22 to 0.40 as cycle time is increased from 60 to 180 minutes while the COP_{ideal} of Design II increases from 0.34 to 0.67 as the cycle time is increased from 10 to 120 min. Comparing the SCP_{ideal} and COP_{ideal} of Designs I and II, as shown in Figure 3-6, indicates that high heat transfer surface area and small fin spacing are two key features of a well-designed adsorber bed for ACS applications and having a proper adsorbent material, such as FAM-Z02, is not necessarily sufficient to reach high ACS performance.

As it can be seen in Figure 3-6a, amount of adsorbed and desorbed material increases with increasing cycle time. This happens as in longer cycle times, there is more time for heat transfer and adsorption/desorption. Figure 3-6b shows that there is an optimal cycle for each design. This trend is with agreement with previous works [118,119]. In shorter cycle times the extent of adsorption and desorption decreases due to poor heat transfer properties and thermal inertia of the system. At a certain cycle time, the maximum SCP is achieved at the prevailing heating and cooling source temperatures. Based on literature, “extending the cycle time further brings forth unfavorable effect on useful cooling as the cycle average cooling capacity decreases“ [118]. It can also be seen in Figure 3-6c that COP is uniformly increasing with cycle time. The reason is that in a longer cycle times, the effects of changing processes in the beds, which involves a significant sensible heat transfer and is transient, plays less important role in heat transfer process.

Total uncertainty divides into systematic and random uncertainty. The systematic uncertainty in the current setup is only due to the accuracy of the mass measurement device, which is 1 gram. As the total reading of the setup is in the order of 27 kg it can be concluded that the accuracy of the balance has minimal effect on the uncertainty of the measurement. The random uncertainty is caused due to different readings in different tests. To address that factor, each test was performed three times and the standard deviations for each set of data were calculated, which is shown as error bars in Figure 3-6.

The detail data and calculated values for $\Delta\omega$, SCP, and COP for Design I and Design II for different cycle times (illustrated in Figure 3-6) are shown in Table 3-2, Table 3-3, and Table 3-4.

Table 3-2 FAM-Z02 COP_{ideal} in Designs I and II vs. different cycle times

Cycle Time [min]	COP	COP Standard Deviation
Design I		
60	0.22	0.006
90	0.32	0.005
120	0.36	0.004
180	0.40	0.011
Design II		
8	0.34	0.011
10	0.40	0.000
15	0.45	0.005
20	0.49	0.000
30	0.54	0.007
60	0.62	0.002
90	0.65	0.012
120	0.67	0.008

Table 3-3 FAM-Z02 SCP_{ideal} in Designs I and II vs. different cycle times

Cycle Time [min]	SCP [W/kg]	SCP Standard Deviation
Design I		
60	23.82	0.635
90	28.82	0.423
120	29.31	0.317
180	27.11	0.733
Design II		
8	110.41	3.408
10	112.86	0.000
15	98.75	1.049
20	91.32	0.000
30	82.09	1.049
60	73.76	0.262
90	65.83	1.224
120	63.15	0.787

Table 3-4 FAM-Z02 water uptake difference between adsorption and desorption processes in Designs I and II vs. different cycle times

Cycle Time [min]	Δω %	Δω Standard Deviation
Design I		
60	3.49	0.093
90	6.34	0.093
120	8.60	0.093
180	11.94	0.323
Design II		
8	2.16	0.067
10	2.76	0.000
15	3.62	0.038
20	4.47	0.000
30	6.02	0.077
60	10.82	0.038
90	14.49	0.269
120	18.53	0.231

3.4. In-situ water uptake rate measurements of calcium chloride confined within silica gel

As a part of experimental setup, in-situ water uptake rate measurements of calcium chloride confined within silica gel developed in LAEC was studied. The test setup used in the previous section was used for this experiment. However, the only heat exchanger used was the first design from before. In this experiment, the adsorber was exposed to the evaporator and condenser until it reached its saturation condition. Figure 3-7 (a) shows that the pressure of adsorber bed increased quickly from vacuum and reached the saturation pressure of the water vapor coming from the condenser/evaporator container. Because of proper vapor supply to the adsorber bed, the water uptake rate of silica gel-CaCl2 improved significantly. At this stage, the water adsorption/desorption rate of silica gel-CaCl2 could be studied.

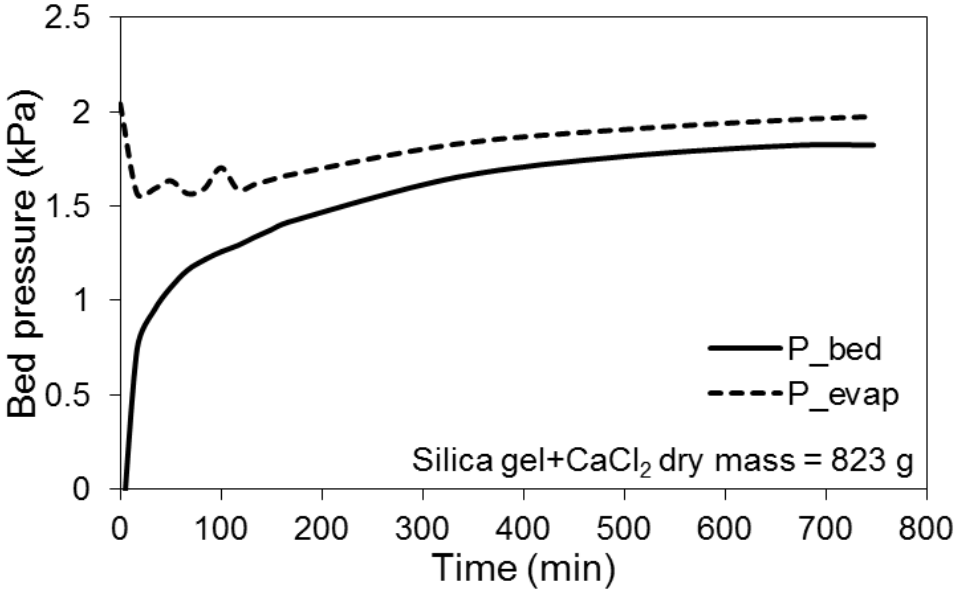

(a)

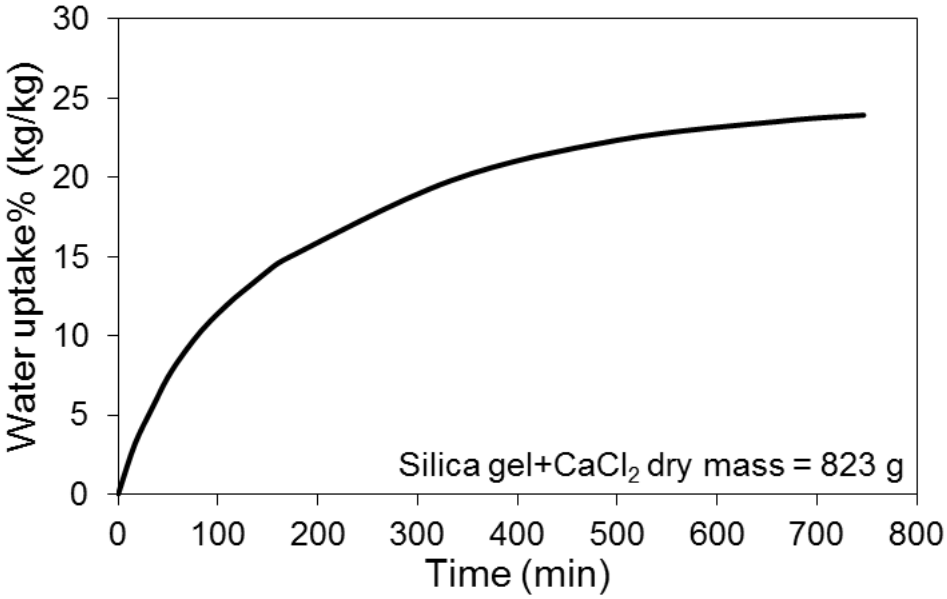

(b)

Figure 3-7 (a) adsorber bed and evaporator pressure, and (b) water uptake rate during adsorption vs. time.

To run a set of adsorption/desorption processes, the heating and cooling fluid inlet temperatures to the adsorber bed were set at 90°C and 30°C, and the condenser/evaporator temperature was maintained at 20°C. Adsorption and desorption of the adsorber bed were repeated a few times and it was noticed that the water uptake rate

of silica gel-$CaCl_2$ was reduced in later cycles, as shown in Figure 3-8. It can be seen in the demarcated region in Figure 3-8(a) that the minimum pressure of the adsorber bed at the end of desorption increased. Due to the increase of the pressure of the adsorber bed, the water uptake rate of silica gel-$CaCl_2$ was reduced, as shown in Figure 3-8(b). To resolve the issue, the silica gel-$CaCl_2$ particles were dried out by heating and the experiments were repeated. The same results were achieved.

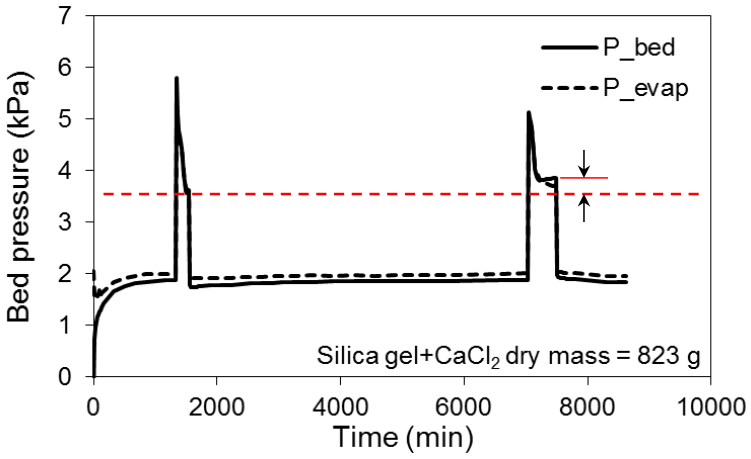

(a)

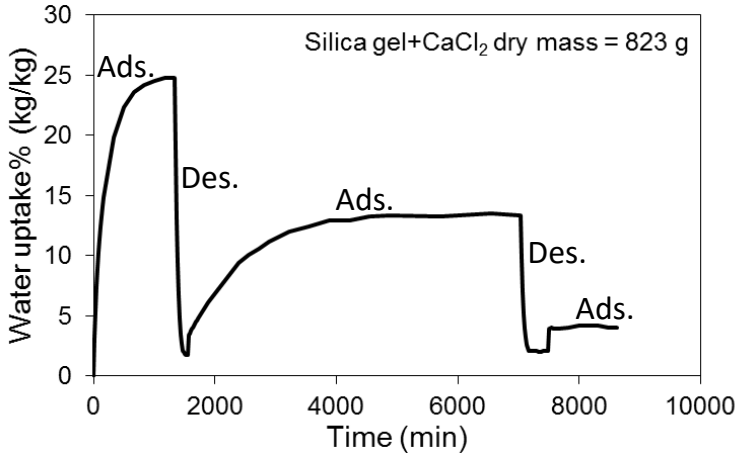

(b)

Figure 3-8 (a) Adsorber bed pressure and (b) water uptake rate of silica gel-$CaCl_2$ during adsorption and desorption in the third experimental setup. The heating and cooling inlet temperatures to the adsorber beds are 90°C and 30°C, and the condenser/evaporator temperature is 20°C.

By opening the adsorber bed and removing the silica gel-$CaCl_2$ from the adsorber bed, we noticed that the copper was corroded, as shown in Figure 3-9(b). Also,

Figure 3-9(c) shows that the silica gel-CaCl2 particles were clumped together due to the $CaCl_2$ leakage to the surface of the silica gel particles. Literature review and further analysis indicated that galvanic corrosion was happened inside the adsorber bed made of copper and aluminum at the presence of water. In addition, $CaCl_2$ accelerated the corrosion rate. Corrosion of the copper generated a background gas inside the adsorber bed and reduced the water uptake rate of silica gel-$CaCl_2$.

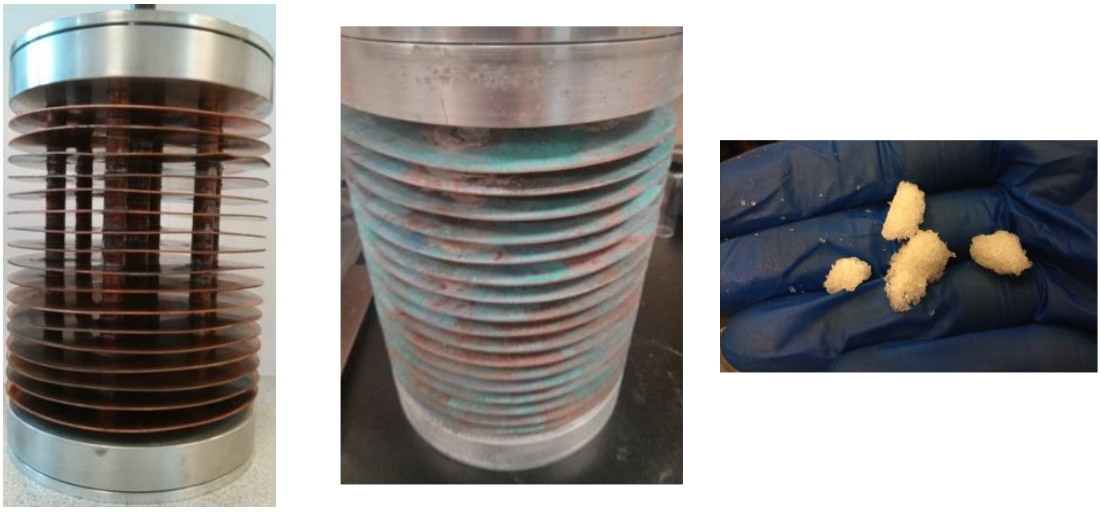

(a) (b) (c)

Figure 3-9 (a) Adsorber bed before packing with silica gel-$CaCl_2$, (b) corrosion of copper due to $CaCl_2$, and (c) silica gel-$CaCl_2$ particles were clumped together due to $CaCl_2$ leakage to the surface of silica gel.

Chapter 4. Numerical modeling

This chapter begins with an introduction to computational fluid dynamic modeling and its application in adsorption cooling systems. This is followed by a short summary of the solution technique, governing equations and simplifying assumptions. Geometry and boundary conditions are described, and finally, this chapter shows the results of the modeling.

4.1. Heat transfer in the adsorber bed

During regeneration (adsorption) within adsorber beds, the bed is heated up (cooled down) with a secondary fluid called the heat transfer fluid. To increase thermal performance and keep the size of the system as small as possible, the heat transfer fluid should be liquid (to have higher convective heat transfer coefficient) and have high thermal capacity (to be affected less by heat generation in the adsorber bed). Water is the best heat transfer fluid (for operating conditions between 0°C and 100°C). It is crucial to have a thermal network model to evaluate the thermal performance of an adsorber bed. In this thermal network, there are five thermal resistances between the heat transfer fluid and adsorber material:

- Convective heat transfer resistance between heat exchanger pipe and the heat transfer fluid (R1)
- Conductive heat transfer resistance through the body of the heat exchanger (R2)
- Thermal contact resistance (TCR) between the adsorbent and the heat exchanger (R3)
- Convective heat transfer resistance between the heat exchanger and the refrigerant (R4)
- Conductive heat transfer resistance through the adsorbent (R5)

The convective heat transfer inside the adsorber bed can be neglected as the working pressure and velocity in adsorber beds are very small. The convective heat transfer resistance between the heat exchanger and the heat transfer fluid is inversely

proportional to the fluid velocity. This resistance can be calculated by having the convective heat transfer coefficient by using 4-1.

$$R_1 = \frac{1}{h_i} \quad , \quad R_4 = \frac{1}{h_o} \tag{4-1}$$

The conductive heat transfer resistance through the heat exchanger (adsorbent) is inversely proportional to the thermal conductivity of the heat exchanger (adsorbent) material and directly proportional to the thickness of the heat exchanger wall (adsorbent layer). The contribution of the heat transfer resistance of the heat exchanger to the total thermal resistance is very small since the materials of the heat exchanger are highly conductive. On the other hand, the thermal resistance of the adsorbent is an important parameter due to the low thermal conductivity of typical adsorber materials [120]. The conductive heat transfer resistance can be calculated from the thickness of the conductive layer and its thermal conductivity as follows:

$$R_2 = \frac{t_{wall}}{k_{wall}} \quad , \quad R_5 = \frac{t_{ads}}{k_{ads}} \tag{4-2}$$

TCR plays a major role in granular configurations, as there is no pressure applied on the grains. This resistance can be decreased by using adsorbent coatings or consolidated adsorbents. Different approaches had been introduced to measure the value of the TCR. One of the easiest and most reliable approaches is to use the two thickness method on a guarded flux meter. In this method, bulk thermal resistance of two different sample is measured. Subtraction of those results can be used to determine the thermal conductivity of adsorbent. Once thermal conductivity of adsorbent is calculated, the thermal contact resistance can be calculated. The detail information about this technique is presented in [121]. A schematic of the thermal resistance and temperature profile within an adsorber bed is shown in Figure 4-1.

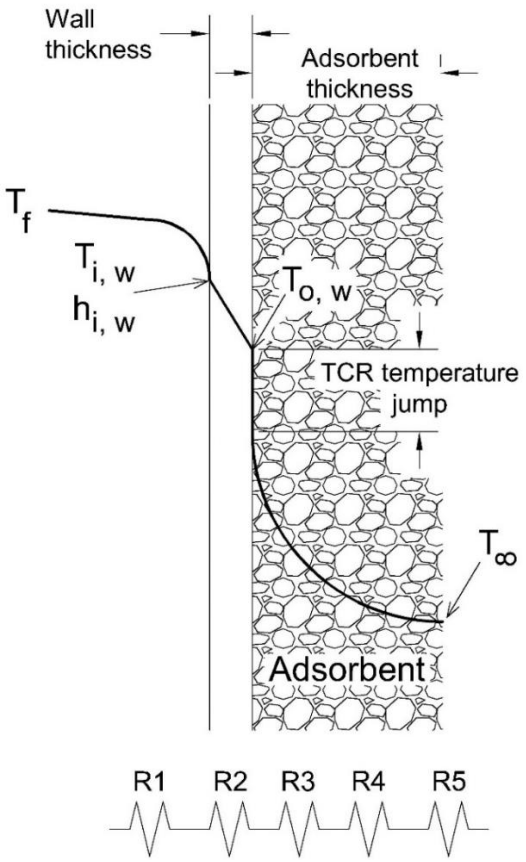

Figure 4-1 Schematic of thermal resistance network in an adsorber bed

4.2. Mathematical model

ANSYS Fluent, a commercial CFD software, was used to simulate heat and mass transfer in the adsorber bed. Since adsorption is a time-dependent process, some assumptions were made to simplify the geometry and reduce the computation time. In this study, ANSYS Fluent was used as a core solver, and boundary conditions, the adsorption uptake rate equation, and source terms were coupled with Fluent by developing a user defined function (UDF) file. Boundary conditions in an adsorber bed vary during adsorption and desorption processes. In addition, the effects of TCR between particles and the heat transfer surface were taken into account.

4.3. Governing equations

A full CFD model for the adsorption and desorption processes within an adsorber bed is presented here. The Navier-Stokes equations are the governing equations for any fluid flow problem. The Navier-Stokes equations are linear partial differential equations (PDE), which do not have an analytical solution for most real world problems. However, using CFD these equations can be solved numerically. These equations can be divided into a mass conservation equation and a momentum conservation equation. The other governing equation for adsorption is the energy equation, which is used in heat transfer problems. The energy equation is a linear transport equation. The mass conservation equation or continuity equation has the differential form

$$\frac{\partial \rho}{\partial t} + \nabla.\left(\rho \vec{v}\right) = S_m \qquad \text{4-3}$$

where ρ is density, t is time, ν is the velocity vector and S_m is a mass source term that represents the mass added to the continuous phase from the dispersed second phase. In adsorption applications, the source term in this equation will represent the vapor adsorbed/desorbed into/from the adsorbent surface.

The momentum conservation equation in differential form of this equation is

$$\frac{\partial}{\partial t}\left(\rho \vec{v}\right) + \nabla.\left(\rho \vec{v}\vec{v}\right) = -\nabla p + \nabla.\left(\bar{\bar{\tau}}\right) + \rho \vec{g} + \vec{F} \qquad \text{4-4}$$

where p is the static pressure, $\bar{\bar{\tau}}$ is the stress tensor, and ρg and F represent gravitational and external body forces respectively. F also contains other model dependent source terms in this equation.

The stress tensor introduced in 4-4 is defined as

$$\bar{\bar{\tau}} = \mu\left[\left(\nabla \vec{v} + \nabla \vec{v}^T\right) - \frac{2}{3}\nabla.\vec{v}I\right] \qquad \text{4-5}$$

where μ is the molecular viscosity, I is the unit tensor, and the second term on the right hand side is the effect of volume dilation

The general form of the energy equation is

$$\frac{\partial}{\partial t}(\rho E)+\nabla.\left(\vec{v}\left(\rho E+p\right)\right)=-\nabla.\left(k_{eff}\nabla T-\sum_{j}h_{j}\vec{J}_{j}+\left(\overline{\overline{\tau}}_{eff}.\vec{v}\right)\right)+S_{h} \qquad 4\text{-}6$$

where E represents the internal energy, k_{eff} is the effective thermal conductivity, h_j represents the enthalpy of species j, and J_j is the diffusion flux of species j. The first three terms on the right-hand side of 4-6 represent energy transfer due to conduction, species diffusion, and viscous dissipation, respectively. S_h is the heat of chemical reaction, and any other volumetric heat sources.

4.3.1. Uptake as a scalar

One parameter that plays a major role in adsorption cooling is the uptake, which is defined as the ratio of mass of adsorbate to adsorbent mass. This parameter is not one of the main quantities (mass, momentum, and energy) in the ANSYS Fluent database. However, new scalars can be defined in ANSYS Fluent using a user defined scalar (UDS). The general transport equation is governing the UDS:

$$\frac{\partial\rho\phi_{k}}{\partial t}+\frac{\partial}{\partial x_{i}}\left(\rho u_{i}\phi_{k}-\Gamma_{k}\frac{\partial\phi_{k}}{\partial x_{i}}\right)=S_{\phi_{k}}\quad k=1,2,...,\mathrm{N} \qquad 4\text{-}7$$

This equation is the general form of a transport equation of an arbitrary scalar $\phi_k$where Γ_k and S_{ϕ_k} are the diffusion coefficient and source term supplied for each of the N scalar equations. The source of this equation, when it is applied for the adsorption process, will represent the uptake of the adsorbate.

The equations above are the general form of the conservation equation of mass, momentum, energy, and a scalar. However, as adsorbent material is a porous material, some modification to these equations are required. In addition, the source term of each equation will be discussed in detail in the following section.

4.3.2. Linear driving force (LDF) model

The source terms in the continuity and energy equations depend on the uptake rate of the adsorbate. In other words, the mass generation in the continuity equation depends on the uptake rate, and the amount of energy released in the energy equation depends on the rate with which adsorbate is adsorbed or desorbed. Therefore, it is important to provide an accurate definition for the uptake rate. One of the most commonly used models for uptake rate is the linear driving force (LDF) model. This model describes the adsorption rate as

$$\frac{\partial \omega}{\partial t} = \frac{15 D_{eff}}{r_p^2}\left(\omega_{eq} - \omega\right) \qquad 4\text{-}8$$

where ω is the uptake value, D_{eff} is the effective diffusivity, r_p is the particle radius, and ω_{eq} is the equilibrium value for uptake at any temperature and pressure. Based on this equation the uptake rate at any time depends linearly on the difference between the equilibrium and actual uptake values [106].

4.3.3. Conservation of user defined scalar (UDS)

The transport equation introduced for the UDS in 4-7 has four terms: the first term represents the change of the scalar over time, the second term is convective portion of transfer phenomenon, the third term takes into account diffusion effects and the fourth term is the source term. Comparing 4-7 and 4-8 one can conclude that by neglecting the convective and diffusive terms in 4-8, the transport equation of defined scalar (uptake) can be simplified to the source term in the LDF model. Now if the unity value is associated with density, the simplified equation for the UDS is

$$\frac{\partial \rho \phi}{\partial t} = S_{\phi} \qquad 4\text{-}9$$

Assuming constant density for the refrigerant, dividing both sides of 4-9 by density and substituting the result into 4-8 leads to the source term for the UDS transport equation:

$$S_{\omega} = \frac{15 D_{eff}}{r_p^2}\left(\omega_{eq} - \omega\right) \qquad 4\text{-}10$$

The values for ω_{eq} depends on the pressure, temperature and the working pair. The governing equations for different working pairs as a function of pressure and temperature is shown in Table 4-1.

Table 4-1 Equilibrium adsorbate uptake and enthalpy of adsorption of different working pairs, reprinted with permission from Elsevier [98]

Working Pair	Equilibrium equation	Enthalpy of adsorption (J/kg)	Constant parameters	Ref.
Zeolite 4A – Water	$\ln(p) = a(\omega) + \frac{b(\omega)}{T_{adsorbent}}$ $a(\omega) = a_0 + a_1\omega + a_2\omega^2 + a_3\omega^3$ $b(\omega) = b_0 + b_1\omega + b_2\omega^2 + b_3\omega^3$	$\Delta h_{ads} = \frac{R_u}{M_{adsorbate}} b(\omega)$	$a_0 = 14.8979,\ b_0 = -7898.85$ $a_1 = 95.408,\ b_1 = 21498$ $a_2 = -636.66,\ b_2 = -184598.0$ $a_3 = 1848.8,\ b_3 = 512605.0$ $R_u = 8.314\,J/mol.K$ $M_{adsorbate} = 0.018\,kg/mol$	[171]
Zeolite 13X – Water	$\ln(p) = a(\omega) + \frac{b(\omega)}{T_{adsorbent}}$ $a(\omega) = a_0 + a_1\omega + a_2\omega^2 + a_3\omega^3$ $b(\omega) = b_0 + b_1\omega + b_2\omega^2 + b_3\omega^3$	$\Delta h_{ads} = \frac{R_u}{M_{adsorbate}} b(\omega)$	$a_0 = 13.4244,\ b_0 = -7373.78$ $a_1 = 110.854,\ b_1 = 6722.92$ $a_2 = -731.76,\ b_2 = 5624.47$ $a_3 = 1644.8,\ b_3 = -3486.7$ $R_u = 8.314\,J/mol.K$ $M_{adsorbate} = 0.018\,kg/mol$	[171]
Act. Carbon – Ethanol	$\ln(p) = a(\omega) + \frac{b(\omega)}{T_{adsorbent}}$ $a(\omega) = a_0 + a_1\omega + a_2\omega^2 + a_3\omega^3$ $b(\omega) = b_0 + b_1\omega + b_2\omega^2 + b_3\omega^3$	$\Delta h_{ads} = \frac{R_u}{M_{adsorbate}} b(\omega)$	$a_0 = 20.3305,\ b_0 = -6003.58$ $a_1 = 6.53035,\ b_1 = 6315.16$ $a_2 = -16.6841, b_2 = -26058.7$ $a_3 = 52.3793,\ b_3 = 40537.9$ $R_u = 8.314\,J/mol.K$ $M_{adsorbate} = 0.032\,kg/mol$	[171]

Table 4-1 (Cont'd) Equilibrium adsorbate uptake and enthalpy of adsorption of different working pairs, reprinted with permission from Elsevier [98]

Working pair	Equilibrium equation	Enthalpy of adsorption (J/kg)	Constant parameters	Ref.
Act. Carbon ethanol	$\omega_{eq} = \omega_0 \exp\left[-A\left[T_{adsorbent}\left(\frac{p_{sat.@T_{adsorbent}}}{p_{cond.\ or\ evap.}}\right)\right]^2\right]$	$\frac{\Delta h_{ads} - h_{fg}}{E} = \left[\ln\left(\frac{\omega_0}{\omega_{eq}}\right)\right]^{1/n} + a\left[\frac{T_{adsorbent}}{T_c}\right]$	$\omega_0 = 0.797\,kg/kg$ $A = 1.716\times10^{-6}\,K^{-2}$ $a = 6.717,\ b = 9.75$ $n = 2,\ E = 138\,kJ/kg$ $T_c = 789.15\,K$	[37]
RD silica gel – water	$\omega_{eq} = \frac{K_0 \exp\left(\frac{\Delta h_{ads} M_{adsorbate}}{R_u T_{adsorbent}}\right) p}{\left[1 + \left[\frac{K_0}{\omega_m}\exp\left(\frac{\Delta h_{ads} M_{adsorbate}}{R_u T_{adsorbent}}\right) p\right]^n\right]^{1/n}}$	$\Delta h_{ads} = 2693\,kJ/kg$	$K_0 = 7.3\times10^{-11}\,mbar^{-1}$ $\omega_m = 0.45\,kg/kg$ $n = 12$ $R_u = 8.314\,J/mol.K$ $M_{adsorbate} = 0.018\,kg/mol$	[172]
Silica gel CaCl2 - water	$\omega_{eq} = \frac{\omega_m K_0 \exp\left(\frac{\Delta h_{ads} M_{adsorbate}}{R_u T_{adsorbent}}\right) p}{\left[1 + \left[K_0 \exp\left(\frac{\Delta h_{ads} M_{adsorbate}}{R_u T_{adsorbent}}\right)\right]^n\right]^{1/n}}$	$\Delta h_{ads} = 2760\,kJ/kg$	$K_0 = 2.0\times10^{-10}\,mbar^{-1}$ $\omega_m = 0.8\,kg/kg$ $n = 1.1$ $R_u = 8.314\,J/mol.K$ $M_{adsorbate} = 0.018\,kg/mol$	[118, 173]

4.3.4. Continuity equation

The general form of the continuity equation was introduced in 4-3. However, this equation in porous media with adsorption is written as

$$\frac{\partial\left(\varepsilon\rho_{refrigerant}\right)}{\partial t}+\nabla.\left(\rho_{refrigerant}\vec{v}\right)+\left(1-\varepsilon\right)\rho_{adsorbent}\frac{d\omega}{dt}=0 \qquad 4\text{-}11$$

The first term in this equation is the change of density over time or mass storage in the control volume. The second term is the convective term, which represents mass transfer through the boundaries, and the last term represents the unsteady source term of the adsorption process, which can be modeled by the LDF model.

4.3.5. Conservation of momentum equation

The equation of conservation of momentum in porous media is

$$\frac{\partial}{\partial t}\left(\rho\vec{v}\right)+\nabla.\left(\frac{\rho\vec{v}\vec{v}}{\varepsilon}\right)=-\varepsilon\nabla p+\nabla.\left(\vec{\tau}\right)-\left(\frac{\varepsilon\mu}{K}\vec{v}+\frac{\varepsilon C_2}{2}\rho\left|\vec{v}\right|\vec{v}\right) \qquad 4\text{-}12$$

In this equation ε represents the porosity of the medium and K is the inverse of the permeability, which can be calculated by the Blake-Kozeny equation [122]:

$$K=\frac{R_p^2\varepsilon^3}{37.5\left(1-\varepsilon\right)^2} \qquad 4\text{-}13$$

Equation 4-12 can be used for modeling adsorption process without any modification.

4.3.6. Energy equation

The energy equation in porous media with adsorption is

$$\left[\rho_s\left(\left(1-\varepsilon\right)C_{p,s}+\omega\varepsilon C_{p,ref}\right)\right]\frac{\partial T}{\partial t}+\vec{\nabla}\left(\rho_s\vec{u}C_{p,ref}T\right)=$$
$$\left(1-\varepsilon\right)\rho_s\Delta h_{ads}\frac{d\omega}{dt}+\vec{\nabla}\left(k\vec{\nabla}T\right) \qquad 4\text{-}14$$

The first term on the left hand side of Equation 4-14 represent the energy stored in the adsorbent and adsorbate, and the second term is convective term in the heat transfer equation. The first term on the right hand side is the source term derived from the linear driving force model, and the last term is conduction heat transfer in the adsorbent.

It must be noted that Δh_{ads} in Equation 4-14 is specific heat of adsorption, which is defined as the ratio between amount of heat created (absorbed) during adsorption (desorption) per unit mass of adsorbent. The equilibrium water uptake of AQSOA-FAM-Z02 as a function of pressure and temperature can be calculated by using

$$\omega_{eq} = \frac{1}{n_s} \frac{\sum_{j=1}^{n_s} \left(K^0 \, p \big/ p^0 \right)^j \exp\left(-\frac{\Delta h_j}{RT} \right) / (j-1)!}{1 + \sum_{j=1}^{n_s} \left(K^0 \, p \big/ p^0 \right)^j \exp\left(-\frac{\Delta h_j}{RT} \right) / (j)!} \quad (kg / kg) \qquad 4\text{-}15$$

In this equation ns=11, p0=100000 Pa, and the other constants are tabulated in Table 4-2 [73].

Table 4-2 Constants to calculate the equilibrium uptake value of the working pair of FAM-Z02 and water, , reprinted with permission from Elsevier [73]

j	$\Delta h_j/R$
1	8442
2	11010
3	22494
4	29352
5	35460
6	39303
7	46491
8	53541
9	64641
10	67908
11	78372

All the governing equations were solved simultaneously to study heat and mass transfer inside the adsorber bed.

4.4. Effects of thermal contact resistance

Thermal contact resistance occurs when two solid surfaces are in contact with each other. The value of the thermal contact resistance depends on many parameters, which are out of scope of this study. To take into account the effects of TCR in this model, an equivalent thickness concept was introduced. The equivalent thickness of TCR is the virtual thickness of a material with the same thermal conductivity of the adsorbent and the same thermal resistance of TCR. It was assumed that this layer works as temperature jump (drop) during adsorption (desorption) and this temperature drop happens suddenly. Therefore, a solid material with equivalent thickness of TCR was added to geometry. In addition, to eliminate the effects of thermal inertia in this layer, the density and thermal capacity of this layer were assumed to be zero. Thus, the heat conduction equation for this layer can be written is

$$\rho c_p \frac{\partial T}{\partial t} = \nabla^2 T \Rightarrow 0 = \nabla^2 T \qquad \text{4-16}$$

Solving this equation yields a linear temperature distribution within the TCR layer, which can be an acceptable representative of the TCR between the heat exchanger fins and the adsorbent.

A schematic of the TCR layer modeling technique used in this study is illustrated in Figure 4-2. The brownish color represents the TCR layer and the grey color shows the adsorbent. The thermal properties of each layer are mentioned in the figure.

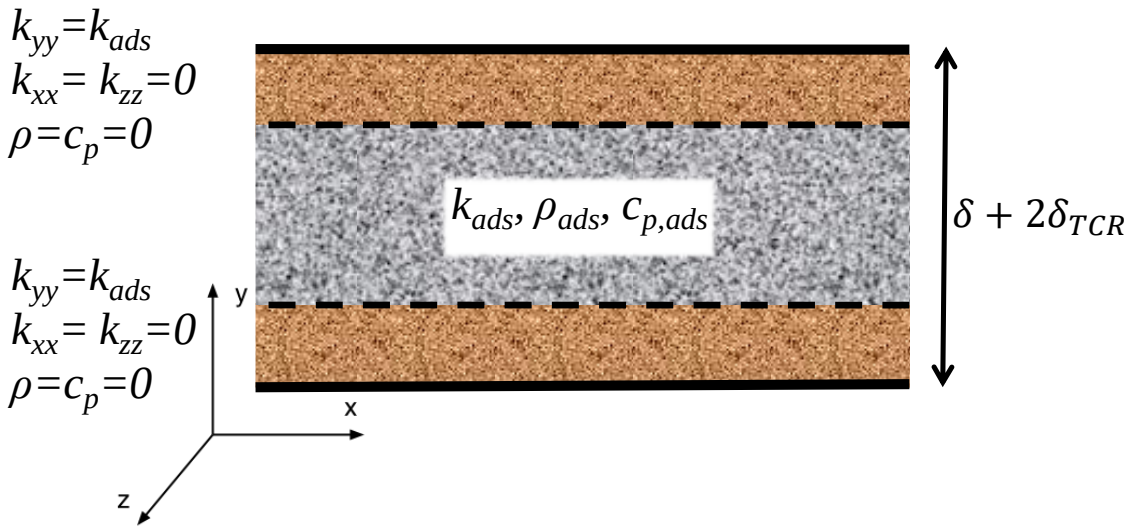

Figure 4-2 Schematic of thermal contact resistance modeling

4.5. Geometry and domain definition

The geometry investigated in this study is a simplified version of the geometry of the experiments conducted in our laboratory. The adsorber bed was comprised of an engine oil cooler adopted as the heat exchanger placed inside a vacuum chamber. The actual heat exchanger is shown in Figure 4-3(A). The adsorbent material (FAM-Z02) was poured in between the fins as illustrated in Figure 4-3(B) and a stainless steel mesh was used to hold the material in place.

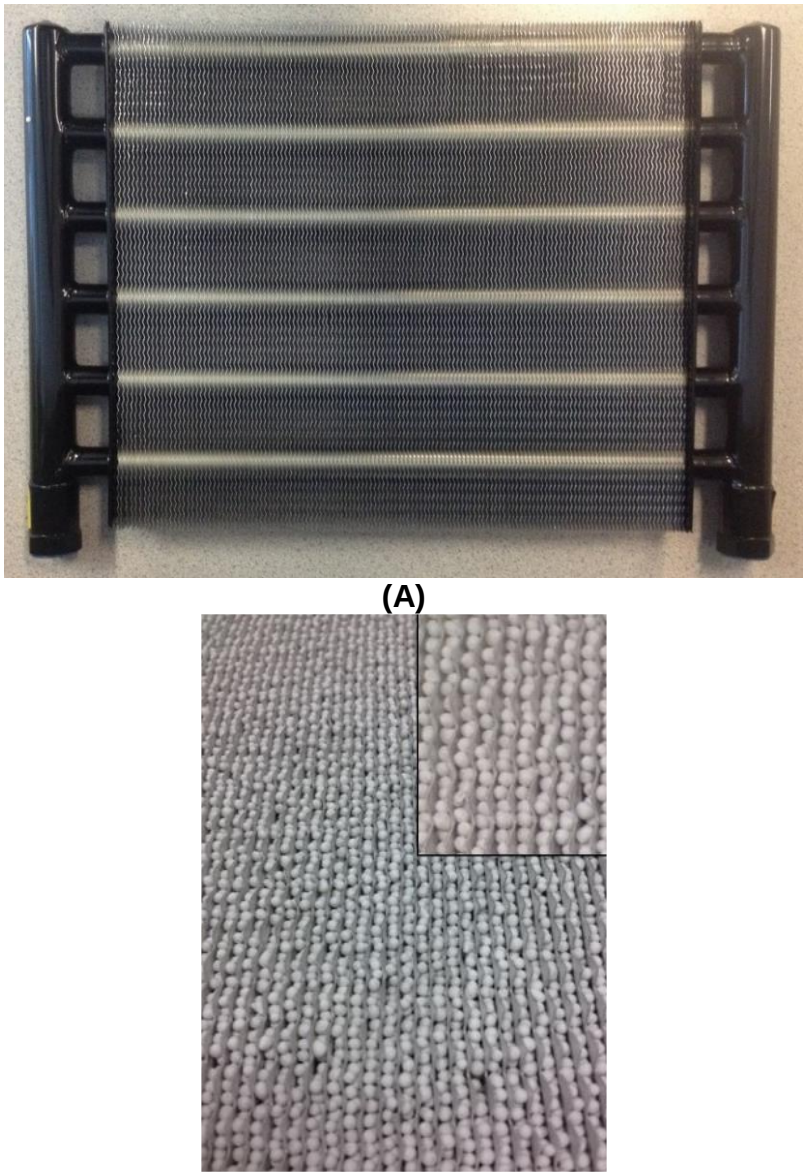

Figure 4-3 The actual heat exchanger used as adsorber bed

To reduce the computation time, the numerical domain modeled in this study was simplified as shown in Figure 4-4. Only one fin spacing was considered as the computational domain and by using symmetry lines and periodic boundary conditions, the geometry can be extended to the entire heat exchanger and vacuum chamber. It must be noted that the effects of the corners of the vacuum chamber are neglected and it is assumed that all the fins and adsorbent material will experience similar conditions.

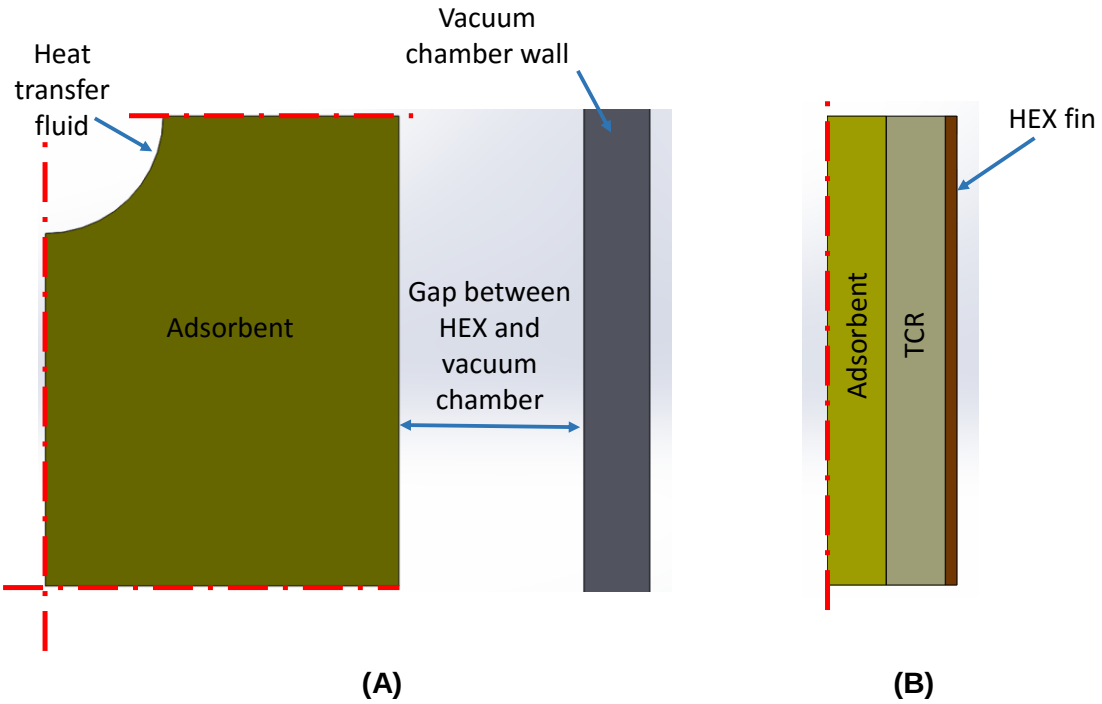

Figure 4-4 Schematic of numerical domain of model (A) front view, (B) side view

4.6. Initial conditions

Since an ACS generates cooling during repeated cooling and heating cycles, the initial conditions do not affect the final results once it reaches to a repetitive pattern for all parameters. However, choosing the appropriate initial conditions will significantly decrease the convergence time. The initial conditions inside the bed for this model were the same pressure and temperature as the outlet of the domain.

To simplify the geometry and decrease the computation time, several symmetry lines were used in the numerical domain. The wall of the vacuum chamber assumed to be insulated (similar to experimental tests), and the pressure and temperature at the boundaries were set to be the same as the measured pressure and its saturation temperature inside evaporator/condenser. To investigate the effects of an ideal evaporator/condenser on the system, the saturation pressure of the working temperature of the evaporator and condenser were applied at the boundaries as sudden changes.

4.7. Results and model verification

Results of the numerical modeling were compared to experimental data in order to verify the model. The parameter of interest for validation is the uptake. Using the numerical model, uptake at any time can be calculated. In addition, real time mass measurements provides data on uptake as a function of time and working conditions. Two cases were studied to verify the model. In the first case, it was assumed that fully dried material was exposed to the evaporator for a very long time until it reached equilibrium. Once there is no change in the measured mass (or in other words, the bed reaches its equilibrium value), the bed is heated up and exposed to the condenser until it reaches equilibrium again. For model verification, the same boundary conditions were applied for a very long cycle time. The comparison between the experimental and numerical model for adsorption and desorption are illustrated in Figure 4-5 and Figure 4-6, respectively. As can be seen, both data follow the same trend and there is a good agreement between the values obtained from each method.

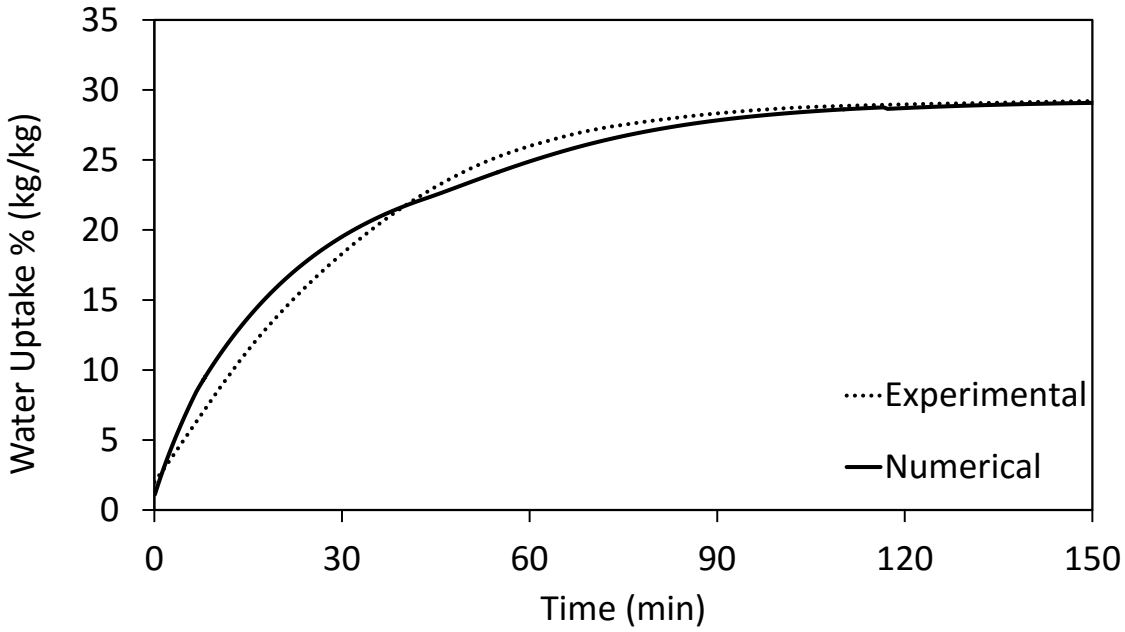

Figure 4-5 comparison between numerical and experimental data for adsorption

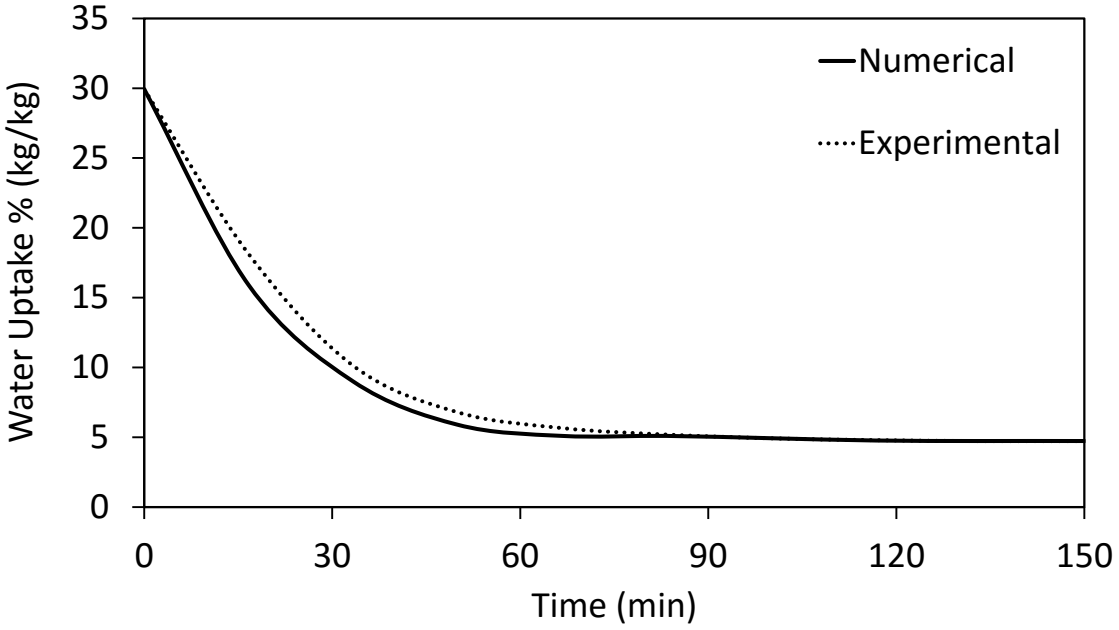

Figure 4-6 comparison between numerical and experimental data for desorption

As another approach to verify the model, the results for cyclic operation were compared. In this comparison the parameter of interest was the difference between

maximum and minimum of uptake value during the cyclic operation. This difference shows the ability of system in adsorbing and desorbing over time and directly related to the SCP. The model was verified against data from experimental tests for cycle times of 480 s, 600 s, 900 s. The results of this comparison are shown in Figure 4-7.

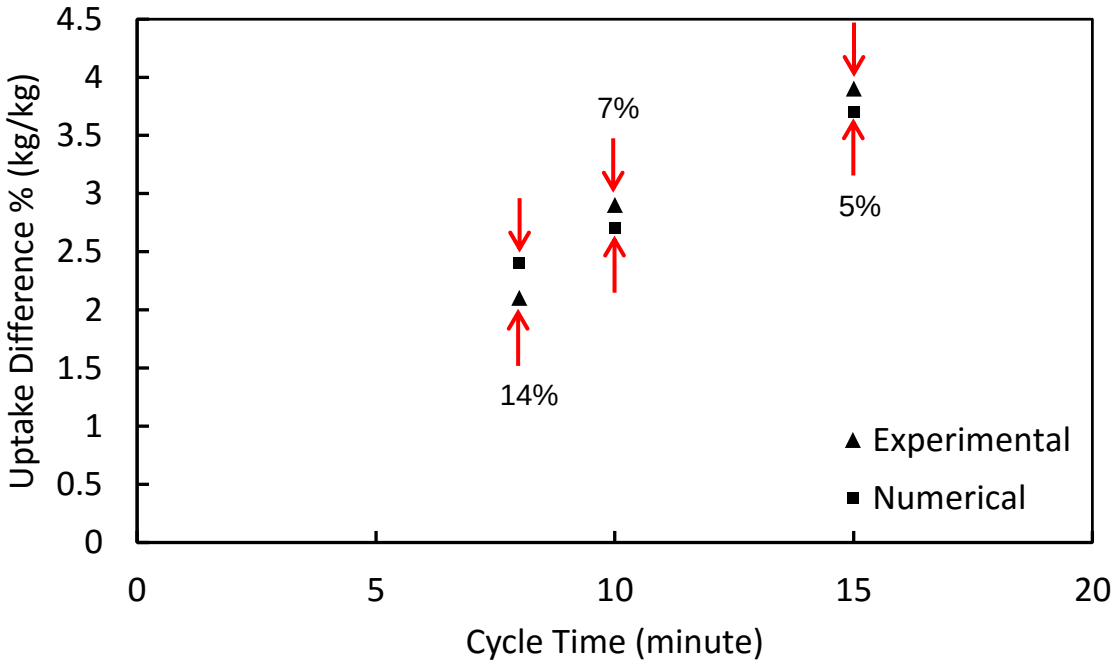

Figure 4-7 comparison between numerical and experimental data for cyclic operation of the adsorption cooling system.

4.8. Parametric study on the thermal conductivity of the adsorbent

Thermal performance of an adsorber bed can be increased by increasing the effective thermal conductivity of the adsorbent. The effective thermal conductivity in an adsorber bed is divided between the bulk resistance and the contact resistance. The bulk resistance can be decreased by adding thermally conductive material to the adsorbent [67], and contact resistance can be decreased by using a coating instead of a loose grain material [123]. In this section the effects of adding graphite as a highly conductive material to the working pair of water and FAM-Z02 adsorbent is studied. Although adding graphite to the adsorbent increases the effective thermal conductivity, it decreases the amount of

active material in the bed. Therefore, it is important to perform a parametric study to see how adding graphite flakes to the adsorbent can affect the thermal performance of the adsorber bed. The previous geometry was chosen for the parametric study, however, it was assumed that the evaporator and condenser are ideal (i.e. the pressure of the evaporator and condenser is constant over time and is not affected by the adsorber bed). In addition, it was assumed that heating and cooling down the adsorber bed is performed with an ideal heat transfer fluid, which does not have thermal inertia. The changes in the thermal conductivity of dry FAM-Z02 as a result of adding different amount of graphite flakes was based on transient plane source (TPS) measurements as shown in Table 4-3.

Table 4-3 Thermal conductivity enhancement with respect to mass percentage of added graphite

Mass percentage of graphite (%)	Thermal conductivity (W/m·K)
0	0.266
5	0.310
10	0.363
20	0.594

The results (Table 4-4 and Figure 4-8) show that, although adding graphite increases thermal efficiency of the adsorber bed, the overall performance of the bed is decreased due to the decreased amount of active material. Heat transfer can be evaluated by calculating the average temperature in the midsection of the adsorbent. This parameter shows how much hotter or colder the bed gets as a result of the increased thermal conductivity of the adsorbent. The difference between the average temperature at the midsection of the adsorbent for different amount of graphite additive and cycle times is shown in Table 4-4. It must be noted that although this temperature difference relatively small value, it is occurring in 1.2 millimeters.

Table 4-4 Temperature difference in midsection of adsorbent for different amounts of graphite additive compared to the sample without graphite

Cycle time (s)	0% graphite	5% graphite	10% graphite	20% graphite
480	0 °C	0.2 °C	0.5 °C	1.1 °C
600	0 °C	0.2 °C	0.5 °C	1.1 °C
900	0 °C	0.2 °C	0.5 °C	1.1 °C

To study the performance of the adsorber bed, changes in uptake were monitored for different cycle times and different amounts of graphite flake. By comparing the amount of adsorbed water, see Figure 4-8, it can be seen that the performance of the system is decreased by the addition of graphite. This is because graphite, which cannot adsorb water, is replacing the active adsorbent.

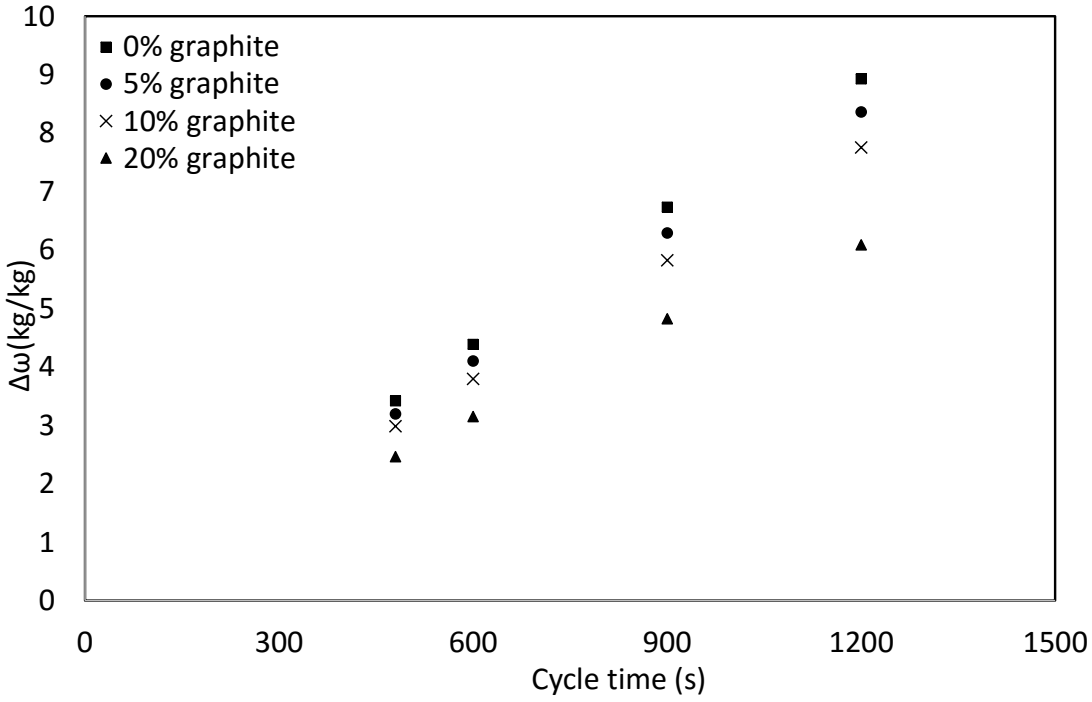

Figure 4-8 the difference between the maximum and minimum value of uptake in cyclic operation for different amount of graphite additive

4.9. Graphite adsorber beds

One of the hot topics in the field of adsorption cooling systems is using heat exchangers made out of graphite. Graphite shows high thermal conductivity in the through-plane direction, while they have low thermal conductivity in in-plane direction. Graphite heat exchangers can be used in adsorption cooling application as they show high corrosion resistance and most adsorbents can be easily coated onto graphite sheet. As a part of this research, a comparison was made between the performance of a graphite heat exchanger and aluminum heat exchanger with the same geometry. A 2D axisymmetric geometry was assumed for both heat exchangers the same thermal contact resistance and dimensions were assumed for both cases. A schematic of the studied geometry is illustrated in Figure 4-9.

Figure 4-9 schematic of axisymmetric geometry studied for comparison between aluminum heat exchanger and graphite heat exchanger

To compare these two cases, the uptake value of the adsorbent was studied at different cycle times. It was assumed that the evaporator and condenser were working ideally, i.e. their pressure will be equal to saturation pressure of water at their operating temperature. The applied boundary conditions for a 5 minute cycle time are shown in Figure 4-10. At each multiple of half the cycle time (here 150s), the pressure at the outlet and the temperature at the pipe are changing to the adsorption or desorption condition.

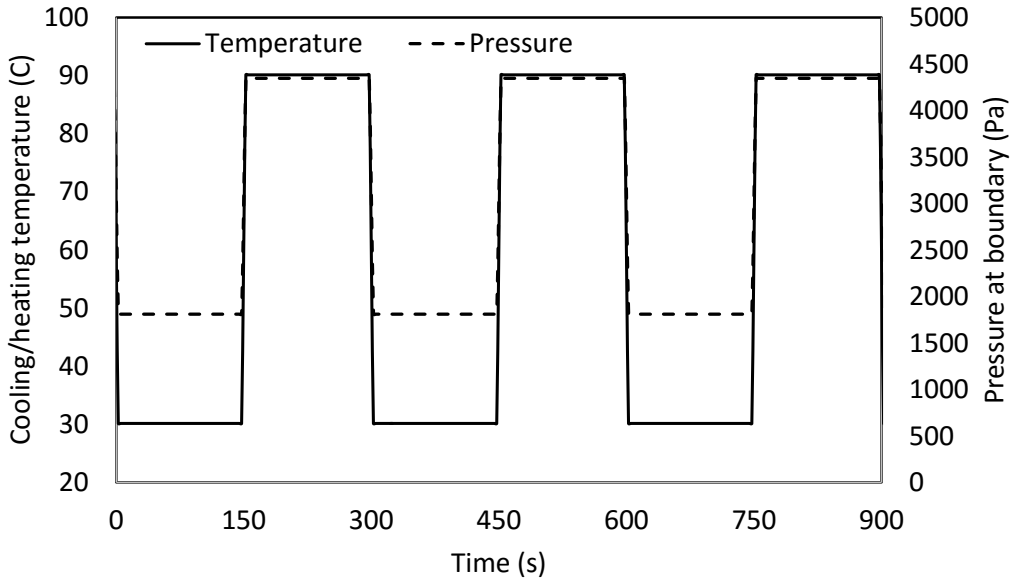

Figure 4-10 Boundary conditions applied to evaporator and heat transfer fluid in comparison between aluminum HEX and graphite HEX (τ=300s)

The changes in uptake value over time for a 5 minute cycle time are shown in Figure 4-11. Although the boundary conditions are changing at multiples of half the cycle time, there is a delay in uptake. This delay occurs due to thermal inertia of the system.

Once the boundary condition is changed, a few seconds are required to see the effects of this change at the boundaries. It must be noted that the parameter that should be measured is not the difference between maximum and minimum of the uptake, because right after changing from adsorption to desorption, the adsorber bed in disconnected from evaporator and cooling effect cannot be provided at evaporator. The thermal inertia of the aluminum heat exchanger is higher than the thermal inertia of the graphite heat exchanger (due to higher density and thermal capacity of aluminum), therefore, it is expected that the graphite heat exchanger performs better compared to aluminum. Based on the modeling results, for 5 minute cycle time, the performance of the graphite HEX is about 31% higher than aluminum heat exchanger. It is expected that the effects of the thermal inertia of the heat exchanger decrease with increasing cycle time. The difference between the performance of the graphite HEX and the aluminum HEX for different cycle time is shown in Table 4-5.

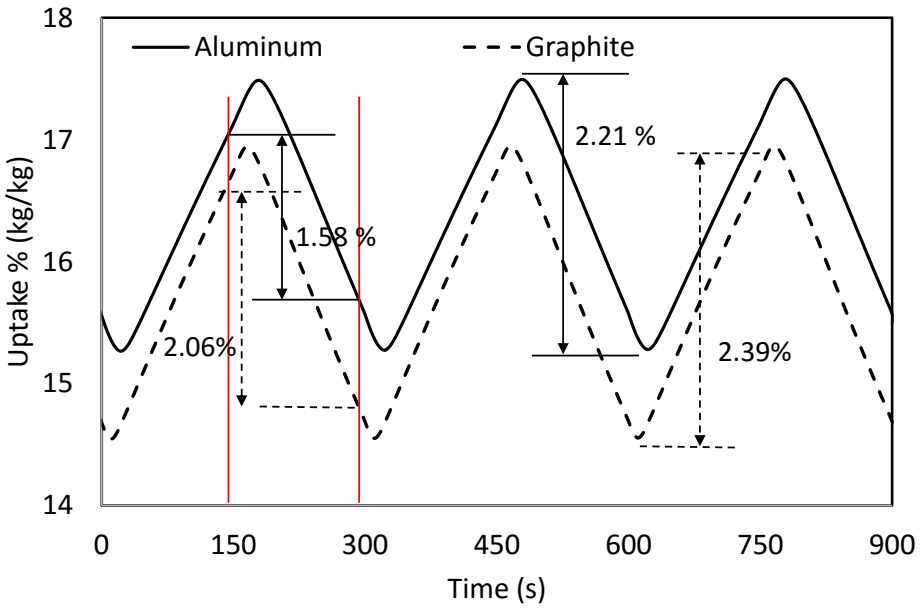

Figure 4-11 Uptake change over time for an aluminum HEX and a graphite HEX (τ=300s)

Table 4-5 Comparison of uptake value between an aluminum HEX and a graphite HEX

Cycle time (s)	Δω (kg/kg %)		Difference
	Aluminum HEX	Graphite Hex	
300	1.58 %	2.02 %	27.8 %
480	3.11 %	3.56 %	14.5 %
600	4.12 %	4.62 %	12.1 %
900	6.57 %	7.05 %	7.3 %

As the next step, a comparison between two different graphite heat exchanger was made. In this model, it was assumed one graphite heat exchanger has fins with in-plane thermal conductivity of 200 (W/m·K) and through-plane thermal conductivity of 5 (W/m·K) and one isotropic graphite heat exchanger has a thermal conductivity of 200 (W/m·K). The same boundary conditions and cycle times were applied to these two heat exchanger to study the effect of the low thermal conductivity of graphite in the through-plane direction. Based on the results from the numerical model, shown in Table 4-6, it can be seen that though-plane thermal conductivity does not play a major role in heat transfer inside an adsorber bed. Heat transfer in an adsorber bed is mostly limited by heat transfer in the adsorber material and the low thermal conductivity of graphite in the through-plane direction contributes much less to the total thermal resistance. Performance enhancement from using isotropic material is minimal, which shows that the low through-plane thermal conductivity is not an important factor for use in adsorber beds.

Table 4-6 Comparison between isotropic and anisotropic graphite

Cycle Time (s)	Δω of anisotropic graphite (kg/kg %)	Δω of isotropic graphite (kg/kg %)	Enhancement
300	2.02 %	2.06 %	2.0 %
480	3.56 %	3.60 %	1.1 %
600	4.62 %	4.67 %	1.1 %
900	7.05 %	7.10 %	0.7 %

4.10. Discussion

Based on the comparison made between the numerical and experimental data, it can be concluded that numerical model can predict the performance of an adsorber bed at different working conditions. The developed UDF can be implemented into any geometry, with any boundary conditions, and give insight about the performance of the adsorber bed. Using this model, a sensitivity analysis and a parametric study can be performed. As an example there are numerous studies focused on improving the thermal conductivity of adsorbent material. Using this model, the effects of changes in the thermal conductivity of an adsorbent can be investigated and light shed on the importance of that parameter.

Although adsorption process is a very complex phenomenon and several factors play role in its dynamics, it is shown that numerical modeling can be a useful tool for predicting the performance of these systems [111].

Chapter 5. Conclusion and future work

This research was focused on modeling and testing an adsorber bed for use in mobile applications. Two different setups for testing two adsorber bed designs were built and tested. In addition, a numerical model was developed that can predict the performance of adsorber bed at different conditions.

5.1. Experimental work

An in-situ mass measurement test setup was developed, built, and tested. Two different heat exchanger designs were studied and compared. The effects of different adsorber bed designs on the performance of an ACS were studied by in-situ water uptake rate measurements of FAM-Z02. The results of a comprehensive literature review showed that large-scale adsorbate uptake rate mass measurements could result in closer performance prediction of an ACS than the adsorbate uptake rate measurements from a TGA. TGA measurements are based on mass change of few milligrams of adsorbent under controlled pressure and temperature, however, in actual adsorber bed desorption and desorption occur under large pressure jumps and non-isothermal conditions. In addition, the TGA result does not include the effects of adsorber bed geometry, interparticle mass transfer resistances, and pressure drop, because the sample size in a TGA is on the order of milligrams. These differences between the TGA and the actual adsorber bed lead to lower performance of adsorber bed compared to the value expected from the TGA measurements. This claim has been also made by N'Tsoukpoe et al. where they say “a common mistake consists in TGA/DSC (thermogravimetric analysis/differential scanning calorimetry) measurements using very small amounts of materials while the story would be very different at large scale” [124].

In addition, other issues affected the mass measurements, such as changes in the density of the heat transfer fluid and variations in the stiffness of the flexible hosing connected to the adsorber beds. In this study, a systematic procedure was introduced to de-convolute these parameters from the in-situ mass measurements to get a precise adsorbate uptake rate and uptake difference measurements. The performance of an ACS

was studied under different cycle times and the results showed that high heat transfer surface area and small fin spacing were key features of a good adsorber bed design for ACS applications. Finally, the results indicated that a combination of high quality adsorbent (FAM-Z02) and a well-designed adsorber bed could produce a SCP_{ideal} of 112.9 W/kg and a COP_{ideal} of 0.34 at cycle time of 10 min.

5.2. Numerical modelling

A full three-dimensional computational fluid dynamic model was developed. The model was based finite volume method and was developed in ANSYS Fluent. The user defined function was developed in the C programing language to create unsteady nonlinear source terms for the mass and heat transfer equations. The code can be used for FAM-Z02, RD silica gel and silica gel confined with $CaCl_2$. The developed code can be used in any geometry (2D and 3D) regardless of boundary conditions. A parametric study was performed using the numerical model. The results show that although thermal conductivity plays an important role in heat transfer of adsorber bed, it is not the only parameter to look into. It was shown that if thermal conductivity improvement is performed by adding some non-adsorptive material like graphite, it could decrease the adsorption performance of the adsorber bed. It was also shown that using a graphite heat exchanger can improve the overall performance of the adsorber bed due to the lower thermal inertia of graphite compared to copper or aluminum.

5.3. Future work

The following topics and concerns can be addressed as the continuation of the experimental part of this dissertation:

1. In-situ mass measurements for different working conditions. Effects of cooling and heating fluid temperature, as well as chilled water temperature and condenser temperature can be studied in in-situ mass measurements.
2. Testing different designs for evaporator and condenser. In this study a chamber worked as evaporator and condenser at the same time. Performance assessment of adsorber bed connected to different designs of evaporator and condenser can be performed.

The following studies can be performed using the numerical model:

1. Adding the effects of uptake value on thermal properties of an adsorbent. Although thermal properties of materials were assumed to be a function of temperature and pressure, the effects of water content in the adsorber was not added into the model. This could be a factor, especially to the thermal capacity of the adsorbent, as water has high thermal capacity and the effective thermal capacity of the wet material can be different from the dry material. Water content can also affect effective thermal conductivity of the medium.
2. Studying the effects of the ideal evaporator and condenser. Boundary conditions of this study were driven by the experimental data. An ideal evaporator and condenser can supply a constant pressure through adsorption and desorption, while pressure in the actual evaporator and condenser is affected by the adsorber bed. A study can be performed to see the effects of an ideal evaporator and condenser and find out the importance of each component in this cycle.

References

[1] J.S. Sim, J.S. Ha, Experimental study of heat transfer characteristics for a refrigerator by using reverse heat loss method, Int. Commun. Heat Mass Transf. 38 (2011) 572–576.

[2] P. Goyal, P. Baredar, A. Mittal, A.R. Siddiqui, Adsorption refrigeration technology - An overview of theory and its solar energy applications, Renew. Sustain. Energy Rev. 53 (2016) 1389–1410.

[3] C.F. Pinnola, J.V.C. Vargas, C.L. Buiar, J.C. Ordonez, Energy consumption reduction in existing HVAC-R systems via a power law controlling kit, Appl. Therm. Eng. 82 (2015) 341–350.

[4] J. Farrington, R; Rugh, Impact of vehicle air-conditioning on fuel economy, tailpipe emissions, and electric vehicle range, in: Proceeding Earth Technol. Forum. Washington, DC, 2000.

[5] B.O. Bolaji, Z. Huan, Ozone depletion and global warming: Case for the use of natural refrigerant - A review, Renew. Sustain. Energy Rev. 18 (2013) 49–54.

[6] V. Oruç, A.G. Devecioğlu, U. Berk, İ. Vural, Experimental comparison of the energy parameters of HFCs used as alternatives to HCFC-22 in split type air conditioners, Int. J. Refrig. 63 (2016) 125–132.

[7] J.M. Mendoza-Miranda, A. Mota-Babiloni, J. Navarro-Esbrí, Evaluation of R448A and R450A as low-GWP alternatives for R404A and R134a using a micro-fin tube evaporator model, Appl. Therm. Eng. 98 (2016) 330–339.

[8] Z. Yang, L. Kou, J. Lu, W. Zhang, W. Mao, J. Lu, Isothermal vapor–liquid equilibria measurements for binary systems of 2,3,3,3-tetrafluoropropene (HFO-1234yf) + 2-chloro-3,3,3-trifluoropropene (HCFO-1233xf) and 2-chloro-3,3,3-trifluoropropene (HCFO-1233xf) + 2-chloro-1,1,1,2-tetrafluoropropane (HCFC-244, Fluid Phase Equilib. 414 (2016) 143–148.

[9] K. Assawamartbunlue, M.J. Brandemuehl, K. Assawamartbunlue, Refrigerant Leakage Detection and Diagnosis for a Distributed Refrigeration System.pdf, 9669 (2016).

[10] M. Aneke, B. Agnew, C. Underwood, M. Menkiti, Thermodynamic analysis of alternative refrigeration cycles driven from waste heat in a food processing application, Int. J. Refrig. 35 (2012) 1349–1358.

[11] M. Cengel, YA; Boles, Thermodynamcis: An Engineering Approach, 6th ed., McGraw-Hill, New York, 2006.

[12] M. a. Karri, E.F. Thacher, B.T. Helenbrook, Exhaust energy conversion by thermoelectric generator: Two case studies, Energy Convers. Manag. 52 (2011) 1596–1611.

[13] D.S. Kim, C. a. Infante Ferreira, Solar refrigeration options – a state-of-the-art review, Int. J. Refrig. 31 (2008) 3–15.

[14] A. Sharafianardakani, Waste heat-driven adsorption cooling systems for vehicle air conditioning applications, 2015.

[15] P. Boatto, C. Boccaletti, G. Cerri, C. Malvicino, Internal combustion engine waste heat potential for an automotive absorption system of air conditioning Part 1: tests on the exhaust system of a spark-ignition engine, Proc. I MECH E Part D J. Automob. Eng. 214 (2000) 979–982.

[16] P. Boatto, C. Boccaletti, G. Cerri, C. Malvicino, Internal combustion engine waste heat potential for an automotive absorption system of air conditioning Part 2: The automotive absorption system, Proc. Inst. Mech. Eng. Part D J. Automob. Eng. 214 (2000) 983–989.

[17] T.H.C. Yeo, I. a. W. Tan, M.O. Abdullah, Development of adsorption air-conditioning technology using modified activated carbon – A review, Renew. Sustain. Energy Rev. 16 (2012) 3355–3363.

[18] H.Z. Hassan, A. a. Mohamad, A review on solar-powered closed physisorption cooling systems, Renew. Sustain. Energy Rev. 16 (2012) 2516–2538.

[19] L. Montastruc, P. Floquet, V. Mayer, I. Nikov, S. Domenech, Kinetic Modeling of Isothermal or Non-isothermal Adsorption in a Pellet: Application to Adsorption Heat Pumps, Chinese J. Chem. Eng. 18 (2010) 544–553.

[20] T.X. Li, R.Z. Wang, J.K. Kiplagat, L.W. Wang, R.G. Oliveira, A conceptual design and performance analysis of a triple-effect solid–gas thermochemical sorption refrigeration system with internal heat recovery, Chem. Eng. Sci. 64 (2009) 3376–3384.

[21] K.R. Ullah, R. Saidur, H.W. Ping, R.K. Akikur, N.H. Shuvo, A review of solar thermal refrigeration and cooling methods, Renew. Sustain. Energy Rev. 24 (2013) 499–513.

[22] R.I. Masel, Principles of Adsorption and Reaction on Solid Surfaces, John Wiley & Sons, Inc., 1996.

[23] H. Demir, M. Mobedi, S. Ülkü, A review on adsorption heat pump: Problems and solutions, Renew. Sustain. Energy Rev. 12 (2008) 2381–2403.

[24] D.M. Nevskaia, E. Castillejos-Lopez, A. Guerrero-Ruiz, V. Muñoz, Effects of the

surface chemistry of carbon materials on the adsorption of phenol–aniline mixtures from water, Carbon N. Y. 42 (2004) 653–665.

[25] C. Sangwichien, G.. Aranovich, M.. Donohue, Density functional theory predictions of adsorption isotherms with hysteresis loops, Colloids Surfaces A Physicochem. Eng. Asp. 206 (2002) 313–320.

[26] K. Nakai, J. Sonoda, H. Iegami, H. Naono, High precision volumetric gas adsorption apparatus, Adsorption. 11 (2005) 227–230.

[27] D.M. Pan, M. Jaroniec, Adsorption and thermogravimetric studies of unmodified and oxidized active carbons, Langmuir. 12 (1996) 3657–3665.

[28] R.Z. Wang, Z.Z. Xia, L.W. Wang, Z.S. Lu, S.L. Li, T.X. Li, et al., Heat transfer design in adsorption refrigeration systems for efficient use of low-grade thermal energy, Energy. 36 (2011) 5425–5439.

[29] E.E. Anyanwu, Review of solid adsorption solar refrigeration II: An overview of the priciples and theory, Energy Convers. Manag. 45 (2004) 1279–1295.

[30] Z. Lu, R. Wang, Z. Xia, L. Gong, Experimental investigation adsorption chillers using micro-porous silica gel–water and compound adsorbent-methanol, Energy Convers. Manag. 65 (2013) 430–437.

[31] R.P. Sah, B. Choudhury, R.K. Das, A review on adsorption cooling systems with silica gel and carbon as adsorbents, Renew. Sustain. Energy Rev. 45 (2015) 123–134.

[32] L.W. Wang, R.Z. Wang, R.G. Oliveira, A review on adsorption working pairs for refrigeration, Renew. Sustain. Energy Rev. 13 (2009) 518–534.

[33] D.C. Wang, Y.H. Li, D. Li, Y.Z. Xia, J.P. Zhang, A review on adsorption refrigeration technology and adsorption deterioration in physical adsorption systems, Renew. Sustain. Energy Rev. 14 (2010) 344–353.

[34] A. a. Askalany, M. Salem, I.M. Ismael, A.H.H. Ali, M.G. Morsy, B.B. Saha, An overview on adsorption pairs for cooling, Renew. Sustain. Energy Rev. 19 (2013) 565–572.

[35] N.C. Srivastava, I.W. Eames, A review of adsorbents and adsorbates in solid–vapour adsorption heat pump systems, Appl. Therm. Eng. 18 (1998) 707–714.

[36] D. Menard, X. Py, N. Mazet, Activated carbon monolith of high thermal conductivity for adsorption processes improvement: Part A: Adsorption step, Chem. Eng. Process. Process Intensif. 44 (2005) 1029–1038.

[37] B.B. Saha, I.I. El-Sharkawy, a. Chakraborty, S. Koyama, Study on an activated

carbon fiber–ethanol adsorption chiller: Part I – system description and modelling, Int. J. Refrig. 30 (2007) 86–95.

[38] U. Jakob, W. Mittelbach, Development and investigation of a compact silica gel/water adsorption chiller integrated in solar cooling systems, VII Minsk Int. Semin. “Heat Pipes, Heat Pumps, Refrig. Power Sources.” (2008).

[39] H. Demir, M. Mobedi, S. Ülkü, Effects of porosity on heat and mass transfer in a granular adsorbent bed, Int. Commun. Heat Mass Transf. 36 (2009) 372–377.

[40] I.S. Glaznev, Y.I. Aristov, The effect of cycle boundary conditions and adsorbent grain size on the water sorption dynamics in adsorption chillers, Int. J. Heat Mass Transf. 53 (2010) 1893–1898.

[41] T. Eun, H. Song, J. Hun, K. Lee, J. Kim, Enhancement of heat and mass transfer in silica-expanded graphite composite blocks for adsorption heat pumps : Part I . Characterization of the composite blocks, Int. J. Refrig. 23 (2000) 64–73.

[42] a. Freni, L. Bonaccorsi, E. Proverbio, G. Maggio, G. Restuccia, Zeolite synthesised on copper foam for adsorption chillers: A mathematical model, Microporous Mesoporous Mater. 120 (2009) 402–409.

[43] G.. Cacciola, G. Restuccia, Progress on adsorption heat pumps, Heat Recover. Syst. CHP. 14 (1994) 409–420.

[44] S.C. Sugarman, HVAC Fundamentals, The Fairmont Press, Inc., 2004.

[45] M. Afshin, A. Sohankar, M. Dehghan Manshadi, M. Kazemi Esfeh, An experimental study on the evaluation of natural ventilation performance of a two-sided wind-catcher for various wind angles, Renew. Energy. 85 (2016) 1068–1078.

[46] L. Jian, Designing, Modeling, Monitoring and Control of Air Conditioning Systems, The Chinese University of Hong Kong, 2006.

[47] A. Sharafian, C. McCague, M. Bahrami, Impact of fin spacing on temperature distribution in adsorption cooling system for vehicle A/C applications, Int. J. Refrig. 51 (2015) 135–143.

[48] Z.Z. Xia, R.Z. Wang, D.C. Wang, Y.L. Liu, J.Y. Wu, C.J. Chen, Development and comparison of two-bed silica gel–water adsorption chillers driven by low-grade heat source, Int. J. Therm. Sci. 48 (2009) 1017–1025.

[49] A.R. Masoud Rezk, Theoretical and experimental investigation of silica gel / water adsorption refrigeration systems, University of Birmingham, 2012.

[50] X. Wang, H.T. Chua, A comparative evaluation of two different heat-recovery schemes as applied to a two-bed adsorption chiller, Int. J. Heat Mass Transf. 50

(2007) 433–443.

[51] Z.S. Lu, R.Z. Wang, L.W. Wang, Dynamic characteristics of a novel adsorption refrigerator with compound mass-heat recovery, Int. J. ENERGY Res. 37 (2013) 59–68.

[52] Z.S. Lu, R.Z. Wang, Performance improvement and comparison of mass recovery in CaCl2/activated carbon adsorption refrigerator and silica gel/LiCl adsorption chiller driven by low grade waste heat, Int. J. Refrig. (2013).

[53] G. Maggio, a. Freni, G. Restuccia, A dynamic model of heat and mass transfer in a double-bed adsorption machine with internal heat recovery, Int. J. Refrig. 29 (2006) 589–600.

[54] R.Z.Z. Wang, Performance improvement of adsorption cooling by heat and mass recovery operation, Int. J. Refrig. 24 (2001) 602–611.

[55] A. Akahira, K.C. a. Alam, Y. Hamamoto, A. Akisawa, T. Kashiwagi, Mass recovery adsorption refrigeration cycle—improving cooling capacity, Int. J. Refrig. 27 (2004) 225–234.

[56] Z.S. Lu, L.W. Wang, R.Z. Wang, Experimental analysis of an adsorption refrigerator with mass and heat-pipe heat recovery process, Energy Convers. Manag. 53 (2012) 291–297.

[57] Y.L. Liu, R.Z. Wang, Z.Z. Xia, Experimental performance of a silica gel–water adsorption chiller, Appl. Therm. Eng. 25 (2005) 359–375.

[58] C.J. Chen, R.Z. Wang, Z.Z. Xia, J.K. Kiplagat, Study on a silica gel–water adsorption chiller integrated with a closed wet cooling tower, Int. J. Therm. Sci. 49 (2010) 611–620.

[59] I. Daßler, W. Mittelbach, Solar cooling with adsorption chillers, Energy Procedia. 30 (2012) 921–929.

[60] B.B. Saha, S. Koyama, J.B. Lee, K. Kuwahara, K.C. a. Alam, Y. Hamamoto, et al., Performance evaluation of a low-temperature waste heat driven multi-bed adsorption chiller, Int. J. Multiph. Flow. 29 (2003) 1249–1263.

[61] M.Z.I. Khan, B.B. Saha, K.C. a. Alam, a. Akisawa, T. Kashiwagi, Study on solar/waste heat driven multi-bed adsorption chiller with mass recovery, Renew. Energy. 32 (2007) 365–381.

[62] T. Miyazaki, A. Akisawa, B.B. Saha, The performance analysis of a novel dual evaporator type three-bed adsorption chiller, Int. J. Refrig. 33 (2010) 276–285.

[63] B.B. Saha, S. Koyama, K. Choon Ng, Y. Hamamoto, A. Akisawa, T. Kashiwagi,

Study on a dual-mode, multi-stage, multi-bed regenerative adsorption chiller, Renew. Energy. 31 (2006) 2076–2090.

[64] Y. Hamamoto, K.C. Amanul Alam, A. Akisawa, T. Kashiwagi, Performance evaluation of a two-stage adsorption refrigeration cycle with different mass ratio, Int. J. Refrig. 28 (2005) 344–352.

[65] M.Z.I. Khan, K.C. a. Alam, B.B. Saha, a. Akisawa, T. Kashiwagi, Performance evaluation of multi-stage, multi-bed adsorption chiller employing re-heat scheme, Renew. Energy. 33 (2008) 88–98.

[66] H. Demir, M. Mobedi, S. Ülkü, The use of metal piece additives to enhance heat transfer rate through an unconsolidated adsorbent bed, Int. J. Refrig. 33 (2010) 714–720.

[67] a. Rezk, R.K. Al-Dadah, S. Mahmoud, a. Elsayed, Effects of contact resistance and metal additives in finned-tube adsorbent beds on the performance of silica gel/water adsorption chiller, Appl. Therm. Eng. 53 (2012) 278–284.

[68] A. Sharafian, M. Bahrami, Assessment of adsorber bed designs in waste-heat driven adsorption cooling systems for vehicle air conditioning and refrigeration, Renew. Sustain. Energy Rev. 30 (2014) 440–451.

[69] A. Sharafian, P.C. Dan, W. Huttema, M. Bahrami, Performance analysis of a novel expansion valve and control valves designed for a waste heat-driven two-adsorber bed adsorption cooling system, Int. J. Refrig. 100 (2015) under review.

[70] B. Dawoud, On the Effect of Grain Size on the Kinetics of Water Vapor Adsorption and Desorption into/from Loose Pellets of FAM-Z02 under a Typical Operating Condition of Adsorption Heat Pumps, J. Chem. Eng. Japan. 40 (2007) 1298–1306.

[71] S.K. Henninger, F.P. Schmidt, H.-M. Henning, Water adsorption characteristics of novel materials for heat transformation applications, Appl. Therm. Eng. 30 (2010) 1692–1702.

[72] K. Okamoto, M. Teduka, T. Nakano, S. Kubokawa, H. Kakiuchi, The development of AQSOA water vapor adsorbent and AQSOA coated heat exchanger, in: Int. Symp. Innov. Mater. Process. Energy Syst., Singapor, 2010.

[73] M.J. Goldsworthy, Measurements of water vapour sorption isotherms for RD silica gel, AQSOA-Z01, AQSOA-Z02, AQSOA-Z05 and CECA zeolite 3A, Microporous Mesoporous Mater. 196 (2014) 59–67.

[74] A. Sharafian, S.M. Nemati Mehr, W. Huttema, M. Bahrami, Effects of different adsorber bed designs on in-situ water uptake rate measurements of AQSOA FAM-Z02 for vehicle air conditioning applications, Appl. Therm. Eng. 98 (2016) 568–574.

[75] B. Dawoud, Y.I. Aristov, Experimental study on the kinetics of water vapor sorption on selective water sorbents, silica gel and alumina under typical operating conditions of sorption heat pumps, Int. J. Heat Mass Transf. 46 (2003) 273–281.

[76] Y.I. Aristov, I.S. Glaznev, a. Freni, G. Restuccia, Kinetics of water sorption on SWS-1L (calcium chloride confined to mesoporous silica gel): Influence of grain size and temperature, Chem. Eng. Sci. 61 (2006) 1453–1458.

[77] Y.I. Aristov, B. Dawoud, I.S. Glaznev, a. Elyas, A new methodology of studying the dynamics of water sorption/desorption under real operating conditions of adsorption heat pumps: Experiment, Int. J. Heat Mass Transf. 51 (2008) 4966–4972.

[78] B. Dawoud, U. Vedder, E.-H. Amer, S. Dunne, Non-isothermal adsorption kinetics of water vapour into a consolidated zeolite layer, Int. J. Heat Mass Transf. 50 (2007) 2190–2199.

[79] I.S. Glaznev, Y.I. Aristov, Kinetics of water adsorption on loose grains of SWS-1L under isobaric stages of adsorption heat pumps: The effect of residual air, Int. J. Heat Mass Transf. 51 (2008) 5823–5827.

[80] B.N. Okunev, a. P. Gromov, V.L. Zelenko, I.S. Glaznev, D.S. Ovoshchnikov, L.I. Heifets, et al., Effect of residual gas on the dynamics of water adsorption under isobaric stages of adsorption heat pumps: Mathematical modelling, Int. J. Heat Mass Transf. 53 (2010) 1283–1289.

[81] I. Glaznev, D. Ovoshchnikov, Y.I. Aristov, Effect of Residual Gas on Water Adsorption Dynamics Under Typical Conditions of an Adsorption Chiller, Heat Transf. Eng. 31 (2010) 924–930.

[82] G. Storch, G. Reichenauer, F. Scheffler, a. Hauer, Hydrothermal stability of pelletized zeolite 13X for energy storage applications, Adsorption. 14 (2008) 275–281.

[83] L. Schnabel, M. Tatlier, F. Schmidt, A. Erdem-Şenatalar, Adsorption kinetics of zeolite coatings directly crystallized on metal supports for heat pump applications (adsorption kinetics of zeolite coatings), Appl. Therm. Eng. 30 (2010) 1409–1416.

[84] D.B. Riffel, U. Wittstadt, F.P. Schmidt, T. Núñez, F. a. Belo, A.P.F. Leite, et al., Transient modeling of an adsorber using finned-tube heat exchanger, Int. J. Heat Mass Transf. 53 (2010) 1473–1482.

[85] İ. Solmuş, C. Yamalı, B. Kaftanoğlu, D. Baker, A. Çağlar, Adsorption properties of a natural zeolite–water pair for use in adsorption cooling cycles, Appl. Energy. 87 (2010) 2062–2067.

[86] D.S. Ovoshchnikov, I.S. Glaznev, Y.I. Aristov, Water sorption by the calcium chloride/silica gel composite: The accelerating effect of the salt solution present in

the pores, Kinet. Catal. 52 (2011) 620–628.

[87] A. a. Askalany, M. Salem, I.M. Ismail, A.H.H. Ali, M.G. Morsy, Experimental study on adsorption–desorption characteristics of granular activated carbon/R134a pair, Int. J. Refrig. 35 (2012) 494–498.

[88] Y.I. Aristov, I.S. Glaznev, I.S. Girnik, Optimization of adsorption dynamics in adsorptive chillers : Loose grains configuration, Energy. 46 (2012) 484–492.

[89] Y.I. Aristov, Experimental and numerical study of adsorptive chiller dynamics: Loose grains configuration, Appl. Therm. Eng. 61 (2013) 841–847.

[90] A. Chakraborty, B. Baran, Y.I. Aristov, Dynamic behaviors of adsorption chiller : Effects of the silica gel grain size and layers, Energy. 78 (2014) 304–312.

[91] B. Dawoud, Water vapor adsorption kinetics on small and full scale zeolite coated adsorbers; A comparison, Appl. Therm. Eng. (2011) 1–7.

[92] L. Gordeeva, A. Frazzica, A. Sapienza, Y.I. Aristov, A. Freni, Adsorption cooling utilizing the “LiBr/silica – ethanol” working pair: Dynamic optimization of the adsorber/heat exchanger unit, Energy. 75 (2014) 390–399.

[93] S. Santamaria, A. Sapienza, A. Frazzica, A. Freni, I.S. Girnik, Y.I. Aristov, Water adsorption dynamics on representative pieces of real adsorbers for adsorptive chillers, Appl. Energy. 134 (2014) 11–19.

[94] A. Frazzica, G. Füldner, A. Sapienza, A. Freni, L. Schnabel, Experimental and theoretical analysis of the kinetic performance of an adsorbent coating composition for use in adsorption chillers and heat pumps, Appl. Therm. Eng. 73 (2014) 1022–1031.

[95] A. Sapienza, S. Santamaria, A. Frazzica, A. Freni, Y.I. Aristov, Dynamic study of adsorbers by a new gravimetric version of the Large Temperature Jump method, Appl. Energy. 113 (2014) 1244–1251.

[96] L. Gordeeva, Y.I. Aristov, Dynamic study of methanol adsorption on activated carbon ACM-35.4 for enhancing the specific cooling power of adsorptive chillers, Appl. Energy. 117 (2014) 127–133.

[97] A. Freni, L. Bonaccorsi, L. Calabrese, A. Caprì, A. Frazzica, A. Sapienza, SAPO-34 coated adsorbent heat exchanger for adsorption chillers, Appl. Therm. Eng. 82 (2015) 1–7.

[98] A. Sharafian, M. Bahrami, Critical analysis of thermodynamic cycle modeling of adsorption cooling systems for light-duty vehicle air conditioning applications, Renew. Sustain. Energy Rev. 48 (2014) Under review.

[99] L.M. Sun, N.B.E.N. Amar, F. Meunier, Numerical study on coupled heat and mass transfers in an adsorber with external fluid heating, Heat Recover. Syst. CHP. 15 (1995) 19–29.

[100] N.B. Amar, L.M. Sun, F. Meunier, Numerical analysis of adsorptive temperature wave regenerative heat pump, Appl. Therm. Eng. 16 (1996) 405–418.

[101] L.Z. Zhang, A three-dimensional non-equilibrium model for an intermittent adsorption cooling system, Sol. Energy. 69 (2000) 27–35.

[102] L. Marletta, G. Maggio, A. Freni, M. Ingrasciotta, G. Restuccia, A non-uniform temperature non-uniform pressure dynamic model of heat and mass transfer in compact adsorbent beds, Int. J. Heat Mass Transf. 45 (2002) 3321–3330.

[103] G. Restuccia, A. Freni, G. Maggio, A zeolite-coated bed for air conditioning adsorption systems: parametric study of heat and mass transfer by dynamic simulation, Appl. Therm. Eng. 22 (2002) 619–630.

[104] K.C. Leong, Y. Liu, Numerical study of a combined heat and mass recovery adsorption cooling cycle, Int. J. Heat Mass Transf. 47 (2004) 4761–4770.

[105] K.C. Leong, Y. Liu, Numerical modeling of combined heat and mass transfer in the adsorbent bed of a zeolite/water cooling system, Appl. Therm. Eng. 24 (2004) 2359–2374.

[106] Y. Liu, K.C. Leong, Numerical modeling of a zeolite/water adsorption cooling system with non-constant condensing pressure, Int. Commun. Heat Mass Transf. 35 (2008) 618–622.

[107] G.G. Ilis, M. Mobedi, S. Ülkü, A dimensionless analysis of heat and mass transport in an adsorber with thin fins; uniform pressure approach, Int. Commun. Heat Mass Transf. 38 (2011) 790–797.

[108] İ. Solmuş, D.A.S. Rees, C. Yamalı, D. Baker, B. Kaftanoğlu, Numerical investigation of coupled heat and mass transfer inside the adsorbent bed of an adsorption cooling unit, Int. J. Refrig. 35 (2012) 652–662.

[109] H. Niazmand, I. Dabzadeh, Numerical simulation of heat and mass transfer in adsorbent beds with annular fins, Int. J. Refrig. 35 (2012) 581–593.

[110] H. Talebian, H. Niazmand, M. Mahdavikhah, Numerical Modeling of Combined Heat and Mass Transfer in an Adsorbent Bed with Rectangular Fins, in: Int. Conf. Mech. Eng. Adv. Technol., 2012: pp. 1–7.

[111] A.O. Yurtsever, G. Karakas, Y. Uludag, Modeling and computational simulation of adsorption based chemical heat pumps, Appl. Therm. Eng. 50 (2013) 401–407.

[112] F. Poyelle, J.J. Guilleminot, F. Meunier, Experimental tests and predictive model of an adsorptive air conditioning unit, Ind. Eng. Chem. Res. 38 (1999) 298–309.

[113] Z. Tamainot-Telto, R.E. Critoph, Monolithic carbon for sorption refrigeration and heat pump applications, Appl. Therm. Eng. 21 (2001) 37–52.

[114] A. Freni, M.M. Tokarev, G. Restuccia, A.G. Okunev, Y.I. Aristov, Thermal conductivity of selective water sorbents under the working conditions of a sorption chiller, Appl. Therm. Eng. 22 (2002) 1631–1642.

[115] A. Sharafian, M. Bahrami, Adsorbate uptake and mass diffusivity of working pairs in adsorption cooling systems, Int. J. Heat Mass Transf. 59 (2013) 262–271.

[116] Y. Aristov, Concept of adsorbent optimal for adsorptive cooling/heating, Appl. Therm. Eng. 72 (2014) 166–175.

[117] S.S. Himooka, K.O. Shima, The evaluation of direct cooling and heating desiccant device coated with FAM, J. Chem. Eng. Japan. 40 (2007) 1330–1334.

[118] B.B. Saha, A. Chakraborty, S. Koyama, Y.I.I. Aristov, A new generation cooling device employing CaCl2-in-silica gel–water system, Int. J. Heat Mass Transf. 52 (2009) 516–524.

[119] Y.I.I. Aristov, A. Sapienza, D.S.S. Ovoshchnikov, A. Freni, G. Restuccia, Reallocation of adsorption and desorption times for optimisation of cooling cycles, Int. J. Refrig. 35 (2012) 525–531.

[120] M. Tatlıer, A. Erdem-Şenatalar, The effects of thermal and mass diffusivities on the performance of adsorption heat pumps employing zeolite synthesized on metal supports, Microporous Mesoporous Mater. 28 (1999) 195–203.

[121] A. Sharafian, K. Fayazmanesh, C. McCague, M. Bahrami, Thermal conductivity and contact resistance of mesoporous silica gel adsorbents bound with polyvinylpyrrolidone in contact with a metallic substrate for adsorption cooling system applications, Int. J. Heat Mass Transf. 79 (2014) 64–71.

[122] H. Demir, The effect of microwave regenerated adsorbent bed on the performance of an adsorption heat pump, Appl. Therm. Eng. 50 (2013) 134–142.

[123] D. Zhu, S. Wang, Experimental investigation of contact resistance in adsorber of solar adsorption refrigeration, Sol. Energy. 73 (2002) 177–185.

[124] K.E. N'Tsoukpoe, G. Restuccia, T. Schmidt, X. Py, The size of sorbents in low pressure sorption or thermochemical energy storage processes, Energy. 77 (2014) 983–998.

[125] N. Douss, F. Meunier, M. Douss, Experimental study of cascading adsorption

cycles, Chem. Eng. Sci. 44 (1989) 225–235.

[126] R.E. Critoph, Towards a one tonne per day solar ice maker, Renew. Energy. 9 (1996) 626–631.

[127] Z. Tamainot-Telto, R.E.E. Critoph, Adsorption refrigerator using monolithic carbon-ammonia pair, Int. J. Refrig. 20 (1997) 146–155.

[128] R.E. Critoph, Rapid cycling solar/biomass powered adsorption refrigeration system, Renew. Energy. 16 (1999) 673–678.

[129] K. Oertel, M. Fischer, Adsorption cooling system for cold storage using methanol/silicagel, Appl. Therm. Eng. 18 (1998) 773–786.

[130] L.Z. Zhang, L. Wang, Momentum and heat transfer in the adsorbent of a waste-heat adsorption cooling system, Energy. 24 (1999) 605–624.

[131] L.Z.L.Z. Zhang, L. Wang, Effects of coupled heat and mass transfers in adsorbent on the performance of a waste heat adsorption cooling unit, Appl. Therm. Eng. 19 (1999) 195–215.

[132] L.Z. Zhang, Design and testing of an automobile waste heat adsorption cooling system, Appl. Therm. Eng. 20 (2000) 103–114.

[133] S. Jiangzhou, R.Z. Wang, Y.Z. Lu, Y.X. Xu, J.Y. Wu, Experimental investigations on adsorption air-conditioner used in internal-combustion locomotive driver-cabin, Appl. Therm. Eng. 22 (2002) 1153–1162.

[134] Y.Z.Z. Lu, R.Z.Z. Wang, S. Jianzhou, M. Zhang, Y.X. Xu, J.Y. Wu, Performance of a diesel locomotive waste-heat-powered adsorption air conditioning system, Adsorption. 10 (2004) 57–68.

[135] G. Restuccia, a. Freni, S. Vasta, Y.I. Aristov, Selective water sorbent for solid sorption chiller: experimental results and modelling, Int. J. Refrig. 27 (2004) 284–293.

[136] D. Magnetto, Thermally Operated Mobile Air Conditioning Systems, 2005.

[137] D.C. Wang, Z.Z. Xia, J.Y. Wu, R.Z. Wang, H. Zhai, W.D. Dou, Study of a novel silica gel–water adsorption chiller. Part I. Design and performance prediction, Int. J. Refrig. 28 (2005) 1073–1083.

[138] D.C. Wang, J.Y. Wu, Z.Z. Xia, H. Zhai, R.Z. Wang, W.D. Dou, Study of a novel silica gel–water adsorption chiller. Part II. Experimental study, Int. J. Refrig. 28 (2005) 1084–1091.

[139] D.C. Wang, Z.X. Shi, Q.R. Yang, X.L. Tian, J.C. Zhang, J.Y. Wu, Experimental research on novel adsorption chiller driven by low grade heat source, Energy Convers. Manag. 48 (2007) 2375–2381.

[140] G. Restuccia, A. Freni, F. Russo, S. Vasta, Experimental investigation of a solid adsorption chiller based on a heat exchanger coated with hydrophobic zeolite, Appl. Therm. Eng. 25 (2005) 1419–1428.

[141] G.Z. Yang, Z.Z. Xia, R.Z. Wang, D. Keletigui, D.C. Wang, Z.H. Dong, et al., Research on a compact adsorption room air conditioner, Energy Convers. Manag. 47 (2006) 2167–2177.

[142] L.W. Wang, R.Z. Wang, Z.S. Lu, C.J. Chen, J.Y. Wu, Comparison of the adsorption performance of compound adsorbent in a refrigeration cycle with and without mass recovery, Chem. Eng. Sci. 61 (2006) 3761–3770.

[143] Z.S. Lu, R.Z. Wang, L.W. Wang, C.J. Chen, Performance analysis of an adsorption refrigerator using activated carbon in a compound adsorbent, Carbon N. Y. 44 (2006) 747–752.

[144] C.J. Chen, R.Z. Wang, L.W. Wang, Z.S. Lu, Studies on cycle characteristics and application of split heat pipe adsorption ice maker, Energy Convers. Manag. 48 (2007) 1106–1112.

[145] A. Freni, F. Russo, S. Vasta, M. Tokarev, Y.I. Aristov, G. Restuccia, An advanced solid sorption chiller using SWS-1L, Appl. Therm. Eng. 27 (2007) 2200–2204.

[146] K. Daou, R.Z. Wang, Z.Z. Xia, G.Z. Yang, Experimental comparison of the sorption and refrigerating performances of a CaCl2 impregnated composite adsorbent and those of the host silica gel, Int. J. Refrig. 30 (2007) 68–75.

[147] A. Sapienza, S. Santamaria, A. Frazzica, A. Freni, Influence of the management strategy and operating conditions on the performance of an adsorption chiller, Energy. 36 (2011) 5532–5538.

[148] M. Verde, J.M. Corberan, R. de Boer, S. Smeding, Modelling of a waste heat driven silica gel/water adsorption cooling system comparison with experimental results, in: ISHPC Conf., Padua, Italy, 2011: pp. 7–8.

[149] D. Laurent, F. Meunier, Experimental temperature fronts for adsorptive heat pump applications, Appl. Therm. Eng. 16 (1996) 395–404.

[150] R.Z. Wang, J.Y. Wu, Y.X. Xu, W. Wang, Performance researches and improvements on heat regenerative adsorption refrigerator and heat pump, Energy Convers. Manag. 42 (2001) 233–249.

[151] Y.T. and W.S. R. Z. Wang, J. Y. Wu, Y. X. Xu, R.Z. Wang, J.Y. Wu, Y.X. Xu, Y.

Teng, W. Shi, Experimental on a continuous heat regenerative adsorption refrigerator using spiral plate heat exchanger as adsorbers, Appl. Therm. Eng. 18 (1998) 13–23.

[152] T.F. Qu, R.Z. Wang, W. Wang, Study on heat and mass recovery in adsorption refrigeration cycles, Appl. Therm. Eng. 21 (2001) 439–452.

[153] R.Z. Wang, Adsorption refrigeration research in Shanghai Jiao Tong University, Renew. Sustain. Energy Rev. 5 (2001) 1–37.

[154] D. Wang, J. Wu, H. Shan, R. Wang, W. Dechang, W. Jingyi, et al., Experimental study on the dynamic characteristics of adsorption heat pumps driven by intermittent heat source at heating mode, Appl. Therm. Eng. 25 (2005) 927–940.

[155] D. Wang, J. Wu, Influence of intermittent heat source on adsorption ice maker using waste heat, Energy Convers. Manag. 46 (2005) 985–998.

[156] R.G. Oliveira, V. Silveira, R.Z. Wang, Experimental study of mass recovery adsorption cycles for ice making at low generation temperature, Appl. Therm. Eng. 26 (2006) 303–311.

[157] R.E.E. Critoph, Simulation of a continuous multiple-bed regenerative adsorption cycle, Int. J. Refrig. 24 (2001) 428–437.

[158] R.E. Critoph, Multiple bed regenerative adsorption cycle using the monolithic carbon–ammonia pair, Appl. Therm. Eng. 22 (2002) 667–677.

[159] Z. Tamainot-Telto, R.E. Critoph, Advanced solid sorption air conditioning modules using monolithic carbon–ammonia pair, Appl. Therm. Eng. 23 (2003) 659–674.

[160] Z. Tamainot-Telto, S.J. Metcalf, R.E. Critoph, Novel compact sorption generators for car air conditioning, Int. J. Refrig. 32 (2009) 727–733.

[161] R.E. Critoph, Y. Zhong, Review of trends in solid sorption refrigeration and heat pumping technology, Proc. Inst. Mech. Eng. Part E J. Process Mech. Eng. 219 (2005) 285–300.

[162] S.J. Metcalf, Z. Tamainot-Telto, R.E. Critoph, Application of a compact sorption generator to solar refrigeration: Case study of Dakar (Senegal), Appl. Therm. Eng. 31 (2011) 2197–2204.

[163] X. Wang, H.T. Chua, K.C. Ng, Experimental investigation of silica gel–water adsorption chillers with and without a passive heat recovery scheme, Int. J. Refrig. 28 (2005) 756–765.

[164] A. Akahira, K.C.A. Alam, Y. Hamamoto, A. Akisawa, T. Kashiwagi, Mass recovery four-bed adsorption refrigeration cycle with energy cascading, Appl. Therm. Eng.

25 (2005) 1764–1778.

[165] K.C. a. Alam, M.Z.I. Khan, A.S. Uyun, Y. Hamamoto, A. Akisawa, T. Kashiwagi, Experimental study of a low temperature heat driven re-heat two-stage adsorption chiller, Appl. Therm. Eng. 27 (2007) 1686–1692.

[166] Y.L. Liu, R.Z. Wang, Z.Z. Xia, Experimental study on a continuous adsorption water chiller with novel design, Int. J. Refrig. 28 (2005) 218–230.

[167] D.C. Wang, Z.Z. Xia, J.Y. Wu, Design and performance prediction of a novel zeolite–water adsorption air conditioner, Energy Convers. Manag. 47 (2006) 590–610.

[168] A. Akahira, K.C.A. Alam, Y. Hamamoto, A. Akisawa, T. Kashiwagi, Experimental investigation of mass recovery adsorption refrigeration cycle, Int. J. Refrig. 28 (2005) 565–572.

[169] W.S. Chang, C.-C. Wang, C.-C. Shieh, Experimental study of a solid adsorption cooling system using flat-tube heat exchangers as adsorption bed, Appl. Therm. Eng. 27 (2007) 2195–2199.

[170] T. Núñez, W. Mittelbach, H.-M. Henning, Development of an adsorption chiller and heat pump for domestic heating and air-conditioning applications, Appl. Therm. Eng. 27 (2007) 2205–2212.

[171] G. Cacciola, G. Restuccia, Reversible adsorption heat pump: a thermodynamic model, Int. J. Refrig. 18 (1995) 100–106.

[172] H.T. Chua, K.C. Ng, A. Chakraborty, N.M. Oo, M.A. Othman, Adsorption Characteristics of Silica Gel + Water Systems, J. Chem. Eng. Data. 47 (2002) 1177–1181.

[173] Y.I. Aristov, M.M. Tokarev, G. Cacciola, G. Restuccia, Selective water sorbents for multiple applications, 1. CaCl2 confined in mesopores of silica gel: sorption properties, React. Kinet. Catal. Lett. 59 (1996) 325–333.

Appendix A.

UDF code used in ANSYS Fluent

```
#include "udf.h"
#include "math.h"
#include "unsteady.h"

/* Material Properties */
#define R_p_RD 3.75E-4              /*m*/
#define R_p_CaCl2 3.75E-4           /*m*/
#define R_p_FAM 9.5E-4              /*m*/

#define porosity 0.60

#define roh_ads_RD 800              /*kg/m^3*/
#define roh_ads_CaCl2 800           /*kg/m^3*/
#define roh_ads_FAM 750             /*kg/m^3*/


/* Cycle Parameters */
#define cycle_time 900.0          /*s*/
#define change_time 2               /*s*/
#define cycle_counts 300.0

/* Temperatures */
#define T_cond 30.0                 /*C*/
#define T_evap 15.0                 /*C*/
#define T_cooling 30.0              /*C*/
#define T_heating 90.0              /*C*/

/* Constants */
#define w_m_RD 0.45                 /*kg/kg*/
#define w_m_CaCl2 0.8               /*kg/kg*/
#define w_m_FAM 0.30                /*kg/kg*/

#define K0_RD 7.3E-11               /*mbar^-1*/
#define K0_CaCl2 2E-10              /*mbar^-1*/
#define K0_FAM 1.97604E-7

#define del_h_ads_RD 2693.0E3       /*J/kg*/
#define del_h_ads_CaCl2 2760.0E3    /*J/kg*/
#define del_h_ads_FAM 3350.0E3      /*J/kg*/

#define R_u 8.314                   /*J/mol/K*/
#define MW_ads 0.018                /*kg/mol*/

#define n_RD 12.0
#define n_CaCl2 1.1

#define D_s0_RD 2.54E-4             /*m^2/s*/
#define D_s0_CaCl2 2.54E-4          /*m^2/s*/
#define D_s0_FAM 35.0E-10            /*m^2/s*/
```

```
#define E_a_RD 42000.0              /*J/mol*/
#define E_a_CaCl2 42000.0           /*J/mol*/
#define E_a_FAM 8450                /*J/mol*/

/* Saturation Constants */
#define a_s 20.5896
#define b_s -5098.26


/*****************************************************************/
/*Unsteady term in uptake rate equatuion*/
/*****************************************************************/
DEFINE_UDS_UNSTEADY(my_uds_unsteady,c,t,i,apu,su)
{
real physical_dt, vol, rho, phi_old;
physical_dt = RP_Get_Real("physical-time-step");
vol = C_VOLUME(c,t);
rho = 1.0;                                  /*C_R_M1(c,t);*/
*apu = -rho*vol / physical_dt;              /*implicit part*/
phi_old = C_STORAGE_R(c,t,SV_UDSI_M1(i));
*su = rho*vol*phi_old/physical_dt;          /*explicit part*/
}
/*****************************************************************/
/*Source term in uptake rate equatuion*/
/*****************************************************************/
DEFINE_SOURCE(uptake_source_RD,c,t,dS,eqn)
{
real p_op,P_abs,const1,source,w_eq;
real k1,k2,k_m;

p_op = RP_Get_Real("operating-pressure");
P_abs = (C_P(c,t) + p_op) * 1.0E-2;             /*mbar*/
const1 = K0_RD * exp(del_h_ads_RD * MW_ads / (R_u * C_T(c,t))) * P_abs;
w_eq = const1 / pow(1.0 + pow((const1/w_m_RD),n_RD), 1.0/n_RD);
k1 = 15.0 * D_s0_RD / pow(R_p_RD,2.0);          /*1/s*/
k2 = E_a_RD / R_u;                              /*K*/
k_m = k1 * exp(-k2 / C_T(c,t));                 /*1/s*/

source = (1.0 - porosity) * k_m * (w_eq - C_UDSI(c,t,0));
dS[eqn] = (-k_m) * (1.0 - porosity);
return source;
}

DEFINE_SOURCE(uptake_source_CaCl2,c,t,dS,eqn)
{
real p_op,P_abs,const1,source,w_eq;
real k1,k2,k_m;

p_op = RP_Get_Real("operating-pressure");
P_abs = (C_P(c,t) + p_op) * 1.0E-2;         /*mbar*/
const1 = K0_CaCl2 * exp(del_h_ads_CaCl2 * MW_ads / (R_u * C_T(c,t))) * P_abs;
w_eq = w_m_CaCl2 * const1 / pow(1.0 + pow(const1,n_CaCl2), 1.0/n_CaCl2);
k1 = 15.0 * D_s0_CaCl2 / pow(R_p_CaCl2,2.0);    /*1/s*/
k2 = E_a_CaCl2 / R_u;                           /*K*/
k_m = k1 * exp(-k2 / C_T(c,t));                 /*1/s*/
```

```
source = (1.0 - porosity) * k_m * (w_eq - C_UDSI(c,t,0));
dS[eqn] = (-k_m) * (1.0 - porosity);
return source;
}

DEFINE_SOURCE(uptake_source_FAM,c,t,dS,eqn)
{
real p_op,P_abs,const1,const2,source,w_eq;
real k1,k2,k_m, p0, C1,C2,C3,C4,C5,C6,C7,C8,C9,C10,C11;

p0=100000.0;
C1=8442.0;
C2=11010.0;
C3=22494.0;
C4=29352.0;
C5=35460.0;
C6=39303.0;
C7=46491.0;
C8=53541.0;
C9=64641.0;
C10=67908.0;
C11=78372.0;

p_op = RP_Get_Real("operating-pressure");
P_abs = (C_P(c,t) + p_op);        /*Pa*/
const1 =
(pow((K0_FAM*P_abs/p0),(1.0))*exp(C1/C_T(c,t)))/(1.0)+(pow((K0_FAM*P_abs/p0),(2.0)
)*exp(C2/C_T(c,t)))/(1.0)+(pow((K0_FAM*P_abs/p0),(3.0))*exp(C3/C_T(c,t)))/(2.0)+
       (pow((K0_FAM*P_abs/p0),(4.0))*exp(C4/C_T(c,t)))/(6.0)+(pow((K0_FAM*P_abs/p0
),(5.0))*exp(C5/C_T(c,t)))/(24.0)+(pow((K0_FAM*P_abs/p0),(6.0))*exp(C6/C_T(c,t)))/
(120.0)+
       (pow((K0_FAM*P_abs/p0),(7.0))*exp(C7/C_T(c,t)))/(720.0)+(pow((K0_FAM*P_abs/
p0),(8.0))*exp(C8/C_T(c,t)))/(5040.0)+(pow((K0_FAM*P_abs/p0),(9.0))*exp(C9/C_T(c,t
)))/(40320.0)+
       (pow((K0_FAM*P_abs/p0),(10.0))*exp(C10/C_T(c,t)))/(362880.0)+(pow((K0_FAM*P
_abs/p0),(11.0))*exp(C11/C_T(c,t)))/(3628800.0);

const2 =
(pow((K0_FAM*P_abs/p0),(1.0))*exp(C1/C_T(c,t)))/(1.0)+(pow((K0_FAM*P_abs/p0),(2.0)
)*exp(C2/C_T(c,t)))/(2.0)+(pow((K0_FAM*P_abs/p0),(3.0))*exp(C3/C_T(c,t)))/(6.0)+
       (pow((K0_FAM*P_abs/p0),(4.0))*exp(C4/C_T(c,t)))/(24.0)+(pow((K0_FAM*P_abs/p
0),(5.0))*exp(C5/C_T(c,t)))/(120.0)+(pow((K0_FAM*P_abs/p0),(6.0))*exp(C6/C_T(c,t))
)/(720.0)+
       (pow((K0_FAM*P_abs/p0),(7.0))*exp(C7/C_T(c,t)))/(5040.0)+(pow((K0_FAM*P_abs
/p0),(8.0))*exp(C8/C_T(c,t)))/(40320.0)+(pow((K0_FAM*P_abs/p0),(9.0))*exp(C9/C_T(c
,t)))/(362880.0)+
       (pow((K0_FAM*P_abs/p0),(10.0))*exp(C10/C_T(c,t)))/(3628800.0)+(pow((K0_FAM*
P_abs/p0),(11.0))*exp(C11/C_T(c,t)))/(39916800.0);

w_eq = (w_m_FAM *const1)/((1.0+const2)*11.0);

k1 = 15.0 * D_s0_FAM/ pow(R_p_FAM,2.0);          /*1/s*/
k2 = E_a_FAM / R_u;                              /*K*/
k_m = k1 * exp(-1*k2 / C_T(c,t));                /*1/s*/
```

```
source = (1.0 - porosity) * k_m * (w_eq - C_UDSI(c,t,0));
dS[eqn] = (-k_m) * (1.0 - porosity);
return source;
}
/*****************************************************************/
/*Source term in continuity equatuion*/
/*****************************************************************/
DEFINE_SOURCE(continuity_source_RD,c,t,dS,eqn)
{
real p_op,w_eq,P_abs,const1,source;
real k1,k2,k_m;

p_op = RP_Get_Real("operating-pressure");
P_abs = (C_P(c,t) + p_op) * 1.0E-2;        /*mbar*/

const1 = K0_RD * exp (del_h_ads_RD * MW_ads / (R_u * C_T(c,t))) * P_abs;
w_eq = const1 / pow(1.0 + pow((const1/w_m_RD),n_RD), 1.0/n_RD);

k1 = 15.0 * D_s0_RD / pow(R_p_RD,2.0);   /*1/s*/
k2 = E_a_RD / R_u;                       /*K*/
k_m = k1 * exp(-k2 / C_T(c,t));          /*1/s*/

source = -(1.0 - porosity)* roh_ads_RD *  k_m * (w_eq - C_UDSI(c,t,0));
dS[eqn] = (1.0 - porosity)* roh_ads_RD * k_m;
return source;
}

DEFINE_SOURCE(continuity_source_CaCl2,c,t,dS,eqn)
{
real p_op,w_eq,P_abs,const1,source;
real k1,k2,k_m;

p_op = RP_Get_Real("operating-pressure");
P_abs = (C_P(c,t) + p_op) * 1.0E-2;/*mbar*/

const1 = K0_CaCl2 * exp (del_h_ads_CaCl2 * MW_ads / (R_u * C_T(c,t))) * P_abs;
w_eq = w_m_CaCl2 * const1 / pow(1.0 + pow(const1,n_CaCl2), 1.0/n_CaCl2);

k1 = 15.0 * D_s0_CaCl2 / pow(R_p_CaCl2,2.0); /*1/s*/
k2 = E_a_CaCl2 / R_u;                  /*K*/
k_m = k1 * exp(-k2 / C_T(c,t));  /*1/s*/

source = -(1.0 - porosity)* roh_ads_CaCl2 *  k_m * (w_eq - C_UDSI(c,t,0));
dS[eqn] = (1.0 - porosity)* roh_ads_CaCl2 * k_m;
return source;
}

DEFINE_SOURCE(continuity_source_FAM,c,t,dS,eqn)
{
real p_op,P_abs,const1,const2,source,w_eq;
real k1,k2,k_m, p0, C1,C2,C3,C4,C5,C6,C7,C8,C9,C10,C11;

p0=100000.0;
C1=8442.0;
C2=11010.0;
C3=22494.0;
```

```
C4=29352.0;
C5=35460.0;
C6=39303.0;
C7=46491.0;
C8=53541.0;
C9=64641.0;
C10=67908.0;
C11=78372.0;

p_op = RP_Get_Real("operating-pressure");
P_abs = (C_P(c,t) + p_op);        /*Pa*/
const1 =
(pow((K0_FAM*P_abs/p0),(1.0))*exp(C1/C_T(c,t)))/(1.0)+(pow((K0_FAM*P_abs/p0),(2.0)
)*exp(C2/C_T(c,t)))/(1.0)+(pow((K0_FAM*P_abs/p0),(3.0))*exp(C3/C_T(c,t)))/(2.0)+
       (pow((K0_FAM*P_abs/p0),(4.0))*exp(C4/C_T(c,t)))/(6.0)+(pow((K0_FAM*P_abs/p0
),(5.0))*exp(C5/C_T(c,t)))/(24.0)+(pow((K0_FAM*P_abs/p0),(6.0))*exp(C6/C_T(c,t)))/
(120.0)+
       (pow((K0_FAM*P_abs/p0),(7.0))*exp(C7/C_T(c,t)))/(720.0)+(pow((K0_FAM*P_abs/
p0),(8.0))*exp(C8/C_T(c,t)))/(5040.0)+(pow((K0_FAM*P_abs/p0),(9.0))*exp(C9/C_T(c,t
)))/(40320.0)+
       (pow((K0_FAM*P_abs/p0),(10.0))*exp(C10/C_T(c,t)))/(362880.0)+(pow((K0_FAM*P
_abs/p0),(11.0))*exp(C11/C_T(c,t)))/(3628800.0);

const2 =
(pow((K0_FAM*P_abs/p0),(1.0))*exp(C1/C_T(c,t)))/(1.0)+(pow((K0_FAM*P_abs/p0),(2.0)
)*exp(C2/C_T(c,t)))/(2.0)+(pow((K0_FAM*P_abs/p0),(3.0))*exp(C3/C_T(c,t)))/(6.0)+
       (pow((K0_FAM*P_abs/p0),(4.0))*exp(C4/C_T(c,t)))/(24.0)+(pow((K0_FAM*P_abs/p
0),(5.0))*exp(C5/C_T(c,t)))/(120.0)+(pow((K0_FAM*P_abs/p0),(6.0))*exp(C6/C_T(c,t))
)/(720.0)+
       (pow((K0_FAM*P_abs/p0),(7.0))*exp(C7/C_T(c,t)))/(5040.0)+(pow((K0_FAM*P_abs
/p0),(8.0))*exp(C8/C_T(c,t)))/(40320.0)+(pow((K0_FAM*P_abs/p0),(9.0))*exp(C9/C_T(c
,t)))/(362880.0)+
       (pow((K0_FAM*P_abs/p0),(10.0))*exp(C10/C_T(c,t)))/(3628800.0)+(pow((K0_FAM*
P_abs/p0),(11.0))*exp(C11/C_T(c,t)))/(39916800.0);

w_eq = (w_m_FAM *const1)/((1+const2)*11.0);


k1 = 15.0 * D_s0_FAM/ pow(R_p_FAM,2.0);          /*1/s*/
k2 = E_a_FAM / R_u;                            /*K*/
k_m = k1 * exp(-1*k2 / C_T(c,t));            /*1/s*/

source = -(1.0 - porosity)* roh_ads_FAM *  k_m * (w_eq - C_UDSI(c,t,0));
dS[eqn] = (1.0 - porosity)* roh_ads_FAM * k_m;
return source;
}


/************************************************************/
/*Source term in energy equatuion of solid porous material*/
/************************************************************/
DEFINE_SOURCE(energy_source_RD,c,t,dS,eqn)
{
real p_op,w_eq,P_abs,const1,source;
real k1,k2,k_m;
```

```
p_op = RP_Get_Real("operating-pressure");
P_abs = (C_P(c,t) + p_op) * 1.0E-2;/*mbar*/

const1 = K0_RD * exp (del_h_ads_RD * MW_ads / (R_u * C_T(c,t))) * P_abs;
w_eq = const1 / pow(1.0 + pow((const1/w_m_RD),n_RD), 1.0/n_RD);

k1 = 15.0 * D_s0_RD / pow(R_p_RD,2.0); /*1/s*/
k2 = E_a_RD / R_u;                    /*K*/
k_m = k1 * exp(-k2 / C_T(c,t));  /*1/s*/

source = (1.0 - porosity)* roh_ads_RD * del_h_ads_RD *  k_m * (w_eq -
C_UDSI(c,t,0));
dS[eqn] = -(1.0 - porosity)* roh_ads_RD * del_h_ads_RD * k_m;
return source;
}

DEFINE_SOURCE(energy_source_CaCl2,c,t,dS,eqn)
{
real p_op,w_eq,P_abs,const1,source;
real k1,k2,k_m;

p_op = RP_Get_Real("operating-pressure");
P_abs = (C_P(c,t) + p_op) * 1.0E-2;/*mbar*/

const1 = K0_CaCl2 * exp (del_h_ads_CaCl2 * MW_ads / (R_u * C_T(c,t))) * P_abs;
w_eq = w_m_CaCl2 * const1 / pow(1.0 + pow((const1),n_CaCl2), 1.0/n_CaCl2);

k1 = 15.0 * D_s0_CaCl2 / pow(R_p_CaCl2,2.0); /*1/s*/
k2 = E_a_CaCl2 / R_u;                    /*K*/
k_m = k1 * exp(-k2 / C_T(c,t));  /*1/s*/

source = (1.0 - porosity)* roh_ads_CaCl2 * del_h_ads_CaCl2 *  k_m * (w_eq -
C_UDSI(c,t,0));
dS[eqn] = -(1.0 - porosity)* roh_ads_CaCl2 * del_h_ads_CaCl2 * k_m;
return source;
}

DEFINE_SOURCE(energy_source_FAM,c,t,dS,eqn)
{
real p_op,P_abs,const1,const2,source,w_eq;
real k1,k2,k_m, p0, C1,C2,C3,C4,C5,C6,C7,C8,C9,C10,C11;

p0=100000;
p0=100000.0;
C1=8442.0;
C2=11010.0;
C3=22494.0;
C4=29352.0;
C5=35460.0;
C6=39303.0;
C7=46491.0;
C8=53541.0;
C9=64641.0;
C10=67908.0;
C11=78372.0;
```

```
p_op = RP_Get_Real("operating-pressure");
P_abs = (C_P(c,t) + p_op);        /*Pa*/
const1 =
(pow((K0_FAM*P_abs/p0),(1.0))*exp(C1/C_T(c,t)))/(1.0)+(pow((K0_FAM*P_abs/p0),(2.0)
)*exp(C2/C_T(c,t)))/(1.0)+(pow((K0_FAM*P_abs/p0),(3.0))*exp(C3/C_T(c,t)))/(2.0)+
       (pow((K0_FAM*P_abs/p0),(4.0))*exp(C4/C_T(c,t)))/(6.0)+(pow((K0_FAM*P_abs/p0
),(5.0))*exp(C5/C_T(c,t)))/(24.0)+(pow((K0_FAM*P_abs/p0),(6.0))*exp(C6/C_T(c,t)))/
(120.0)+
       (pow((K0_FAM*P_abs/p0),(7.0))*exp(C7/C_T(c,t)))/(720.0)+(pow((K0_FAM*P_abs/
p0),(8.0))*exp(C8/C_T(c,t)))/(5040.0)+(pow((K0_FAM*P_abs/p0),(9.0))*exp(C9/C_T(c,t
)))/(40320.0)+
       (pow((K0_FAM*P_abs/p0),(10.0))*exp(C10/C_T(c,t)))/(362880.0)+(pow((K0_FAM*P
_abs/p0),(11.0))*exp(C11/C_T(c,t)))/(3628800.0);

const2 =
(pow((K0_FAM*P_abs/p0),(1.0))*exp(C1/C_T(c,t)))/(1.0)+(pow((K0_FAM*P_abs/p0),(2.0)
)*exp(C2/C_T(c,t)))/(2.0)+(pow((K0_FAM*P_abs/p0),(3.0))*exp(C3/C_T(c,t)))/(6.0)+
       (pow((K0_FAM*P_abs/p0),(4.0))*exp(C4/C_T(c,t)))/(24.0)+(pow((K0_FAM*P_abs/p
0),(5.0))*exp(C5/C_T(c,t)))/(120.0)+(pow((K0_FAM*P_abs/p0),(6.0))*exp(C6/C_T(c,t))
)/(720.0)+
       (pow((K0_FAM*P_abs/p0),(7.0))*exp(C7/C_T(c,t)))/(5040.0)+(pow((K0_FAM*P_abs
/p0),(8.0))*exp(C8/C_T(c,t)))/(40320.0)+(pow((K0_FAM*P_abs/p0),(9.0))*exp(C9/C_T(c
,t)))/(362880.0)+
       (pow((K0_FAM*P_abs/p0),(10.0))*exp(C10/C_T(c,t)))/(3628800.0)+(pow((K0_FAM*
P_abs/p0),(11.0))*exp(C11/C_T(c,t)))/(39916800.0);

w_eq = (w_m_FAM *const1)/((1+const2)*11.0);

k1 = 15.0 * D_s0_FAM/ pow(R_p_FAM,2.0);          /*1/s*/
k2 = E_a_FAM / R_u;                              /*K*/
k_m = k1 * exp(-1*k2 / C_T(c,t));                /*1/s*/

source = (1.0 - porosity)* roh_ads_FAM * del_h_ads_FAM *  k_m * (w_eq -
C_UDSI(c,t,0));
dS[eqn] = -(1.0 - porosity)* roh_ads_FAM * del_h_ads_CaCl2 * k_m;
return source;
}

/*****************************************************************/
/*Water Temperature Profile - Pipe - Function of time*/
/*****************************************************************/
DEFINE_PROFILE(water_temp,t,i)
{
real water_temp;
real time;
real k;
face_t f;

time = CURRENT_TIME;
k = floor (time/(cycle_time));

if (k<cycle_counts)

       if (abs(cycle_time-480.0)<1E-3)
       {
              if ((k*cycle_time<=time) && (time<0.5*(2*k+1)*cycle_time))
```

```
                    water_temp=273.15+21.9322*exp(-0.0121*(time-
k*cycle_time))+35.3797*exp(-0.1788*(time-k*cycle_time))+30.8024;

             if ((0.5*(2*k+1)*cycle_time<=time) &&
(time<(0.5*(2*k+1)*cycle_time+44)))
                    water_temp=273.15+12107.1926*exp(0.0000172*(time-
(k+0.5)*cycle_time))-37.41927*exp(-0.19854*(time-(k+0.5)*cycle_time))-12037.044;

             if ((0.5*(2*k+1)*cycle_time+44<=time) && (time<(k+1)*cycle_time))
                    water_temp=273.15+394.00096*exp(0.000057*(time-
(k+0.5)*cycle_time))-10.25342*exp(-0.01816*(time-(k+0.5)*cycle_time))-311.079;
      }

      if (abs(cycle_time-600.0)<1E-3)
      {
             if ((k*cycle_time<=time) && (time<0.5*(2*k+1)*cycle_time))
                    water_temp=273.15+22.2808*exp(-0.0133*(time-
k*cycle_time))+34.3047*exp(-0.1879*(time-k*cycle_time))+31.5718;

             if ((0.5*(2*k+1)*cycle_time<=time) &&
(time<0.5*(2*k+1)*cycle_time+48))
                    water_temp=273.15+6170.3867*exp(0.000039*(time-
(k+0.5)*cycle_time))-35.4224*exp(-0.212148003707*(time-(k+0.5)*cycle_time))-
6101.6133;

             if ((0.5*(2*k+1)*cycle_time+48<=time) && (time<(k+1)*cycle_time))
                    water_temp=273.15+15.7553*exp(0.0003*(time-
(k+0.5)*cycle_time))-14.4154*exp(-0.0158*(time-(k+0.5)*cycle_time))+70.658;
      }

      if (abs(cycle_time-900.0)<1E-3)
      {
             if ((k*cycle_time<=time) && (time<k*cycle_time+39))
                    water_temp=273.15+33.8127*exp(-0.1785*(time-
k*cycle_time))+53.6982*exp(-0.0050*(time-k*cycle_time));

             if ((k*cycle_time+39<=time) && (time<k*cycle_time+128))
                    water_temp=273.15+0.1308*exp(0.04524*(time-k*cycle_time))-
0.5323*exp(0.03603*(time-k*cycle_time))+45.64;

             if ((k*cycle_time+128<=time) && (time<0.5*(2*k+1)*cycle_time))
                    water_temp=273.15+10.0000*exp(-0.3426*(time-
k*cycle_time))+11.25*exp(-0.01113*(time-k*cycle_time))+31.94;

             if ((0.5*(2*k+1)*cycle_time<=time) &&
(time<0.5*(2*k+1)*cycle_time+27))
                    water_temp=273.15+63.63*exp(0.00646*(time-
(k+0.5)*cycle_time))-31.64*exp(-0.2885*(time-(k+0.5)*cycle_time));

             if ((0.5*(2*k+1)*cycle_time+27<=time) && (time<(k+1)*cycle_time))
                    water_temp=273.15+6.647*exp(0.00014*(time-
(k+0.5)*cycle_time))-17.62*exp(-0.01586*(time-(k+0.5)*cycle_time))+80.52;
      }

      if (abs(cycle_time-1200.0)<1E-3)
      {
```

```
              if ((k*cycle_time<=time) && (time<k*cycle_time+39))
                     water_temp=273.15+33.8127*exp(-0.1785*(time-
k*cycle_time))+53.6982*exp(-0.0050*(time-k*cycle_time));

              if ((k*cycle_time+39<=time) && (time<k*cycle_time+128))
                     water_temp=273.15+0.1308*exp(0.04524*(time-k*cycle_time))-
0.5323*exp(0.03603*(time-k*cycle_time))+45.64;

              if ((k*cycle_time+128<=time) && (time<0.5*(2*k+1)*cycle_time))
                     water_temp=273.15+10.0000*exp(-0.3426*(time-
k*cycle_time))+11.25*exp(-0.01113*(time-k*cycle_time))+31.94;

              if ((0.5*(2*k+1)*cycle_time<=time) &&
(time<0.5*(2*k+1)*cycle_time+27))
                     water_temp=273.15+63.63*exp(0.00646*(time-
(k+0.5)*cycle_time))-31.64*exp(-0.2885*(time-(k+0.5)*cycle_time));

              if ((0.5*(2*k+1)*cycle_time+27<=time) && (time<(k+1)*cycle_time))
                     water_temp=273.15+6.647*exp(0.00014*(time-
(k+0.5)*cycle_time))-17.62*exp(-0.01586*(time-(k+0.5)*cycle_time))+80.52;
       }

       if (abs(cycle_time-1800.0)<1E-3)
       {
              if ((k*cycle_time<=time) && (time<k*cycle_time+55))
                     water_temp=273.15+13.4769*exp(-0.8052*(time-
k*cycle_time))+31.9208*exp(-0.0785*(time-k*cycle_time))+43.2488;

              if ((k*cycle_time+55<=time) && (time<k*cycle_time+110))
                     water_temp=273.15+0.2059*exp(0.0441*(time-k*cycle_time))-
0.6004*exp(0.0371*(time-k*cycle_time))+45.9856;

              if ((k*cycle_time+110<=time) && (time<k*cycle_time+300))
                     water_temp=273.15+1013.8944*exp(-0.0555*(time-
k*cycle_time))+35.7577*exp(-0.00028*(time-k*cycle_time));

              if ((k*cycle_time+300<=time) && (time<0.5*(2*k+1)*cycle_time))
                     water_temp=273.15+0.7072*exp(-0.0057*(time-k*cycle_time-
300))+32.211*exp(-0.000009*(time-k*cycle_time-300));

              if ((0.5*(2*k+1)*cycle_time<=time) &&
(time<0.5*(2*k+1)*cycle_time+27))
                     water_temp=273.15+63.63*exp(0.00646*(time-
(k+0.5)*cycle_time))-31.64*exp(-0.2885*(time-(k+0.5)*cycle_time));

              if ((0.5*(2*k+1)*cycle_time+27<=time) && (time<(k+1)*cycle_time))
                     water_temp=273.15+6.647*exp(0.00014*(time-
(k+0.5)*cycle_time))-17.62*exp(-0.01586*(time-(k+0.5)*cycle_time))+80.52;
       }

       if (abs(cycle_time-24000.0)<1E-3)

       {
              if ((k*cycle_time<=time) && (time<k*cycle_time+25))
                     water_temp=273.15+19.7494*exp(-0.0072*(time-
k*cycle_time))+10.0462*exp(0.0129*(time-k*cycle_time));
```

```
		if ((k*cycle_time+25<=time) && (time<k*cycle_time+390))
			water_temp=273.15+32.7182*exp(-0.00088*(time-k*cycle_time))-
4.7961*exp(-0.0282*(time-k*cycle_time));

		if ((k*cycle_time+390<=time) && (time<k*cycle_time+5000))
			water_temp=273.15-0.0004111*(time-k*cycle_time)+31.76;

		if ((k*cycle_time+5000<=time) && (time<0.5*(2*k+1)*cycle_time))
			water_temp=273.15+29.7;

		if ((0.5*(2*k+1)*cycle_time<=time) &&
(time<0.5*(2*k+1)*cycle_time+4))
			water_temp=273.15+29.7;

		if ((0.5*(2*k+1)*cycle_time+4<=time) &&
(time<0.5*(2*k+1)*cycle_time+36))
			water_temp=273.15+62.9550*exp(0.0055*(time-
(k+0.5)*cycle_time))-94.0800*exp(-0.2548*(time-(k+0.5)*cycle_time));

		if ((0.5*(2*k+1)*cycle_time+33<=time) &&
(time<0.5*(2*k+1)*cycle_time+147))
			water_temp=273.15+81.4767*exp(0.0002*(time-
(k+0.5)*cycle_time))-10.9568*exp(-0.0144*(time-(k+0.5)*cycle_time));

		if ((0.5*(2*k+1)*cycle_time+147<=time) &&
(time<0.5*(2*k+1)*cycle_time+1000))
			water_temp=273.15+87.4347*exp(0.000002*(time-
(k+0.5)*cycle_time))-27.3549*exp(-0.01172*(time-(k+0.5)*cycle_time));

		if ((0.5*(2*k+1)*cycle_time+1000<=time) &&
(time<0.5*(2*k+1)*cycle_time+5000))
			water_temp=0.0004724*(time-(k+0.5)*cycle_time-999)+360.76;

		if ((0.5*(2*k+1)*cycle_time+5000<=time) && (time<(k+1)*cycle_time))
			water_temp=273.15+89.50;
	}


	begin_f_loop(f,t)
	{
		F_PROFILE(f,t,i)=water_temp;
	}
	end_f_loop(f,t);
}

/*****************************************************************/
/*Pressure Profile (Evaporator/Condensor) - Function of time*/
/*****************************************************************/
DEFINE_PROFILE(pressure,t,i)
{
real pressure;
real time, step, p_evap, p_cond;
real k;
face_t f;
```

```
time = CURRENT_TIME;
p_evap=100*exp(a_s+b_s/(T_evap+273.15));
p_cond=100*exp(a_s+b_s/(T_cond+273.15));
k = floor (time/(cycle_time));

if (k<cycle_counts)

       if (abs(cycle_time-480)<1E-3)
       {
              if ((k*cycle_time<=time) && (time<k*cycle_time+10))
                     pressure=18.0184*exp(0.3912*(time-k*cycle_time))-
15.6377*exp(0.4149*(time-k*cycle_time))+3714.621;

              if ((k*cycle_time+10<=time) && (time<0.5*(2*k+1)*cycle_time))
                     pressure=4115.5336*exp(-0.0136*(time-
k*cycle_time))+9.2552*exp(0.01445*(time-k*cycle_time))+28.371;

              if ((0.5*(2*k+1)*cycle_time<=time) &&
(time<0.5*(2*k+1)*cycle_time+42))
                     pressure=957.8733*exp(-0.0623*(time-
(k+0.5)*cycle_time))+7897.201*exp(0.0058*(time-(k+0.5)*cycle_time))-8374.818;

              if ((0.5*(2*k+1)*cycle_time+42<=time) && (time<(k+1)*cycle_time))
                     pressure=31098.877*exp(-0.00007*(time-(k+0.5)*cycle_time))-
4206.666*exp(-0.0099*(time-(k+0.5)*cycle_time))-26459.681;
       }

       if (abs(cycle_time-600)<1E-3)
       {
              if ((k*cycle_time<=time) && (time<k*cycle_time+10))
                     pressure=-30.6922*exp(0.2479*(time-
k*cycle_time))+47.2946*exp(0.1763*(time-k*cycle_time))+3761.529;

              if ((k*cycle_time+10<=time) && (time<0.5*(2*k+1)*cycle_time))
                     pressure= 4164.098*exp(-0.0147*(time-
k*cycle_time))+88.945*exp(0.0051*(time-k*cycle_time));

              if ((0.5*(2*k+1)*cycle_time<=time) &&
(time<0.5*(2*k+1)*cycle_time+14))
                     pressure=-10.567*exp(-30.711*(time-
(k+0.5)*cycle_time))+1.477*exp(0.3473*(time-(k+0.5)*cycle_time))+421.798;

              if ((0.5*(2*k+1)*cycle_time+14<=time) && (time<(k+1)*cycle_time))
                     pressure=-4014.837*exp(-0.0150*(time-
(k+0.5)*cycle_time))+28972.1735*exp(0.000013*(time-(k+0.5)*cycle_time))-25214.194;
       }
       if (abs(cycle_time-900)<1E-3)
       {
              if ((k*cycle_time<=time) && (time<k*cycle_time+22))
                     pressure=-14495.403*exp(0.0119*(time-k*cycle_time))-
26731.378*exp(-0.0066*(time-k*cycle_time))+44923.425;

              if ((k*cycle_time+22<=time) && (time<0.5*(2*k+1)*cycle_time))
                     pressure=3859.1657*exp(-0.0152*(time-
k*cycle_time))+913.591*exp(0.000468*(time-k*cycle_time))-698.032;
```

```
            if ((0.5*(2*k+1)*cycle_time<=time) &&
(time<0.5*(2*k+1)*cycle_time+47))
                  pressure=24477.982*exp(-0.0036*(time-(k+0.5)*cycle_time))+
15576.215*exp(0.0063*(time-(k+0.5)*cycle_time))-39721.389;

            if ((0.5*(2*k+1)*cycle_time+47<=time) && (time<(k+1)*cycle_time))
                  pressure=5290.0241*exp(-0.00075*(time-(k+0.5)*cycle_time))-
4910.212*exp(-0.0089*(time-(k+0.5)*cycle_time));
      }
      if (abs(cycle_time-1200)<1E-3)
      {
            if ((k*cycle_time<=time) && (time<k*cycle_time+14))
                  pressure=-61.9217*exp(0.1540*(time-
k*cycle_time))+3563.1014*exp(0.0034*(time-k*cycle_time));

            if ((k*cycle_time+14<=time) && (time<k*cycle_time+165))
                  pressure=1260*exp(-0.1196*(time-k*cycle_time))+3463*exp(-
0.01241*(time-k*cycle_time))+90.27;

            if ((k*cycle_time+165<=time) && (time<0.5*(2*k+1)*cycle_time))
                  pressure=146.9290*exp(-0.0061*(time-
k*cycle_time))+12100.6517*exp(-0.0291*(time-k*cycle_time))+384.5672;

            if ((0.5*(2*k+1)*cycle_time<=time) &&
(time<0.5*(2*k+1)*cycle_time+15))
                  pressure=325.2688*exp(-0.0311*(time-
(k+0.5)*cycle_time))+66.3108*exp(0.1062*(time-(k+0.5)*cycle_time));

            if ((0.5*(2*k+1)*cycle_time+15<=time) &&
(time<0.5*(2*k+1)*cycle_time+263))
                  pressure=3917.9378*exp(0.00013*(time-(k+0.5)*cycle_time))-
4267.7019*exp(-0.0143*(time-(k+0.5)*cycle_time));

            if ((0.5*(2*k+1)*cycle_time+263<=time) && (time<(k+1)*cycle_time))
                  pressure=5126.6237*exp(-0.00063*(time-(k+0.5)*cycle_time))-
4729.3164*exp(-0.0095*(time-(k+0.5)*cycle_time));
      }

      if (abs(cycle_time-1800)<1E-3)
      {
            if ((k*cycle_time<=time) && (time<k*cycle_time+13))
                  pressure=-251.6180*exp(-0.00734*(time-k*cycle_time))-
10.8036*exp(0.2476*(time-k*cycle_time))+3503.8132;

            if ((k*cycle_time+13<=time) && (time<k*cycle_time+155))
                  pressure=760.0259*exp(-0.05745*(time-
k*cycle_time))+3056.4507*exp(-0.01068*(time-k*cycle_time));

            if ((k*cycle_time+155<=time) && (time<k*cycle_time+300))
                  pressure=21084.7460*exp(-0.0325*(time-
k*cycle_time))+507.2680*exp(-0.00082*(time-k*cycle_time));

            if ((k*cycle_time+300<=time) && (time<0.5*(2*k+1)*cycle_time))
                  pressure=219.1390*exp(-0.0050*(time-
k*cycle_time))+336.1381*exp(0.00013*(time-k*cycle_time));
```

```
            if ((0.5*(2*k+1)*cycle_time<=time) &&
(time<0.5*(2*k+1)*cycle_time+18))
                  pressure=349.8067*exp(-0.01436*(time-
(k+0.5)*cycle_time))+33.1371*exp(0.1328*(time-(k+0.5)*cycle_time));

            if ((0.5*(2*k+1)*cycle_time+18<=time) &&
(time<0.5*(2*k+1)*cycle_time+276))
                  pressure=4029.1867*exp(0.000226*(time-(k+0.5)*cycle_time))-
4391.9449*exp(-0.01380*(time-(k+0.5)*cycle_time));

            if ((0.5*(2*k+1)*cycle_time+276<=time) &&
(time<0.5*(2*k+1)*cycle_time+800))
                  pressure=5141.8451*exp(-0.00053*(time-(k+0.5)*cycle_time))-
5630.6033*exp(-0.0112*(time-(k+0.5)*cycle_time));

            if ((0.5*(2*k+1)*cycle_time+800<=time) && (time<(k+1)*cycle_time))
                  pressure=0.002931771043*pow((time-(k+0.5)*cycle_time),2)-
6.2506*(time-(k+0.5)*cycle_time)+6491.8872;
      }

      if (abs(cycle_time-24000)<1E-3)
      {
            if ((k*cycle_time<=time) && (time<k*cycle_time+106))
                  pressure=776.9487*exp(-0.287529637462*(time-
k*cycle_time))+1258.6075*exp(-0.0040*(time-k*cycle_time));

            if ((k*cycle_time+106<=time) && (time<k*cycle_time+601))
                  pressure=4359.2776*exp(0.00001*(time-
k*cycle_time))+637.552*exp(-0.0070*(time-k*cycle_time))-3843.956;

            if ((k*cycle_time+601<=time) && (time<k*cycle_time+2598))
                  pressure=-0.00718*((time-k*cycle_time)-600)+551;

            if ((k*cycle_time+2598<=time) && (time<k*cycle_time+3800))
                  pressure=-3.0494*exp(0.003015*(time-k*cycle_time-
2500))+506.5231*exp(0.000676*(time-k*cycle_time-2500));

            if ((k*cycle_time+3800<=time) && (time<k*cycle_time+10000))
                  pressure=2078.3084*exp(-0.000013*(time-k*cycle_time-3800))-
990.6468*exp(-0.00046*(time-k*cycle_time-3800));

            if ((k*cycle_time+10000<=time) && (time<0.5*(2*k+1)*cycle_time))
                  pressure=0.003896*(time-k*cycle_time-10000)+1866;

            if ((0.5*(2*k+1)*cycle_time<=time) &&
(time<0.5*(2*k+1)*cycle_time+28))
                  pressure=256.142*exp(-0.2618*(time-
(k+0.5)*cycle_time))+1673.7675*exp(0.0159*(time-(k+0.5)*cycle_time));

            if ((0.5*(2*k+1)*cycle_time+28<=time) &&
(time<0.5*(2*k+1)*cycle_time+1387))
                  pressure=5828.294*exp(-0.00019*(time-(k+0.5)*cycle_time))-
3565.374*exp(-0.0039*(time-(k+0.5)*cycle_time));

            if ((0.5*(2*k+1)*cycle_time+1387<=time) &&
(time<0.5*(2*k+1)*cycle_time+6000))
```

```
                    pressure=3114.308*exp(-0.00057*(time-(k+0.5)*cycle_time-
1300))+1490.99*exp(0.00006*(time-(k+0.5)*cycle_time-1300));

             if ((0.5*(2*k+1)*cycle_time+6000<=time) && (time<(k+1)*cycle_time))
                    pressure=24.928*exp(-0.0014*(time-(k+0.5)*cycle_time-
6000))+2164.574*exp(-0.000003*(time-(k+0.5)*cycle_time-6000));

       }

       begin_f_loop(f,t)
       {
              F_PROFILE(f,t,i)=pressure;
       }
       end_f_loop(f,t);
}


/*****************************************************************/
/*Temperature Profile (Evaporator/Condensor) - Function of time*/
/*****************************************************************/
DEFINE_PROFILE(temperature,t,i)
{
real pressure;
real time, step, p_evap, p_cond;
real k;
face_t f;

time = CURRENT_TIME;
p_evap=100*exp(a_s+b_s/(T_evap+273.15));
p_cond=100*exp(a_s+b_s/(T_cond+273.15));
k = floor (time/(cycle_time));

if (k<cycle_counts)

       if (abs(cycle_time-480)<1E-3)
       {
             if ((k*cycle_time<=time) && (time<k*cycle_time+10))
                    pressure=18.0184*exp(0.3912*(time-k*cycle_time))-
15.6377*exp(0.4149*(time-k*cycle_time))+3714.621;

             if ((k*cycle_time+10<=time) && (time<0.5*(2*k+1)*cycle_time))
                    pressure=4115.5336*exp(-0.0136*(time-
k*cycle_time))+9.2552*exp(0.01445*(time-k*cycle_time))+28.371;

             if ((0.5*(2*k+1)*cycle_time<=time) &&
(time<0.5*(2*k+1)*cycle_time+42))
                    pressure=957.8733*exp(-0.0623*(time-
(k+0.5)*cycle_time))+7897.201*exp(0.0058*(time-(k+0.5)*cycle_time))-8374.818;

             if ((0.5*(2*k+1)*cycle_time+42<=time) && (time<(k+1)*cycle_time))
                    pressure=31098.877*exp(-0.00007*(time-(k+0.5)*cycle_time))-
4206.666*exp(-0.0099*(time-(k+0.5)*cycle_time))-26459.681;
       }

       if (abs(cycle_time-600)<1E-3)
       {
```

```
            if ((k*cycle_time<=time) && (time<k*cycle_time+10))
                  pressure=-30.6922*exp(0.2479*(time-
k*cycle_time))+47.2946*exp(0.1763*(time-k*cycle_time))+3761.529;

            if ((k*cycle_time+10<=time) && (time<0.5*(2*k+1)*cycle_time))
                  pressure= 4164.098*exp(-0.0147*(time-
k*cycle_time))+88.945*exp(0.0051*(time-k*cycle_time));

            if ((0.5*(2*k+1)*cycle_time<=time) &&
(time<0.5*(2*k+1)*cycle_time+14))
                  pressure=-10.567*exp(-30.711*(time-
(k+0.5)*cycle_time))+1.477*exp(0.3473*(time-(k+0.5)*cycle_time))+421.798;

            if ((0.5*(2*k+1)*cycle_time+14<=time) && (time<(k+1)*cycle_time))
                  pressure=-4014.837*exp(-0.0150*(time-
(k+0.5)*cycle_time))+28972.1735*exp(0.000013*(time-(k+0.5)*cycle_time))-25214.194;
      }
      if (abs(cycle_time-900)<1E-3)
      {
            if ((k*cycle_time<=time) && (time<k*cycle_time+22))
                  pressure=-14495.403*exp(0.0119*(time-k*cycle_time))-
26731.378*exp(-0.0066*(time-k*cycle_time))+44923.425;

            if ((k*cycle_time+22<=time) && (time<0.5*(2*k+1)*cycle_time))
                  pressure=3859.1657*exp(-0.0152*(time-
k*cycle_time))+913.591*exp(0.000468*(time-k*cycle_time))-698.032;

            if ((0.5*(2*k+1)*cycle_time<=time) &&
(time<0.5*(2*k+1)*cycle_time+47))
                  pressure=24477.982*exp(-0.0036*(time-(k+0.5)*cycle_time))+
15576.215*exp(0.0063*(time-(k+0.5)*cycle_time))-39721.389;

            if ((0.5*(2*k+1)*cycle_time+47<=time) && (time<(k+1)*cycle_time))
                  pressure=5290.0241*exp(-0.00075*(time-(k+0.5)*cycle_time))-
4910.212*exp(-0.0089*(time-(k+0.5)*cycle_time));
      }
      if (abs(cycle_time-1200)<1E-3)
      {
            if ((k*cycle_time<=time) && (time<k*cycle_time+14))
                  pressure=-61.9217*exp(0.1540*(time-
k*cycle_time))+3563.1014*exp(0.0034*(time-k*cycle_time));

            if ((k*cycle_time+14<=time) && (time<k*cycle_time+165))
                  pressure=1260*exp(-0.1196*(time-k*cycle_time))+3463*exp(-
0.01241*(time-k*cycle_time))+90.27;

            if ((k*cycle_time+165<=time) && (time<0.5*(2*k+1)*cycle_time))
                  pressure=146.9290*exp(-0.0061*(time-
k*cycle_time))+12100.6517*exp(-0.0291*(time-k*cycle_time))+384.5672;

            if ((0.5*(2*k+1)*cycle_time<=time) &&
(time<0.5*(2*k+1)*cycle_time+15))
                  pressure=325.2688*exp(-0.0311*(time-
(k+0.5)*cycle_time))+66.3108*exp(0.1062*(time-(k+0.5)*cycle_time));
```

```
            if ((0.5*(2*k+1)*cycle_time+15<=time) &&
(time<0.5*(2*k+1)*cycle_time+263))
                  pressure=3917.9378*exp(0.00013*(time-(k+0.5)*cycle_time))-
4267.7019*exp(-0.0143*(time-(k+0.5)*cycle_time));

            if ((0.5*(2*k+1)*cycle_time+263<=time) && (time<(k+1)*cycle_time))
                  pressure=5126.6237*exp(-0.00063*(time-(k+0.5)*cycle_time))-
4729.3164*exp(-0.0095*(time-(k+0.5)*cycle_time));
      }

      if (abs(cycle_time-1800)<1E-3)
      {
            if ((k*cycle_time<=time) && (time<k*cycle_time+13))
                  pressure=-251.6180*exp(-0.00734*(time-k*cycle_time))-
10.8036*exp(0.2476*(time-k*cycle_time))+3503.8132;

            if ((k*cycle_time+13<=time) && (time<k*cycle_time+155))
                  pressure=760.0259*exp(-0.05745*(time-
k*cycle_time))+3056.4507*exp(-0.01068*(time-k*cycle_time));

            if ((k*cycle_time+155<=time) && (time<k*cycle_time+300))
                  pressure=21084.7460*exp(-0.0325*(time-
k*cycle_time))+507.2680*exp(-0.00082*(time-k*cycle_time));

            if ((k*cycle_time+300<=time) && (time<0.5*(2*k+1)*cycle_time))
                  pressure=219.1390*exp(-0.0050*(time-
k*cycle_time))+336.1381*exp(0.00013*(time-k*cycle_time));

            if ((0.5*(2*k+1)*cycle_time<=time) &&
(time<0.5*(2*k+1)*cycle_time+18))
                  pressure=349.8067*exp(-0.01436*(time-
(k+0.5)*cycle_time))+33.1371*exp(0.1328*(time-(k+0.5)*cycle_time));

            if ((0.5*(2*k+1)*cycle_time+18<=time) &&
(time<0.5*(2*k+1)*cycle_time+276))
                  pressure=4029.1867*exp(0.000226*(time-(k+0.5)*cycle_time))-
4391.9449*exp(-0.013800828018*(time-(k+0.5)*cycle_time));

            if ((0.5*(2*k+1)*cycle_time+276<=time) &&
(time<0.5*(2*k+1)*cycle_time+800))
                  pressure=5141.8451*exp(-0.00053*(time-(k+0.5)*cycle_time))-
5630.6033*exp(-0.0112*(time-(k+0.5)*cycle_time));

            if ((0.5*(2*k+1)*cycle_time+800<=time) && (time<(k+1)*cycle_time))
                  pressure=0.002931771043*pow((time-(k+0.5)*cycle_time),2)-
6.2506*(time-(k+0.5)*cycle_time)+6491.8872;
      }

      if (abs(cycle_time-24000)<1E-3)
      {
            if ((k*cycle_time<=time) && (time<k*cycle_time+106))
                  pressure=776.9487*exp(-0.287529637462*(time-
k*cycle_time))+1258.6075*exp(-0.0040*(time-k*cycle_time));

            if ((k*cycle_time+106<=time) && (time<k*cycle_time+601))
```

```
                    pressure=4359.2776*exp(0.00001*(time-
k*cycle_time))+637.552*exp(-0.0070*(time-k*cycle_time))-3843.956;

             if ((k*cycle_time+601<=time) && (time<k*cycle_time+2598))
                    pressure=-0.00718*((time-k*cycle_time)-600)+551;

             if ((k*cycle_time+2598<=time) && (time<k*cycle_time+3800))
                    pressure=-3.0494*exp(0.003015*(time-k*cycle_time-
2500))+506.5231*exp(0.000676*(time-k*cycle_time-2500));

             if ((k*cycle_time+3800<=time) && (time<k*cycle_time+10000))
                    pressure=2078.3084*exp(-0.000013*(time-k*cycle_time-3800))-
990.6468*exp(-0.00046*(time-k*cycle_time-3800));

             if ((k*cycle_time+10000<=time) && (time<0.5*(2*k+1)*cycle_time))
                    pressure=0.003896*(time-k*cycle_time-10000)+1866;

             if ((0.5*(2*k+1)*cycle_time<=time) &&
(time<0.5*(2*k+1)*cycle_time+28))
                    pressure=256.142*exp(-0.2618*(time-
(k+0.5)*cycle_time))+1673.7675*exp(0.0159*(time-(k+0.5)*cycle_time));

             if ((0.5*(2*k+1)*cycle_time+28<=time) &&
(time<0.5*(2*k+1)*cycle_time+1387))
                    pressure=5828.294*exp(-0.00019*(time-(k+0.5)*cycle_time))-
3565.374*exp(-0.0039*(time-(k+0.5)*cycle_time));

             if ((0.5*(2*k+1)*cycle_time+1387<=time) &&
(time<0.5*(2*k+1)*cycle_time+6000))
                    pressure=3114.308*exp(-0.00057*(time-(k+0.5)*cycle_time-
1300))+1490.99*exp(0.00006*(time-(k+0.5)*cycle_time-1300));

             if ((0.5*(2*k+1)*cycle_time+6000<=time) && (time<(k+1)*cycle_time))
                    pressure=24.928*exp(-0.0014*(time-(k+0.5)*cycle_time-
6000))+2164.574*exp(-0.000003*(time-(k+0.5)*cycle_time-6000));

       }

       begin_f_loop(f,t)
       {
             F_PROFILE(f,t,i)=b_s/((log(pressure/100)/log(2.7183))-a_s);
       }
       end_f_loop(f,t);
}

/*****************************************************************/
/*Pressure Profile (Ideal Evaporator/Condensor) - Function of time*/
/*****************************************************************/
DEFINE_PROFILE(pressure_ideal,t,i)
{
real pressure_ideal;
real time, step, p_evap, p_cond, fraction;
real k;
face_t f;

time = CURRENT_TIME;
```

```
p_evap=100*exp(a_s+b_s/(T_evap+273.15));
p_cond=100*exp(a_s+b_s/(T_cond+273.15));
k = floor (time/(cycle_time));
fraction=(change_time)/(cycle_time);

if (k<cycle_counts)

       if ((k*cycle_time<=time) && (time<(fraction+k)*cycle_time))
       {      step=(time-k*cycle_time)/(fraction*cycle_time);
              pressure_ideal=0.5*(p_cond+p_evap)-0.5*((p_cond-p_evap)*step);
       }
       if (((fraction+k)*cycle_time<=time) && (time<(0.5-fraction+k)*cycle_time))
       {      step=1.0;
              pressure_ideal=0.5*(p_cond+p_evap)-0.5*((p_cond-p_evap)*step);
       }
       if (((0.5-fraction+k)*cycle_time<=time) &&
(time<(0.5+fraction+k)*cycle_time))
       {      step=-(time-(0.5+k)*cycle_time)/(fraction*cycle_time);
              pressure_ideal=0.5*(p_cond+p_evap)-0.5*((p_cond-p_evap)*step);
       }
       if (((0.5+fraction+k)*cycle_time<=time) && (time<(1-
fraction+k)*cycle_time))
       {      step=-1.0;
              pressure_ideal=0.5*(p_cond+p_evap)-0.5*((p_cond-p_evap)*step);
       }
       if (((1-fraction+k)*cycle_time<=time) && (time<(1+k)*cycle_time))
       {      step=(time-(1+k)*cycle_time)/(fraction*cycle_time);
              pressure_ideal=0.5*(p_cond+p_evap)-0.5*((p_cond-p_evap)*step);
       }

       begin_f_loop(f,t)
       {
              F_PROFILE(f,t,i)=pressure_ideal;
       }
       end_f_loop(f,t);
}

/*****************************************************************/
/*Temperature Profile (Ideal Evaporator/Condensor) - Function of time*/
/*****************************************************************/
DEFINE_PROFILE(temperature_ideal,t,i)
{
real temperature_ideal;
real time, step, fraction;
real k;
face_t f;
fraction=(change_time)/(cycle_time);


time = CURRENT_TIME;
k = floor (time/(cycle_time));

if (k<cycle_counts)

       if ((k*cycle_time<=time) && (time<(fraction+k)*cycle_time))
       {      step=(time-k*cycle_time)/(fraction*cycle_time);
```

```
              temperature_ideal=273.15+0.5*(T_cond+T_evap)-0.5*((T_cond-
T_evap)*step);
       }
       if (((fraction+k)*cycle_time<=time) && (time<(0.5-fraction+k)*cycle_time))
       {      step=1.0;
              temperature_ideal=273.15+0.5*(T_cond+T_evap)-0.5*((T_cond-
T_evap)*step);
       }
       if (((0.5-fraction+k)*cycle_time<=time) &&
(time<(0.5+fraction+k)*cycle_time))
       {      step=-(time-(0.5+k)*cycle_time)/(fraction*cycle_time);
              temperature_ideal=273.15+0.5*(T_cond+T_evap)-0.5*((T_cond-
T_evap)*step);
       }
       if (((0.5+fraction+k)*cycle_time<=time) && (time<(1-
fraction+k)*cycle_time))
       {      step=-1.0;
              temperature_ideal=273.15+0.5*(T_cond+T_evap)-0.5*((T_cond-
T_evap)*step);
       }
       if (((1-fraction+k)*cycle_time<=time) && (time<(1+k)*cycle_time))
       {      step=(time-(1+k)*cycle_time)/(fraction*cycle_time);
              temperature_ideal=273.15+0.5*(T_cond+T_evap)-0.5*((T_cond-
T_evap)*step);
       }

       begin_f_loop(f,t)
       {
              F_PROFILE(f,t,i)=temperature_ideal;
       }
       end_f_loop(f,t);
}

/**********************************************************************/
/*Temperature Profile (Ideal HTF) - Function of time*/
/**********************************************************************/
DEFINE_PROFILE(HTF_temperature_ideal,t,i)
{
real HTF_temperature_ideal;
real time, step, fraction;
real k;
face_t f;
fraction=(change_time)/(cycle_time);


time = CURRENT_TIME;
k = floor (time/(cycle_time));

if (k<cycle_counts)

       if ((k*cycle_time<=time) && (time<(fraction+k)*cycle_time))
       {      step=(time-k*cycle_time)/(fraction*cycle_time);
              HTF_temperature_ideal=273.15+0.5*(T_heating+T_evap)-0.5*((T_heating-
T_evap)*step);
       }
       if (((fraction+k)*cycle_time<=time) && (time<(0.5-fraction+k)*cycle_time))
```

```
	{	step=1.0;
		HTF_temperature_ideal=273.15+0.5*(T_heating+T_cooling)-
0.5*((T_heating-T_cooling)*step);
	}
	if (((0.5-fraction+k)*cycle_time<=time) &&
(time<(0.5+fraction+k)*cycle_time))
	{	step=-(time-(0.5+k)*cycle_time)/(fraction*cycle_time);
		HTF_temperature_ideal=273.15+0.5*(T_heating+T_cooling)-
0.5*((T_heating-T_cooling)*step);
	}
	if (((0.5+fraction+k)*cycle_time<=time) && (time<(1-
fraction+k)*cycle_time))
	{	step=-1.0;
		HTF_temperature_ideal=273.15+0.5*(T_heating+T_cooling)-
0.5*((T_heating-T_cooling)*step);
	}
	if (((1-fraction+k)*cycle_time<=time) && (time<(1+k)*cycle_time))
	{	step=(time-(1+k)*cycle_time)/(fraction*cycle_time);
		HTF_temperature_ideal=273.15+0.5*(T_heating+T_cooling)-
0.5*((T_heating-T_cooling)*step);
	}

	begin_f_loop(f,t)
	{
		F_PROFILE(f,t,i)=HTF_temperature_ideal;
	}
	end_f_loop(f,t);
}
```